REDUCED GRAVITY RANKINE CYCLE SYSTEM DESIGN AND OPTIMIZATION STUDY WITH PASSIVE VORTEX PHASE SEPARATION

A Thesis

by

KEVIN ROBERT SUPAK

Submitted to the Office of Graduate Studies of
Texas A&M University
in partial fulfillment of the requirements for the degree of

MASTER OF SCIENCE

December 2007

Major Subject: Nuclear Engineering

REDUCED GRAVITY RANKINE CYCLE SYSTEM DESIGN AND OPTIMIZATION STUDY WITH PASSIVE VORTEX PHASE SEPARATION

A Thesis

by

KEVIN ROBERT SUPAK

Submitted to the Office of Graduate Studies of
Texas A&M University
in partial fulfillment of the requirements for the degree of

MASTER OF SCIENCE

Approved by:

Chair of Committee,	Frederick Best
Committee Members,	Yassin Hassan
	Obdulia Ley
Head of Department,	John Poston

December 2007

Major Subject: Nuclear Engineering

ABSTRACT

Reduced Gravity Rankine Cycle System Design and Optimization Study with Passive Vortex Phase Separation. (December 2007)
Kevin Robert Supak, B.S., Texas A&M University
Chair of Advisory Committee: Dr. Frederick Best

Liquid-metal Rankine power conversion systems (PCS) coupled with a fission reactor remain an attractive option for space power applications because system specific power and efficiency is very favorable for plant designs of 100 kW(e) or higher. Potential drawbacks to the technology in a reduced gravity environment include two-phase fluid management processes such as liquid-vapor phase separation. The most critical location for phase separation is at the boiler exit where only vapor must be sent to the turbine because blade erosion occurs from high velocity liquid droplets entrained by vapor flow.

Previous studies have proposed that rotary separators be used to separate the liquid and vapor from a two phase mixture. However these devices have complex turbo machinery, require kilowatts of power and are untested for high vapor flow conditions. The Interphase Transport Phenomena (ITP) laboratory has developed a low-power, passive microgravity vortex phase separator (MVS) which has already proven to be an essential component of two-phase systems operating in low gravity environments.

This thesis presents results from flight experiments where a Rankine cycle was operated in a reduced gravity environment for the first time by utilizing the MVS for liquid and vapor phase separation. The MVS was able to operate under saturated conditions and adjust to system transients as it would in the Rankine cycle by controlling the amount of liquid and vapor within the device. A new model is developed for the MVS to predict separation performance at high vapor flow conditions for sizing the separator at the

boiler, condenser, and turbine locations within the cycle by using a volume limiting method. This model factors in the following separator characteristics: mass, pumping power, and available buffer volume for system transients. The study is concluded with overall Rankine efficiency and performance changes due to adding vortex phase separation and a schematic of the Rankine cycle with the integration of the MVS is presented. The results from this thesis indicate the thermal to electric efficiency and specific mass of the cycle can be improved by using the MVS to separate the two phases instead of a rotary separator.

DEDICATION

To my parents: Debra and Robert. Their guidance and support in my life made me the person I am today.

ACKNOWLEDGMENTS

Several individuals have had a great influence on the work I completed for this thesis. Ryoji Oinuma, Michael Ellis, and Richard C. Kurwitz have been invaluable sources of help and support when I had difficulties completing my research. Dr. Frederick Best, my graduate advisor, gave me the opportunity to participate in a research program that has a profound impact on the technologies developed for future space missions. I would also like to thank Paul Schmitz of NASA Glen, Graydon Yoder of Oak Ridge National Laboratory, and William Deter from Hamilton Sunstrand Corp. for their help with the history behind my research. The experimental results presented in this thesis could not be completed without the help from Patrick Magari of Creare Inc. for the calibration of the void fraction sensors. However, I would not be the student of science I am today without my parent's love and support.

NOMENCLATURE

PCS	Power Conversion System
ITP	Interphase Transport Phenomena
kW(e)	Kilowatts-Electric
MVS	Microgravity Vortex Separator
ORNL	Oak Ridge National Laboratory
SNAP	Systems For Nuclear Auxiliary Power
MPRE	Medium Power Reactor Experiment
RFMD	Rotary Fluid Management Device
RPM	Revolutions Per Minute
LPM	Liters Per Minute
SLPM	Standard Liters Per Minute
T	Temperature
s	Entropy
$\dot{W}_{actual}$	Actual Work Done by the System
$\dot{W}_T$	Work Done by the Turbine
$\dot{W}_P$	Work Done by the Pump
$\dot{m}$	Mass Flow
h_{in}	Inlet Enthalpy

h_{out}	Outlet Enthalpy
$h_{out,s}$	Isentropic Outlet Enthalpy
η_T	Turbine Efficiency
η_P	Pump Efficiency
η	Thermal to Electric Efficiency
η_{th}	Plant Thermal Efficiency
$\dot{Q}_{reactor}$	Reactor Thermal Power
h_3	Turbine Inlet Enthalpy
h_4	Turbine Exit Enthalpy
h_1	Feed Pump Inlet Enthalpy
h_2	Feed Pump Exit Enthalpy
h_2	Boiler Inlet Enthalpy
h_3	Boiler Exit Enthalpy
W_n	Separator Nozzle Width
H_n	Separator Nozzle Height
D_{sep}	Separator Diameter
CFD	Computational Fluid Dynamics
ω	Liquid Rotational Speed
R_{sep}	Separator Radius

L_n	Separator Nozzle Characteristic Length
V_n	Separator Nozzle Velocity
μ_l	Liquid Dynamic Viscosity
ρ_l	Liquid Density
Bo	Bond Number
Fr	Froude Number
ρ_g	Vapor Density
R_I	Separator Vapor Core Radius
g	Acceleration
σ	Surface Tension
V	Velocity in the Froude Number
D_I	Separator Vapor Core Diameter
We	Weber Number
σ_{plate}	End Plate Stress of the Separator
t_{plate}	End Plate Thickness of the Separator
k	Factor for Separator Geometry in Stress Calculations
p	Separator Pressure for Stress Calculations
σ_{yield}	Yield Stress of the Material Used for Separator Construction
t_{wall}	Separator Wall Thickness

$\bar{V}_{sep}$	Separator Separation Volume
$\bar{V}_{V}$	Separator Vapor Core Volume
$\bar{V}_{L}$	Separator Liquid Volume
$\bar{V}_{VH}$	Separator Vapor Hold Up Volume
t_r	Separator Radial Transit Time
$\dot{\bar{V}}_{V}$	Vapor Volumetric Flow Rate
X	Separator Vapor Core Diameter Fraction of the Separator Diameter
$\bar{V}_{2\varphi}$	Separator Two-Phase Volume
T_L	Separator Liquid Layer Thickness
t_{iter}	Calculated Radial Transient Time
ΔP	Pump Differential Pressure
P_{EMP}	Electromagnetic Pump Power
η_{EMP}	Electromagnetic Pump Efficiency
P_{mech}	Mechanical Pump Power
η_{mech}	Mechanical Pump Efficiency
V_{pipe}	Pipe Velocity
ΔP_{vel}	Bernouli's Differential Pressure Head
ΔP_{form}	Pressure Drop from Form Losses
β	Loss Coefficient for Form Loss Calculations

NPSH	Net Positive Suction Head
$\dot{Q}_{pump}$	Energy Added to the Separator by the Pump
$\dot{Q}_{2\varphi}$	Energy Added to the Separator by the Heater Tape
$\dot{Q}_{spray\,condenser}$	Energy Removed from the Separator by the Condenser
$\dot{Q}_{ambient}$	Energy Removed from the Separator by Ambient Losses
$\dot{Q}_{gain}$	Net Energy Gained by the Separator
E_{in}	Energy In
E_{out}	Energy Out
E_{gain}	Energy Gained
$\dot{Q}$	Thermal Energy
x	Flowing Quality
h_{fg}	Latent Heat of Vaporization
μ_g	Gas Dynamic Viscosity
α	Void Fraction
EM	Electromagnetic

TABLE OF CONTENTS

Page

CHAPTER Page

LIST OF TABLES

Page

LIST OF FIGURES

Page

Page

Page

Page

CHAPTER I

INTRODUCTION AND LITERATURE REVIEW

Rankine cycle power conversion is used in most commercial power reactors on Earth and is well understood in a 1-g environment. The separation of liquid and vapor from a two-phase mixture in an earth based power plant is driven by buoyancy by phase separation. However, in a reduced gravity environment liquid and vapor do not naturally separate because surface tension and capillary forces overcome buoyancy. To operate efficiently in microgravity, Rankine cycle systems require vapor separation from a two-phase mixture at many locations in the power plant. These locations include: the boiler exit, inter-stage turbine separation, and the condenser. The most critical location is at the boiler exit where only vapor must be sent to the turbine because blade erosion would otherwise occur from high velocity liquid droplets entrained by vapor flow. Phase separation at each Rankine cycle location should require minimal power to operate in order to increase plant power conversion efficiency. A phase separator which is mechanically simple generally offers greater reliability because active devices with internal turbo-machinery and seals are more prone to mechanical failure than passive components. Therefore, the need exists for low power, passive and reliable phase separation at the boiler exit and other plant locations.

The Interphase Transport Phenomena (ITP) laboratory at Texas A&M University (TAMU) has developed a passive microgravity vortex phase separator (MVS) which has already proven to be an essential component of two-phase systems operating in low gravity environments.[1,2,3] This phase separator has been flight tested on thousands of parabolas aboard NASA reduced gravity aircraft and has achieved a NASA technology readiness level (TRL) of 6. Along with its ability to separate liquid and vapor in

---

This thesis follows the style of *Journal of Nuclear Science and Technology*.

micro-gravity, the separator can also act as an accumulator for inventory control and as a direct contact heat exchanger.[2)] For a Rankine system, the MVS is able to manage two-phase flows by returning liquid to the boiler or other plant locations and deliver very high quality vapor to the turbine to increase system performance.

The ITP designed the MVS to use the working fluid's intrinsic momentum to generate a centripetal acceleration field which induces buoyancy in microgravity. The acceleration field is generated by injecting the fluid through a nozzle which is tangentially located on the wall of a cylindrical body. Under microgravity conditions, the liquid within the MVS coupled with the fluid's inlet momentum, creates a liquid vortex which rotates around an axial vapor column. To complete separation, the vapor and liquid are extracted at axially opposite ends of the MVS and delivered to their respective locations within the system. Schematic and photo representations of the MVS can be seen in Fig. 1.

The ITP has recently conducted microgravity flight testing of an experimental test bed which simulated a Rankine cycle power system and used a microgravity vortex separator for vapor and liquid separation. This flight demonstrated the ability of the MVS to successfully operate in a single fluid component saturated state as it would in a Rankine cycle. The study presented in this thesis analyzes the results from this flight and how they apply to space Rankine cycle design with the MVS. Techniques developed by the ITP to design the MVS are used to investigate the characteristics of the device at different locations within the system.

This thesis focuses on the effect that a MVS will have on a microgravity Rankine cycle power conversion system (PCS) in terms of system specific mass and efficiencies. A MVS is sized for use at the boiler exit, an external turbine location and the condenser with techniques developed by the ITP. Future flight experiments and recommended further work for space Rankine cycles with MVS are also discussed.

One of the main advantages of the Rankine cycle for space applications is the power to weight ratio for 100 kW(e) systems and above. To show the effect of adding vortex phase separation to the system, software developed by Oak Ridge National Laboratory (ORNL) is used to estimate component masses. Specifically, the goal of this thesis is to show how a functioning liquid metal space Rankine cycle can be designed and operated in microgravity using the technology and procedures developed by the ITP over the past 20 years.

Background

With the Vision for Space Exploration set forth by President Bush in 2003 to further explore the lunar surface and establish a human presence through out the solar system, engineers have recognized that more efficient and larger power sources are required.[4)] Possible systems include: Brayton, Stirling, Thermionic, Thermoelectric, and Rankine power conversion cycles (PCS). The power requirement for a spacecraft has a direct impact on what type of power conversion cycle would be required to complete a mission because a specific PCS does not scale well over a wide range of power requirements.[5)] Fig. 2 shows scaling of different power conversion systems over the range of power requirements for future missions.

Rankine cycle power conversion becomes an ideal option for a PCS on space missions when the power requirement is 100 kW(e) or higher because the phase change of the working fluid allows more thermal energy per unit mass to be transported through the system. The power to weight ratio is also aided by the reduction in radiator area by the hot working fluid temperatures when compared to single phase systems. These arguments are supported later in the discussion. The system does not scale well in the low power region because the mass of the components needed to operate the system do not size linearly with power requirements.

Rankine cycle power conversion is used in most commercial power reactors on Earth and is well understood in a 1-g environment. A simplified schematic of a Rankine cycle can be seen in Fig. 3. Rankine cycles are two-phase systems in which thermal energy vaporizes a working fluid to provide momentum for driving a turbine-alternator which produces electrical power. The working fluid is condensed after it leaves the turbine and then returned to the boiler.

There are several other reasons why Rankine cycles are attractive for space missions. Rankine cycle technology has the potential to reach thermodynamic efficiencies up to 30%.[6] With increasing efficiency comes a decrease in overall system mass. Fig. 4 displays the fraction of the overall system mass for each component in a general turbo-electric system versus power level. As power level increases, the radiator mass fraction significantly increases. Efforts to decrease this fraction will result in more efficient power conversion cycles in terms of system specific power.

Using liquid metal as the two-phase working fluid allows for low system pressure with high and constant temperature heat rejection in the radiator. The constant temperature heat rejection allows the radiator mass and size to be significantly less than those of Brayton power conversion systems.[8] Fig. 5 displays a plot of the decrease in radiator area as the operating temperature increases for different liquid-metals. Fig. 5 shows why liquid metal two-phase systems are the leading candidates for high-power space power conversion cycles. To show the radiator mass savings in liquid metal Rankine cycles when compared with single-phase systems, such as the Brayton cycle, Fig. 6 displays a plot of radiator area per kilowatt as a function of system operating temperature.

The components required to operate a Rankine cycle have proven to be compact. For example, the design for the potassium secondary side of a Rankine cycle proposed by ORNL for the boiler and condenser are only 2.3 meters and about 0.5 meters in length respectively in a 100 kW(e) system.[9] The pressure vessel for the reactor in the 300

kW(e) SNAP-50 (Systems for Nuclear Auxiliary Power) is approximately 0.4 meters in diameter and 1 meter in height.[10] Rankine cycle components such as the feed pumps and turbines have been lifetime tested for thousands of hours during several liquid-metal space power programs which have provided a strong mechanical basis for Rankine cycle system optimization.[11] Component size and mass will be further investigated in this document when the Rankine cycle programs are discussed.

Although the potential for Rankine cycle technology is positive, the PCS is not currently available for space missions because the behavior of two-phase systems is not known well in reduced gravity environments. Two-phase heat transfer and pressure drop models for heat exchangers in reduced gravity are an immature technology.[11,12,13] The flow regimes which dictate the energy transport process are much different in a reduced gravity environment than on earth. The heat exchanger must be well characterized to understand the quality of the fluid at the exit of the boiler. However, it is argued the most important Rankine cycle technology is vapor separation from a two-phase flow. Rankine cycles depend on liquid and vapor phase separation to operate because system lifetime is affected by the quality of vapor delivered to the turbine. High-velocity liquid droplets entrained in vapor flows will cause turbine blade erosion.

Liquid and vapor separation naturally occurs on earth because of the buoyancy force provided by our gravity field. However, in the absence of an acceleration field, other forces such as the capillary effect and surface tension tend to dominate. NASA has recognized that the lack of knowledge of two-phase fluid management and prediction of steady and transient flow phenomena in microgravity is the major obstacle for Rankine cycle technology for space missions.[4] Therefore, potential drawbacks to the technology in a reduced gravity environment include two-phase fluid management processes such as liquid-vapor phase separation.

History of Space Rankine Cycle Development

Although two-phase technology for space Rankine cycles is underdeveloped, significant progress has been made since the 1950's in ground experiments and system optimization. Early Rankine cycle development started with the Atomics International Systems for Nuclear Auxiliary Power (SNAP) program in 1957.[10] The SNAP program consisted of three different reactor studies. Two of these reactor programs, SNAP-2 and SNAP-8, utilized liquid metal Rankine cycle power conversion while SNAP-10A used thermoelectrics. These three programs provide a rich technical background for present space nuclear power development through the experiments, design and planning of early electrical power systems. Table 1 summarizes the major features of the first three space nuclear power plant designs. It is important to note the turbine inlet temperature is higher than the boiling temperature because the vapor was superheated to ensure moisture would not enter the turbine.

SNAP-2 was a three kW(e) mercury PCS which demonstrated the first startup, steady-state, and shutdown of a space Rankine cycle power plant and development for this program extended over a decade. A simplified schematic of the SNAP-2 power plant can be seen in Fig. 7. The power conversion machinery was mounted on a single mercury lubricated rotating shaft which offered high reliability and ease of design. The combined rotating unit which operated the shaft was only 10 inches long.

Early in the program, thermal energy transfer was recognized to be more difficult in microgravity environments because of the lack of buoyancy forces. To augment heat transfer in the boiler, internal swirl wires were introduced into the flow area. The wires forced the liquid within the two-phase mixture to the wall to increase the heat transfer coefficient. Several flight tests were conducted in 1962 to study boiling and condensing phenomena but an entire system was not constructed for microgravity testing.[7,10] The

success of this program provided a technology basis for future programs such as the SNAP-10A and SNAP-8 reactors.

SNAP-10A has been the only U.S. reactor to fly in space. SNAP-10A orbited the earth for 43 days at full power in 1965. Although this reactor had a thermoelectric PCS and only generated 500 watts of power, it showed that a critical reaction could occur and be controlled from the ground in microgravity. Highly successful programs such as the SNAP-2 and SNAP-10A allowed a second generation of space nuclear power plants to be constructed, the SNAP-8. Initiated in 1960, the SNAP-8 program planned to deliver 30 kW(e) of power with the capability of expanding to 60 kW(e) with a 10,000 hour lifetime. Fig. 8 shows the size of a complete test reactor assembly in the SNAP-8 reactor program. SNAP-8 was similar to the SNAP-2 in that mercury was used as the working fluid in the PCS. Two test reactors with power conversion cycles were completed and tested for thousands of hours in this program.[7,10)] Significant progress was made with operating turbo-machinery to understand which structural materials were compatible with liquid-metals. Liquid metal pumps and turbine-alternator assemblies were start-stop tested for thousands of cycles and lifetime tested for over 10,000 hours. Although these reactors were extensively ground tested, no progress was made in the SNAP-8 program to understand the behavior of the systems in a reduced gravity environment.

The SNAP-50 space nuclear power program existed in the early 1960's until 1973 and had the goal of developing a 300-1200 kW(e) power plant which had a 10,000 hour lifetime.[10)] The plant was again similar to the early SNAP reactors because it utilized Rankine cycle power conversion. However, SNAP-50 used potassium as the working fluid instead of mercury. Engineers again recognized in this program that boiling in micro-gravity is not characterized well. To augment the heat transfer process and make boiling less susceptible to gravitational effects, the heat exchanger for the design built upon the wire swirl generators from the SNAP-2 program. The new design contained 12

channels, each with a twisted tape helical insert. These twisted tape inserts rely on the fluid's intrinsic momentum to provide radial acceleration and drive liquid to the wall of the heat exchanger. To produce superheated potassium vapor, the boiler design was approximately 2.3 meters in length.[10] To better package the boiler in the system and minimize mechanical and thermal stress, the device was circularized to form an arc-shape. The integration of the arc-shaped boiler with the PCS can be seen in Fig. 9.

It was recognized within the SNAP-50 program that vapor condensation within the turbine would drastically reduce turbine lifetime due to blade erosion. Therefore an interspool liquid separator was designed to remove moisture from the first turbine stage. Consequently, this design also removed some vapor with the liquid extraction thus reducing system performance. Each of the components needed to operate the PCS were extensively ground tested including the arc-shaped boiler.[14] However, a complete PCS was not tested due to program termination but was assumed to have high probability of success.[10] The components were never microgravity flight tested and it was unknown if the boiler could effectively operate under space mission conditions.[14] Table 2 outlines the testing of many turbine ground tests performed with potassium to understand turbine lifetime at the high working fluid temperatures during the early reactor programs.

At the conclusion of the early space nuclear power reactor programs such as SNAP and Advanced Space Nuclear Power Program in the early 1970's, engineers had addressed and resolved many technical problems associated with operating a Rankine cycle power plant on space missions.[11,10] However, the physics behind two-phase flow was still at an early stage of development in the early space reactor programs and is still considered to be a major issue to address in today's space systems.[1,3,4,10] The Interphase Transport Phenomena (ITP) laboratory at Texas A&M University has been studying the behavior of two-phase flow in a reduced gravity environment since 1984. The ITP has addressed many problems associated with two-phase flow technology development such as

reduced gravity pressure drop, heat transfer, phase distribution in manifolds, boiling and condensations behavior, and two-phase separation.[3)]

The ITP began two-phase separation development for space Rankine cycles in 1988 during the SP-100 program. The SP-100 program started in 1983 with the major goal of providing a reactor power system capable of supplying 10-100 kW(e) of unattended electrical power over a period of 7-10 years.[15)] One of the proposed configurations for the SP-100 program, which is similar to the schematic in Fig. 3, was a Rankine cycle PCS which utilized lithium for the fast reactor coolant and potassium was used as the working fluid on the secondary side. The design layout was similar to the early SNAP-2 and SNAP-8 reactor programs as previously discussed. A major problem with the SP-100 Rankine cycle design is that lithium can be split by neutrons to form helium gas. It was recognized that the removal of this non-condensable gas would be necessary for effective operation in this design.[1)]

Engineers in the SP-100 program designed a separator/accumulator device to control the helium gas in the system. This separator can be seen in Fig. 10. This device is an inline swirl separator with mesh capillary screens. The swirler induces approximately 2g of radial acceleration to produce buoyancy and drive the gas bubbles toward the center. A lithium wetted capillary mesh was used to separate the outer lithium flow from the core of helium gas. Although this device has been successfully operated on earth with air and water, the SP-100 program was terminated before zero gravity testing or lithium/helium operation and compatibility tests with the capillary material were conducted.

The ITP proposed that a MVS which was 32 centimeters in diameter be used in the primary side of the PCS to remove the non-condensable gas from the reactor coolant.[1)] The MVS is an effective solution to the problem because it could accommodate varying helium evolution rates over the lifetime of the reactor due to the buffer volume which

exists in the separator and does not have special materials such as the mesh screen in the SP-100 separator. Although the SP-100 program ended in 1994, the MVS is recognized as an essential component in Rankine cycle development because of its passive design, ability to effectively separate liquid and vapor, and act as an accumulator for inventory control.[1,2,3)] At the end of the program, the ITP further investigated the abilities of the MVS. Many sizes and configurations for the MVS were flight tested aboard NASA reduced gravity aircraft for over thirty hours using different working fluids and flow rates to understand separator stability for operation in microgravity.[2,3)] The programs which utilized the MVS are discussed later in this thesis.

ORNL Rankine Cycle Design

ORNL has worked with liquid metal Rankine cycles since the 1960's when it was one of the principal design teams for the medium power reactor experiment (MPRE).[6,8)] Since the early space reactor programs began, ORNL has been continually investigating Rankine cycle power systems for space missions. When President Bush announced the Vision for Space Exploration initiative in 2003, Project Prometheus was started to meet the power requirements for future space vehicles.[4)] ORNL became one of the design leads for a Rankine cycle power system because of its previous experience with the MPRE. Research was started where the SNAP-50 and MPRE program left off in the early 1970's in system optimization and material compatibility studies.[6,8)] The goals of the ORNL Rankine cycle team were: to increase specific power of the PCS, develop two-phase fluid management technologies, investigate liquid-metal freeze and thaw transients, and perform scaled experiments which emulate full-size liquid-metal Rankine cycles.

Rankine cycle development for Project Prometheus was partly completed with software developed by ORNL called ALKASYS-SPRS.[6,8,9)] ALKASYS-SPRS is a thermodynamic code which estimates the masses for the components needed to operate a

Rankine cycle in a reduced gravity environment.[16] ALKASYS-SPRS has been used to conduct trade studies which optimized system mass by varying several parameters such as: materials used in the secondary loop, number of feed heaters, number of turbine extractions, and condenser temperature. Specific studies have been conducted to analyze the effect that condenser temperature has on radiator mass with different radiator materials. This ALKASYS-SPRS study for a 100 kW(e) system determined that mercury and potassium fluid temperatures between 800 and 900 Kelvin in the condenser would yield the minimum radiator mass for the range of materials selected.[17]

ORNL also used ALKASYS-SPRS to study the effect that feed heating and reheating has on total system mass and efficiency. A study conducted on a 100 kW(e) system determined that three feed heaters and a reheat temperature of 160 Kelvin would increase cycle efficiency from 23.6% to 31.5% with a mass savings of 436 kg. Without reheat, the efficiency with three feed heaters only increased from 23.6% to 24.8% with a mass savings of 88 kg. From these results, ORNL concluded that Rankine cycle feed heating was not effective.[6] Feed heating did not significantly increase system efficiency and reduce system mass to make up for the penalty of adding the components and increasing system complexity.[6,8] Without feed heating and reheating components, ORNL proposed that a space Rankine cycle PCS take the form of the schematic presented in Fig. 11.

ALKASYS-SPRS utilizes phase separation at interstage and external locations for the turbine at assumed efficiencies which were modeled after terrestrial liquid-metal power plants.[16] The phase separation within ALKASYS-SPRS operates at efficiencies significantly lower than the potential MVS separation rates. The interstage separator is assumed to remove 25% of the moisture which passes through the device and also has an associated penalty by removing 0.25 pounds of vapor with every pound of moisture removed. The external separator is much larger than the interstage separator and is assumed to remove 90% of the moisture which passes through the device. There are two

associated penalties with the external separator in that it removed 0.1 pounds of vapor for every pound of moisture removed and the device has a 1.5 psi pressure drop. ORNL did not explore phase separation efficiency as a parameter for optimizing system mass. The MVS has the potential to greatly improve the PCS performance by offering significantly lower vapor pressure drop and improved phase separation rates and efficiences.[1,3)]

In order to manage the vapor which leaves the condenser in the Rankine cycle developed by ORNL for Project Prometheus, a rotary fluid management device (RFMD) is used to separate vapor from a two phase mixture.[6,8)] The RFMD was also added in later versions of ALKASYS-SPRS in order to account for its mass and efficiency.[18)] This device is designed by Sundstrand to provide the appropriate phase separation rates and net positive suction head to the boiler feed pump needed for plant operation. However, the RFMD is an active rotating machine which has a lot of mass, bearings, and seals which affect the long-term reliability of the device.[19,20)] The complicated turbo-machinery, bearings, and seals add to the difficulty of starting up and shutting down the RFMD in a liquid-metal system because transients normally result in the freezing and thawing of the working fluid within the device.

With the RFMD's internal complexity, freeze/thaw transients could lead to failures within device from un-thawed fragments of the working fluid which could damage internal components. Another major drawback of the RFMD is its large power consumption. Reduced gravity experiments provided separated liquid and vapor flows from a 24 g/s mixture at 150 watts-electric.[19)] Therefore it is estimated from preliminary reduced gravity testing to require 300 to 2000 watts of power to operate in the space Rankine cycle. A schematic of the RFMD can be seen in Fig. 12. This prototype RFMD was operated aboard reduced gravity aircraft over a narrow range of toluene vapor and liquid flow-rates.[20)] Because the mass of the device has not been published it is estimated using the dimensions provided by Bland et al.[19)] The prototype

RFMD has a 17.5 cm outer housing diameter and a 37.3 cm outer housing length. If it is assumed the material used for construction is stainless steel and 20% of the volume is the space available for the working fluid then the prototypic RFMD would have an estimated mass of 60 kg. Therefore it is estimated that the RFMD mass for a space Rankine cycle would be at least 100 to 200 kg to handle the increase in flow rate. No additional development or testing has been published or completed to characterize the capability of this device.

Space Rankine Cycle Components

The components to operate a potassium space Rankine cycle were designed by ORNL during the Prometheus program. Most research was performed in the two-phase heat transfer and management areas such as the boiler and the condenser. As it was reviewed earlier in Table 2, many turbines were tested with potassium as the working fluid for thousands of hours to understand how high temperature potassium interacts with components over time and to investigate turbine blade erosion.[7)] Most components were designed to be able to withstand the temperatures of a potassium system and were made of Niobium with 1% Zirconium (Nb-1%Zr). This section describes the components which were designed and tested for the 100 kW(e) space Rankine cycle by ORNL for the Prometheus program. The component descriptions are summarized as they are found in Yoder et al.[8)]

The potassium Rankine power system was optimized for both the 100 kW(e) and 250 kW(e) systems. The overall masses of these systems are approximately 3100 kg and 6300 kg respectively, each with two totally redundant power conversion units including the mass of the single reactor and shield. Conceptual designs for the components needed to operate a potassium Rankine cycle were developed in order to estimate component mass models for ALKASYS-SRPS. The components were designed to be compact so that the entire system could fit within a heavy launch vehicle.

A conceptual design for the boiler designed for the PCS can be seen in Fig. 13 and Fig. 14. The boiler is a once-through shell-and-tube design with single-phase lithium from the primary side of the system and potassium flowing on the shell side. The boiler was designed to produce approximately 100% quality fluid, however this design was never constructed and the outlet quality was never experimentally verified. Twisted tape inside the boiler tubes were used to provide sufficient swirl flow to increase the heat transfer coefficient by keeping liquid on the walls of the tube. Table 3 lists the typical boiler geometry and operating conditions.

The boiler feed pump consists of a single-stage, partial admission turbine coupled to a single-stage centrifugal pump which operates at 24,000 rpm. The turbine rotor diameter is approximately 11 cm, and the pump impeller diameter is approximately 2.7 cm for the 100 kW(e) system. For this system, the expected pump and turbine efficiencies are 47% and 27% respectively. The hydraulic power required for pumping 0.27 kg/s of potassium with a pressure rise of 840 kPa is approximately 320 watts. The turbine is expected to see 9 grams per second of potassium vapor directly from the boiler to provide the necessary pumped liquid potassium flow for a 100 kW(e) system. The expansion of this vapor through the turbine yields approximately 750 watts of shaft power which produces the necessary hydraulic power for pumping 0.27 kg/s of liquid potassium for the system. This turbo-pump size was chosen from a balance of turbine efficiency and turbo-pump rotational speed based on the power output of the system. The feed pump can be seen in Fig. 15.

A nine-stage, axial flow turbine is used in the ORNL design and uses a tilting pad bearing system which is lubricated with 750 K liquid potassium from the condenser. The turbine is shown in Fig. 16 The shaft power of the turbine is 127 kW at 60,000 . In order to reduce turbine blade erosion due to moisture droplets entrained in the vapor flow, the turbine was sized so that the tip speed was limited to 260 m/s and would

therefore be compact in design. This tip speed made the turbine rotor diameter 8.2 cm and the overall length 27 cm. For these turbine conditions, the efficiency of the device is approximately 74%. Moisture levels within the turbine expansion path are maintained by an external separator at the middle stage, and interstage separators are used between stages to maintain moisture at acceptable levels. The interstage separator can remove 25% of the moisture in the vapor flow but has an associated penalty of removing 113 grams of vapor with each 453 grams of liquid removed. The external separator has a much higher efficiency of 90% moisture removal and 45 grams of vapor removed with every 453 grams of liquid removed. However the external separator has a 10 kPa pressure drop associated with full power operation.

The homopolar inductor alternator was chosen for the potassium Rankine cycle because it is was determined to be the best candidate for high-temperature operation with liquid metal cooling with a rotor temperature limitation of 600 C. The alternator with dimensions can be seen in Fig. 17. The alternator has an efficiency of 86% to 90%. There has been no testing of homopolar inductor alternators for space applications but there have been configurations of the alternator which have been used in similar high temperature environments for military applications. The operating speed of the device is approximately 60,000 RPM because it shares its shaft with the turbine. The 25 cm long and 13 cm in diameter alternator is coupled directly to the turbine with low-conductivity coupling to eliminate external rotating seals and to thermally isolate the alternator from the hot vapor.

Rankine Cycle Experiments

Ground testing of components needed to operate a Rankine cycle power system for Project Prometheus was to be completed at ORNL. Calculations performed by ORNL using the thermal hydraulic code ATHENA investigated the boiler performance of the SNAP-50 and MPRE programs for the given geometry, mass flow rates, and heat flux.

The results of this study verified the ability of the boiler to produce a potassium vapor given the geometry of the original design. However, these calculations did not take into account the geometry of the twisted tape inserts, gravitationally dependent heat transfer, and fluid flow regimes.[21] Building upon the designs from the SNAP-50, SP-100 and MPRE programs, scaled experiments using surrogate working fluids were designed to emulate the boiler and condenser.[9,22] The ORNL boiler design used twisted-tape inserts similar to the designs in earlier space nuclear programs. The scaled twisted-tape boiling experiment can be seen in Fig. 18 and Fig. 19. Ground and flight testing in twisted tapes was planned to study boiling phenomena such as pressure drop, exit quality, and heat transfer, but the experiments were not completed because Project Prometheus was significantly scaled back in 2005 to accommodate changes in the NASA budget.

The ITP has been continually working on models for twisted-tape boiling since the beginning of Project Prometheus. Ground experiments at Texas A&M University similar to the ORNL design of Fig. 18 have been carried out using refrigerant fluids such as R11 and HFE-7000 (3M Corporation) to study the previously mentioned characteristics of twisted-tape boiling.[12] A schematic of the Texas A&M University experiment test loop can be seen in Fig. 20. Significant ground testing and research was completed with this 36 inch horizontal boiler configuration to study the boiling phenomena present in twisted tapes. High speed imagery was used to study flow-regimes and transitions. Bubbly, slug and annular flow regimes were observed during the experiments. In the annular flow regime, disturbance waves, which will cause liquid entrainment to increase the pressure drop, were observed. In all the experiments which have been performed, an all vapor flow was never attained at the boiler exit given the body length and flow rates.

Experiments have been planned to study the effect that pitch (length for 180 degree twist/inside tube diameter) and tube diameter has on twisted tape boiling in order to increase the outlet quality. Friction factors developed by Manglik and Bergles[23,24] were

used with the homogenous model and Lockhart-Martinelli correlations to calculate the two-phase pressure drop across a twisted tape boiler to within 30% of the experimental data. Fig. 21 shows the results from the experiment and the error in using conventional pressure drop models to predict the data. More extensive investigations in flow regime mapping and mass flux data are needed to appropriately model the pressure drop in twisted tape heat exchangers.[12,13)]

Other experiments also using R-113 as the working fluid has been carried out to predict and investigate the adiabatic and diabatic pressure drop in vertical straight tubes with twisted tape inserts at the University of Wisconsin.[25)] Different twisted tape pitches were used in this experiment and it was noted that pressure drop and exit quality increases with the twisted tape pitch. The diabatic testing performed on a 48 inch heated test section yielded a maximum exit quality of 78%. The program was very successful in predicting single phase and two phase pressure drop data from the experiment to within 17% for mass velocities greater than 475 kg/m^2s. The investigators did note that with better empty tube pressure drop predictions, the twisted tape predications at the lower mass velocities should be improved. Little reduced gravity testing of twisted-tape boiling with a reasonable body length has been completed. Ground testing at Texas A&M University and the results from the University of Wisconsin indicate exit quality from a twisted tape boiler may not be sufficient to avoid turbine blade erosion which suggests the need for phase separation at the boiler exit.

From these discussions it is proposed that the need exists for low power, passive, and reliable phase separation in a Rankine cycle power plant. The critical location for phase separation and inventory control is at the boiler exit where only vapor must be sent to the turbine to extend turbine lifetime. Other locations in the power plant have indicated that reliable phase separation would increase the efficiency of components such as the turbine and condenser. The RFMD was previously chosen to provide phase separation for the Rankine cycle, but its power requirement and complicated turbo-machinery make

it less desirable for space systems. The MVS has proven through reduced gravity experiments and ground studies to have high potential for use in a liquid-metal Rankine cycle PCS.

Techniques developed by the ITP to design a MVS for a particular system have been extensively tested with other programs which required microgravity two-phase separation.[26] Failure modes for the separator, such as carry under/over and vortex stability, have also been characterized and accommodated for in the design tools used by the ITP.[1,2,3,26] Many programs the ITP has participated in have indicated the potential of the MVS. In 1998, the MVS successfully separated flow rates of 2 to 9.8 LPM of water and 0.5 to 3.1 SLPM of air in a closed two-phase test loop for a multi-chamber bioreactor and a packed bed device. During the Immobilized Microbe Microgravity Waste-water Processing System program, the MVS provided a buffer volume for the accumulation of fluids over time and is considered to be an integral part of the system. The MVS also became part of the Proton Exchange Membrane fuel cell system in 2003. Testing for this system involved the use of a gas driven ejector with the injection nozzle of the separator. During microgravity operation, the separator was operated with gaseous Nitrogen flow rates up to 180 SLPM and at pressures of 413 kPa. Using the MVS as a direct contact heat exchanger is also being investigated for use as a dehumidifier. The initial results of this system acquired from microgravity testing are promising for providing cold cabin air, condensate removal, and water reclamation for gas flow rates up to 180 SLPM.

Knowledge of two-phase flow systems is a continuing obstacle for NASA and other research partners in order to increase the efficiency of power and thermal management systems. Single-phase systems for space vehicles have reached the point where their mass becomes too large for long-term missions. Two-phase systems, which carry more energy per unit mass, are a more attractive option for reducing component sizes. The ITP is developing two-phase technology for future space missions and continues to

operate experiments on the ground and in reduced gravity aircraft to understand the behavior and improve the models of these systems.

Thesis Organization

This document is broken into several sections which characterize the research completed with space Rankine cycle power systems in this thesis. Included in this document is: the history of space Rankine cycles, the current Rankine cycle research conducted by the ITP, the theory involved in the sizing of a MVS for a Rankine cycle, how the ALKASYS-SPRS program operates, the results of the experiments and calculations, discussion of the results, recommended further work and concluding remarks.

CHAPTER II

THEORY

A Rankine cycle is a two-phase power conversion cycle used in most terrestrial power plants because of their high thermal efficiency and their ability to transport more thermal energy per unit working fluid mass than single-phase plants. Because Rankine cycles are two-phase systems, phase separation is required a several plant locations to effectively operate the plant. Phase separation on the ground is principally dependent on the earth's gravitational acceleration field which separates liquid and vapor by the buoyancy force. Therefore in microgravity environments, two-phase systems are difficult to employ because the liquid and vapor do not naturally separate.

The ITP at Texas A&M University originally began work with microgravity phase separation during the SP-100 space reactor program as reviewed in the introductory chapter. The ITP developed the MVS to be a passive device which separates liquid and vapor by using the intrinsic momentum present in pumped fluid systems to produce a radial acceleration field. MVS operation is principally dependent upon the device's ability to generate an acceleration field in microgravity. This acceleration field produces the buoyancy force needed to separate dissimilar density fluids. Buoyancy is the net force acting on an object as a result of fluid pressure. The MVS principally acts on vapor bubbles which enter the separation volume by first traveling radially and axially through a liquid layer and then coalescing into the vapor column. Fluid pressure is developed in the liquid layer because of the acceleration field present in the MVS.[26)]

The following sections outline the fundamentals of the space Rankine cycle and MVS operation. The tools needed to size and design a MVS for a particular system are also discussed.

Reduced Gravity Rankine Cycles

Space Rankine cycles are similar to terrestrial indirect Rankine cycles in that thermal energy from a reactor is transported by the primary coolant to a heat exchanger in which the working fluid on the secondary side is vaporized in order to drive a turbine for electrical energy production. Once vapor is expanded through the turbine, it is condensed by rejecting thermal energy and pumped back to the boiler to complete the cycle. The main differences between space and terrestrial Rankine cycles are in the way thermal energy is rejected and how two-phase flow is handled. Fig. 22 shows a schematic of a typical Rankine cycle and the areas where phase separation is required to operate the system.

Terrestrial Rankine cycles can reject thermal energy by passing the working fluid through a heat exchanger where the energy is primarily removed by convective heat transfer by relatively cold air or water. The heat sink for the system is usually either a cooling tower or pond. In space, thermal energy can only be rejected by radiated heat transfer. Thermal energy in the condenser passes through a heat exchanger where it is conducted to heat pipes. These heat pipes reject the thermal energy via radiator panels. As indicated by Fig. 22, there are several regions of gravity induced phase separation in a terrestrial Rankine cycle. These areas are: the pressurizer, the heat exchanger which vaporizes the working fluid, and the condenser. Due to the lack of an acceleration field during space missions, these regions of two phase flow must be handled differently than on earth.

As was discussed in the introduction, space Rankine cycle designs utilized active rotary fluid management devices to separate liquid and vapor from a two-phase mixture. However this device has complicated turbo-machinery, glands and seals, and requires 500 to 2000 Watts to operate. It also has not been extensively tested in a microgravity environment. The MVS is a passive device that does not have turbo-machinery and has

been through extensive microgravity testing. Later in this chapter, phase separation using a MVS will be analyzed and discussed for managing the two-phase flows inherent with Rankine cycles.

Fig. 23 displays a temperature-entropy diagram for the secondary side of a Rankine cycle without superheat or reheat and the state-points 1 through 4 correspond to the locations in Fig. 22. Superheat is accomplished in a system by heating the working fluid into the superheated vapor region. Superheat allows the working fluid to enter the turbine at a higher quality thus minimizing turbine blade erosion. Reheat is a process where the working fluid is returned to a heat exchanger after partial expansion in the turbine. However, it was found in studies by ORNL that superheating and reheating the working fluid within the cycle adds complexity and mass to the system which cannot be justified with increase in system efficiency attained by the two optimizing components.[6)] Therefore, space Rankine cycles with superheat and reheat will not be discussed in this thesis.

The dotted lines in Fig. 23, 2s and 4s, represent isentropic compression in the feed pump and expansion in the turbine. The shaded area between the isobars represents the ideal work of the cycle. The actual work of the cycle is the net rate of work generated by the pump and the turbine which forms the relationship in Eq. (2.1). Eq. (2.2) includes the isentropic efficiencies of the pump and turbine from Eq. (2.1). For a pump the differences between the inlet and outlet enthalpy is negative, whereas a turbine has a positive difference between the inlet and outlet enthalpy. Therefore work is supplied to the pump and the turbine delivers the work from the system.

$$\dot{W}_{actual} = \dot{W}_T + \dot{W}_P = \left[\dot{m}\left(h_{in} - h_{out}\right)\right]_T + \left[\dot{m}\left(h_{in} - h_{out}\right)\right]_P \tag{2.1}$$

$$\dot{W}_{actual} = \left[\eta_T \dot{m}\left(h_{in} - h_{out,s}\right)\right]_T + \left[\frac{\dot{m}}{\eta_p}\left(h_{in} - h_{out,s}\right)\right]_P \tag{2.2}$$

If changes in the potential and kinetic energy of the working fluid are neglected, then the plant thermal to electric efficiency, ζ , is represented by Eq. (2.3). Plant thermal to electric efficiency is a ratio of the actual energy produced by the cycle to the amount of thermal energy produced by the reactor. The plant thermal efficiency, ζ_{th} can be reduced to Eq. (2.4) for the system displayed in Fig. 22 if the pump work on the primary side of the system is neglected.

$$\zeta = \frac{\dot{W}_t - \dot{W}_p}{\dot{Q}_{reactor}} \tag{2.3}$$

$$\zeta_{th} = \frac{h_3 - h_4 + h_1 - h_2}{h_3 - h_2} \tag{2.4}$$

Typical terrestrial indirect Rankine cycles have plant efficiencies up to 33% and higher by using superheat and reheat. The designed system efficiency for a 100 kW(e) Rankine cycle presented in Fig. 24 without superheat and reheat proposed by ORNL is 17%.[6)] The thermal efficiency of a Rankine cycle is improved with superheating and reheating the working fluid which reduces the amount of moisture in the vapor flow entering the turbine thus preventing liquid droplet erosion of turbine blades. However the complexity of adding superheating and reheating components for space Rankine cycles is not desired and other methods for reducing the excess moisture in the turbine have been explored such as external moisture separators and an interstage separator. The analysis performed in this thesis will include the performance change due to using a MVS to remove excess moisture from the turbine.

Fig. 24 also shows the three locations (red boxes) where two-phase flow in the Rankine cycle must be managed. The two-phases can be separated at these locations with the aid of the MVS. Sizing the MVS for each location is analyzed in this thesis. The dotted box around the RFMD represents the possible concerns and issues which surround the device.

Because of its high power and internal complexity, the RFMD should be replaced by a MVS.

AKASYS-SRPS Code

The ALKASYS code was originally developed at ORNL in 1987 and has been used extensively by Project Prometheus to perform sensitivity studies on how different components affect system mass. The code was originally written in BASIC and later converted to FORTRAN 77. The code outputs estimated masses for all the components needed to operate a liquid metal space nuclear power system including the reactor, shield, turbine, generator, piping, pumps, and radiator. The output also includes the pressures and temperatures at different thermodynamic points in the cycle.

Newer versions of the code, termed ALKASYS-SRPS, were developed in 2003 and 2004 so that the code would be fully modular with separate modules to calculate the PCS, the radiator, the reactor, and the shield masses. Fig. 25 details each of the modules used to calculate the masses of the system. The code was modified by ORNL to version ALKASYS-SRPS from ALKASYS to offer high fidelity mass calculations for 100 kW(e) systems instead of multi-megawatt.

The design and performance characteristics of the components sized by ALKASYS are determined by engineering sizing procedures from mass and performance data of existing hardware instead of empirical correlations. The cycle is solved in ALKASYS by determining the mass and energy balance around each component from an input deck defined by the user. Turbine moisture levels and radiator condensing temperature are the two largest factors for determining the final system mass. The code has a model with interstage and external separators like those of the turbine reviewed earlier in this thesis. The code is designed to maintain a moisture level less than 12% in the turbine. During the research performed for this thesis, ALKASYS-SRPS was modified to account for

varying efficiency of these separators. Investigations of the performance will be examined later in the results chapter of this thesis.

ALKASYS-SRPS has the RFMD mass model built into the code to provide a net positive suction head of 15 kPa to the boiler feed-pump by separating any excess vapor from the liquid stream and returning it to the condenser. The RFMD in ALKASYS-SRPS replaces the jet-pump needed to provide net positive suction head in the original code ALKASYS. The mass calculation is based on the pressure, temperature, flow rate and pressure rise of the two-phase potassium which enters the device. However the code does not account for the plant efficiency change by using the RFMD. The RFMD was projected to require between 300 and 2000 watts of electrical power. The MVS would be a more effective solution for this location because of its low power requirement, variable buffer volume, and simple design.

The code has the ability to change the inlet turbine quality, but without significant changes to the boiler and piping models a vortex phase separator would be difficult to add to the code at any of the two-phase separation locations in the cycle without significant software development. Therefore ALKASYS-SRPS is primarily used to examine turbine separation efficiency, determine the mass of the components, and to acquire the thermodynamic states the MVS would be operating under for different power levels. The code was also used to construct a saturated potassium thermodynamic property calculator for sizing the MVS at the different locations within the cycle. Both modified codes along with a sample input and output are listed in Appendix B.

Microgravity Vortex Separator

The MVS is a right circular cylinder in which fluid is injected tangentially at the curved wall of the device. This orientation causes the fluid to rotate in a circular path and reduce the presence of secondary flows within the device. Momentum is continuously

provided to the liquid layer by the injection nozzle thus creating centripetal force acting on the fluids in the separator.[26] In accordance with Newton's Third Law of Motion, the fluid reacts to the centripetal force and therefore produces a centrifugal force directed toward the z-axis of the separator. The centrifugal force provided by the radial acceleration fields provides the buoyancy needed to drive liquid to the wall of the MVS and drive vapor bubbles to coalesce with the vapor core along the z-axis. The geometry and normal operation of the device can be seen in Fig. 26.

Fig. 26 shows that the vortex forms along the axis of the cylinder and rotates upon the end face and baffle plate. The vortex diameter is dependent on the amount of liquid and vapor present within the device. System transients can be accommodated by the MVS because of the buffer volume available within the separation chamber as defined by the separator and baffle plate diameter. The separator can be sized to accommodate fluctuations in inlet quality and system flow rates. Separators used by the ITP have ranged from one-half to ten inches in diameter.

Separator performance is also dependent on the driving nozzle size. The nozzle size depends on the phase of the fluid passing through it which provides the necessary momentum for stable vortex formation. Because liquid has more density than vapor and can generally provide more momentum than vapor, the nozzles for mostly liquid flows are larger than mostly vapor flows. Investigation of nozzle geometry for particular systems have been experimentally performed by the ITP from ground and flight testing.[26] The nozzle size for a mostly liquid driven separator is determined from Eq. (2.5) which comes from experiments of tested separators of sizes 2, 4.5, 5.5 and 10 inches in diameter.

$$W_n = 0.00288 D_{sep}$$
$$H_n = 0.0888 D_{sep} \qquad (2.5)$$

Several investigations to understand phase separator performance have been performed by the ITP.[26,28] Computational fluid dynamics (CFD) was used to investigate the liquid velocities at all radial and axial locations within the separation volume.[26] These CFD calculations optimized nozzle design to balance nozzle velocity with pressure drop. Experiments relating separator and nozzle size to the liquid rotational speed have been completed so that the separator's performance can be predicted. Eq. (2.6) relates the rotational speed (ω) from the separator's radius, R_{sep}, nozzle characteristic length, L_n, liquid velocity at the nozzle, V_n, and the fluid properties within the device. The nozzle characteristic length is the square root of the nozzle area. This equation is useful for sizing a separator to a system because the minimum flow rate needed for separator operation and the buffer volume for system transients can be predicted.

$$\omega = \frac{0.394 L_n V_n - 2020.0 \dfrac{\mu_l}{\rho_l}}{R_{sep}^2} \tag{2.6}$$

Vortex stability and failure within the separator are mainly governed by two events: flooding and dryout. These two events are also known as 'Carry-over' and 'Carry-under' respectively. Flooding occurs within the separator when there is liquid in the gas outlet or if an unstable vortex is formed. Dryout occurs when there is gas in the liquid outlet. Flooding tends to take place when the capillary forces overcome the inertial forces and a collimated vortex cannot be formed. This is usually the result of low tangential velocity in the liquid layer. Fig. 27 represents the various forms of flooding in the MVS.

Fig. 28 represents the forces related to the dryout condition for the MVS. Dryout occurs when the injected fluids axial transit time is less than the radial transit time of the vapor bubbles. The vapor transit time is a function of the tangential velocity in the liquid layer. The radial bubble velocity is a function of the buoyancy and drag forces acting on the

bubble. Axial bubble velocity is equal to the liquid axial velocity and is a function of the gas column diameter, liquid inlet and outlet flow rates of the MVS.

Separator performance is dictated by the ability of the device to maintain a cylindrical liquid/gas vortex shown in Fig. 26. Formation of a vortex within the MVS is dependent on the force balance acting on the liquid/gas interface. Under microgravity conditions, the forces which dictate stable vortex formation are the inertial and capillary forces. Using dimensionless parameters, a relationship can be developed which describes the ratio of inertial to surface tension forces which act on the fluid. The Bond number (Bo) shown in Eq. (2.7) is the ratio of the acceleration force to the surface tension force. The Froude number (Fr) shown in Eq. (2.8) is the ratio of inertial force to acceleration force.

$$Bo = \frac{\text{acceleration force}}{\text{surface tension force}} = \frac{\left(\rho_l - \rho_g\right) R_I^2 g}{\sigma} \tag{2.7}$$

$$Fr = \frac{\text{intertial force}}{\text{acceleration force}} = \frac{V^2}{gD_I} \tag{2.8}$$

For cylindrical rotation, Eq. (2.8) is modified to account for circular motion by the relationship shown in Eq. (2.9). With a combination of the Bond number (Bo) and the Froude (Fr) number, the rotational Weber number (We) can be derived which is a function of the liquid rotational speed, gas core diameter (D_I), liquid/vapor densities, and surface tension. This shown is displayed in Eq. (2.10).

$$V = \omega R_I \tag{2.9}$$

$$\begin{aligned} We &= Bo \bullet Fr = \frac{g(\rho_l - \rho_g) D_I^2}{4\sigma} \frac{\omega^2 D_I}{4g} \\ We &= \frac{\omega^2 D_I^3 (\rho_l - \rho_g)}{16\sigma} \end{aligned} \tag{2.10}$$

Unlike cyclonic separators which produce thousands of g's at the wall of the separation volume, the separator developed by the ITP normally maintains a one g acceleration field under microgravity conditions. The small acceleration field allows the device to be operated with very little power, low pressure, and be mechanically simple. However, such a small acceleration field will not produce a stable liquid/gas vortex under earth's gravitational field. Therefore the MVS must be reduced gravity tested in order to verify the separator's vortex stability and separation efficiency under the conditions it would operate in two-phase space systems.

Through reduced gravity testing of the MVS, the ITP has determined that a Weber number of 100 is more than sufficient to produce a stable vortex. Fig. 29 represents a stability plot of the two inch and four and a half inch diameter MVS. The vortex diameter divided by the separator diameter is plotted against the separator RPM. The Weber number lines represent a balance of the capillary force and the dynamic hydrostatic force of the liquid/gas interface. The solid diamonds represent stable cylindrical vortex formations. Most of the stable vortices are above the Weber number line of 100.

Estimating the mass of the separator is dependent on the operating pressure of the device and also mechanical constraints for attaching fittings to all the ports. For this analysis the following sizes will be used: the baffle plate thickness is assumed to be 0.1 inches, the baffle region height (the distance between the bottom of the baffle plate and the liquid outlet) is 0.5 inches, and the baffle plate gap (the distance between the separator wall and the baffle plate) is 0.25 inches. Any material needed to strengthen nozzle locations on the wall of the separator will be neglected. Because the separator geometry is basically a pressure vessel, the maximum stress in the device will occur at the end plates.[29] The thickness of the end plates can be calculated by Eq. (2.11) where σ_{plate} is the end plate stress, p is the pressure in psi, R_{sep} is the radius of the separator, t_{plate} is the end plate thickness, and k is a factor to compensate for the geometry of the plate. For a

uniformly loaded circular plate pinned at its edges, 'k' has a value of 0.75. Using a safety factor of 2.5, the thickness of the end plates can be calculated by Eq. (2.12) with a given yield stress of the material used. The minimum end plate thickness to account for the vapor and liquid outlet fittings is assumed to be 0.1 inches.

$$\sigma_{plate} = k\frac{pR_{sep}^2}{t_{plate}^2} \tag{2.11}$$

$$t_{plate} = \sqrt{\frac{2.5kpR_{sep}^2}{\sigma_{yield}}} \tag{2.12}$$

Separator wall thickness can be estimated with the thin walled cylindrical pressure vessel assumption. Eq. (2.13) gives the hoop stress for a cylindrical pressure vessel of radius r, pressure p, and thickness t_{wall}. If a safety factor of 2.5 is used to calculate the wall thickness, then Eq. (2.14) yields the thickness of the separator wall. The minimum wall thickness for the design is assumed to be 0.1 inches. Table 4 gives the yield stresses of the different materials which would be used in high temperature liquid metal systems. It is good engineering practice to build the separator from the same material as the PCS so that material compatibility thermal strain is minimized among components.

$$\sigma_h = \frac{pR_{sep}}{t_{wall}} \tag{2.13}$$

$$t_{wall} = \frac{2.5pR_{sep}}{\sigma_{yield}} \tag{2.14}$$

Designing a control system for a phase separator in a liquid metal system could be difficult because of the extreme fluid temperatures present on the boiler side of the PCS. A key operating parameter defining the performance of the separator met is the minimum and maximum inventory. Therefore to assure the hydrodynamic limits of the separator have been met, an inventory monitoring system is needed. The primary liquid

inventory monitoring mechanism developed by Texas A&M University and implemented in the NASA "Immobilized Microbe Microgravity Wastewater Processing System" is ultrasonic depth thickness. An ultrasonic transducer can be placed in direct contact with the wall of the separator and measure the thickness of the liquid film on the wall of the separator by knowing the speed of sound through the materials present. This transducer provides instrumentation for the thickness of the liquid layer. However the extreme temperatures make an acoustic system is difficult to implement. Electronics of an acoustic transducer placed on the wall of a separator at 1300K would destroy the gauge. An alternative would be to acoustically couple a standard transducer to the separator wall while thermally isolating it from the extreme temperatures of a separator filled with liquid metal. This can be done using an acoustic finger. A finger is a piece of material or a series of pieces of material that is capable of withstanding the high temperatures and is acoustically coupled to both the transducer and the separator wall. Experience with performing thickness measurements on a dynamic surface such as the gas/liquid interface inside the separator in conjunction with an acoustic finger has proven possible but flight testing is required to calibrate the acoustic gauge.

A third option for inventory control is gamma densitometry. This is a method of thickness measurement that takes advantage of the gamma ray attenuation properties of a material. Because gamma rays are readily available from nuclear fission, the radiation can be used from the reactor to determine the thickness of the liquid layer within the separator. By knowing the materials involved, initial intensity of the gamma rays, and the exiting intensity of the gamma ray, one can determine the amount of material that the gamma rays passed through.

The proposed locations for the MVS in the potassium Rankine cycle designed by ORNL are shown in Fig. 30. Wet vapor exiting the boiler will be sent to a MVS operating at the boiler saturation temperature and pressure. The boiler exit separator will deliver 100% quality vapor to the turbine and return any excess moisture to the boiler feed-pump. An

external separator between turbine stages 8 and 9 will remove any moisture which evolves in the vapor stream from a reduction in temperature and pressure. Excess moisture will also be returned to the boiler feed-pump. The condensing separator will act as the thermal energy rejection system in conjunction with radiator panels. The process by which vapor will condense within the separator will be discussed in the next chapter. The condensing separator will remove any vapor present in the liquid return line to the boiler and also provide the necessary net positive suction head required to operate the boiler feed-pump. A detailed flow loop will be presented later in this thesis for each separator location detail the integration of vortex separation with liquid metal Rankine cycles.

High Vapor Flow Separator Model

A conventional TAMU MVS operates in systems in which vapor must be removed from a two-phase mixture such that the incoming vapor flow rate has little effect on the operation of the separator. Such effects include: displacing the liquid layer by the vapor hold up within the layer, separator rotational stability due to large vapor hold up volumes, and adding rotational momentum from incoming vapor flow. However, in the Rankine cycle PCS designed by ORNL for project Prometheus, a vapor flow rate of approximately 5000 LPM must be attained to drive the turbine at 100 kW(e). Due to the large vapor volumetric flow rate which would be encountered at the boiler exit in the cycle, the TAMU MVS must be properly sized to effectively send vapor to the boiler to share the compact design of the components in the cycle which were previously described.

The TAMU MVS normally operates in a separation mode similar to that of Fig. 31. Vapor enters the separation volume and quickly attains the rotating liquid velocity within the device. The buoyancy force present within the separator drives the vapor bubbles radially towards the vapor core. Incoming vapor bubbles displace the liquid

layer, but under small volumetric flow rates this effect is negligible. When the incoming vapor volumetric flow rate becomes high enough to displace the liquid and shift the liquid-vapor interface radially inward, separator stability changes and the acceleration within the device is not large enough to effectively separate the two phases as shown in Fig. 32.

In order to effectively operate, liquid must be withdrawn from the separation volume as the incoming vapor flow rate increases. The rotational speed of the device must also increase so the radial transit time of the incoming vapor is reduced therefore reducing the vapor hold up volume within the liquid layer. The radial transit time of the vapor is the time in which a vapor bubble enters the separation volume to its coalescence with the vapor core. To successfully separate the two-phases with high vapor volumetric flow rates, it is predicted that the separator performance is best when there is the least amount of liquid volume and the largest vapor core diameter within the device. A separator running in this configuration is displayed in Fig. 33. It is assumed that the liquid layer in Fig. 33 transforms in to a two-phase layer because of the large vapor hold up within the device. The interface between the vapor core and the liquid phase would be effectively replaced by a two-phase mixture of vapor and liquid. It is assumed that the separator can drive the two-phase layer like the liquid layer presented in Fig. 31 for this analysis and that no momentum is gained in the two-phase layer by the incoming vapor flow.

With the development of a new separator model such as Fig. 33, a relationship between separator variables must be derived to determine the separation performance of the system. The results from this model will indicate the operating envelope for various vapor flow rates for each separator size. Rankine cycle system performance with vortex phase separation is mainly affected by the mass of the separator and the liquid volumetric flow rate needed to drive the separator which would determine the pumping power needed for effective separation of the phases.

The MVS is a right circular cylinder and the separation chamber volume of the device, $\forall_{sep}$, is given by Eq. (2.15). The vapor core volume, $\forall_V$, is given by Eq. (2.16) where the vapor core diameter is D_I. The liquid volume within the device, $\forall_L$, is determined from a zero vapor flow rate mode and is given by the expression in Eq. (2.17) which is simply the subtraction of the vapor core volume from the separator volume. The vapor hold-up volume, $\forall_{VH}$, is given by Eq. (2.18) where t_r and $\dot{\forall}_V$ are the radial transit time of the incoming vapor and the vapor flow rate respectively. Once a large vapor flow enters the separation volume, Eq. (2.17) is no longer valid to determine the liquid volume within the device because the liquid layer becomes a mixture of liquid and vapor. An equation must be derived which will be used to generalize the volume of the liquid within the device for any sized separator or vapor flow rate.

$$\forall_{sep} = \frac{\pi}{4} D_{sep}^3 \tag{2.15}$$

$$\forall_V = \frac{\pi}{4} D_{sep} \left(D_I^2 \right) \tag{2.16}$$

$$\forall_L = \frac{\pi}{4} D_{sep} \left(D_{sep}^2 - D_I^2 \right) \tag{2.17}$$

$$\forall_{VH} = \dot{\forall}_V t_r \tag{2.18}$$

The separator liquid volume can be rewritten as a function of the liquid layer thickness without vapor flow and can be seen in Eq. (2.19) where the liquid layer thickness is denoted by T_L. If the final vapor core diameter with vapor flow into the separation volume and original liquid volume within the device were some fraction, X, of the separator diameter, then Eq. (2.15) and (2.16) could be combined to form Eq. (2.20) which is termed the two-phase layer volume, $\forall_{2\varphi}$.

$$\forall_L = \frac{\pi}{4} D_{sep} \left(D_{sep}^2 - \left(D_{sep} - 2T_L \right)^2 \right) \tag{2.19}$$

$$\forall_{2\varphi} = \frac{\pi}{4} D_{sep}^3 \left(1 - X^2 \right) \tag{2.20}$$

An equation can now be derived to describe the available volume within the separator for vapor held up in the two-phase layer. If the volume available for the vapor held up in the two-phase layer is $\forall_{2\varphi}$, and the initial liquid volume in the separator without vapor flow is $\forall_L$, then the difference between these volumes will equal the vapor hold up volume, $\forall_{VH}$. This relationship can be seen in Eq. (2.21).

$$\begin{aligned} \forall_{VH} &= \forall_{2\varphi} - \forall_L \\ \dot{\forall}_V t_r &= \frac{\pi}{4} D_{sep} \left(D_{sep}^2 \left(1 - X^2 \right) - D_{sep}^2 + \left(D_{sep} - 2T_L \right)^2 \right) \end{aligned} \tag{2.21}$$

However, the two-phase volume is principally a function of the incoming vapor flow rate, the separator drive nozzle flow rate, and the vapor core diameter. Therefore Eq. (2.21) is a transcendental equation and must be solved iteratively. Eq. (2.21) is rearranged to find the radial transit time required to effectively separate the vapor phase from an incoming two-phase flow by dividing by the incoming vapor volumetric flow rate. Using a similar iteration process to determine bubble transit time as described in Ellis,[26] a code was written to determine the radial transit time of a MVS with several separator diameters, D_{sep}, and a vapor core diameters, D_I, with the vapor flow rate needed to drive a 100 kW(e) turbine. The geometry within the code was structured so that the inequality in Eq. (2.22) is always satisfied.

$$\forall_{2\varphi} > \forall_L \quad or \quad \forall_{VH} > 0 \tag{2.22}$$

This program calculates the transit time and path taken by a bubble traversing the phase separator operating volume (cylinder volume). In the tangential direction, the bubbles

are assumed to move at the same speed as the liquid flow. In the radial direction, bubble velocity is assumed to result from the balance between buoyancy force and drag force. It is important to note that since this is a microgravity separator, the buoyancy force results from the centripetal acceleration imparted to the fluid as it moves around the cylinder. A minimal bubble radius of 0.1 cm is assumed for the code. It is also assumed that there is no physical interaction between vapor bubbles present in the two-phase layer when determining the radial transit time. The program utilizes correlations attained from rotational speed ground tests to relate the rotational speed to an incoming liquid momentum rates. The nozzle size for each separator is determined from Eq. (2.5) because this system is driven by a liquid injection nozzle.

Once a calculated radial transit time, t_{iter}, is determined for a specific separator diameter, vapor core diameter and drive flow rate, the inequality in Eq. (2.23) must be satisfied in order to solve Eq. (2.21) with 1% error. If it is not satisfied, the drive flow rate to the separator is increased until Eq. (2.21) is satisfied.

$$\frac{\left|\mathrm{t_r} - t_{iter}\right|}{t_r} \leq 0.01 \tag{2.23}$$

The program also calculates several other parameters which help dictate the size of the separator needed to effectively provide the vapor flow rate required for a 100 kW(e) turbine. These parameters include: the Weber number of the separator as described in the previous section, the liquid pressure drop of the separator and the estimated pumping power needed to operate the separator. The separator could be driven by an electromagnetic (EM) or a mechanical pump. EM pumps have a lot more mass and are less efficient than mechanical pumps. However mechanical pumps have seals in them which separate the motor from the impeller and would not react well with liquid metal systems. There has been a lot of research performed in liquid metal mechanical pumping systems but these studies have yet to produce mass and power correlations which could be used for this thesis.[30,31)]

However using an EM pump for boiler exit separator may not be the most efficient method for driving the separator given that EM pumps typically have efficiencies less than 10%. Another feed pump turbine similar to the one which delivers working fluid to the boiler could be used to drive the separator but this system could lead to operational stability issues since the pump would be directly coupled with the vapor delivered by the separator. More mass flow through the boiler and separator would also be required to drive this feed pump turbine. This thesis will investigate the use of an EM and mechanical pump for driving the separator assuming that there are no materials issues with mechanical pump seals or bearings.

The pumping power and pump mass correlations are computed by using correlations presented in the ALKASYS-SRPS code manual for an alkaline metal electromagnetic (EM) pump.[16] The estimated pumping power for the EM pump is a function of the mass flow rate, pressure rise of the fluid and the density of the fluid which is given by Eq. (2.24). The EM pump efficiency is given by Eq. (2.25). The units of these two equations are: the differential pressure developed by the pump, ΔP, in psi, the liquid potassium flow rate, $\dot{m}$, in kg/s, and the liquid density, ρ_l, in lb/ft^3. The mass of the EM pump in kilograms can also be related by the correlation presented in Eq. (2.26). The theoretical mechanical pump power will be related by Eq. (2.27). The mass and efficiency of the pump will be estimated by similar pumps used in liquid metal tests by the Navy.[30]

$$P_{EMP} = \frac{(\Delta P)^{1.317/\dot{m}}}{0.115\rho_l} \tag{2.24}$$

$$\eta_{EMP} = 0.0495(\dot{m}\Delta P)^{0.2405} \tag{2.25}$$

$$m_{EMP} = 5.72(\dot{m}\Delta P)^{0.66} \tag{2.26}$$

$$P_{mech} = \frac{\Delta P \dot{m}}{\rho_l \eta_{mech}} \tag{2.27}$$

To estimate the pumping power required to operate the separator, the total pressure drop of the separator must be determined. The separator pressure drop is assumed to occur primarily in the nozzle and from the form loss associated with the area change from the nozzle to the separation chamber. Because the nozzle converts pressure head into velocity, the pressure drop of the nozzle is given by Eq. (2.28). The pipe velocity, V_{pipe}, is the velocity of the fluid prior to entering the nozzle. It is assumed that the pipe size is 1 inch ID because this size matches the piping system proposed by the ORNL PCS design. The form loss within the separator is given by Eq. (2.29). The coefficient of expansion is a loss coefficient based on the area ratio between the nozzle and the separation chamber. The coefficient, β, is calculated to be 0.8 as given by Fox and McDonald.[32)]

$$\Delta p_{vel} = \frac{\rho\left(V_n^2 - V_{pipe}^2\right)}{2} \tag{2.28}$$

$$\Delta p_{form} = \frac{\beta \rho_l V_{nozzle}^2}{2} \tag{2.29}$$

There are other pressure drop mechanisms associated with a saturated phase separator system such as: the frictional losses on the separator walls, the pressure drop associated with the eductor, form losses from valves and pipe diameter changes, and frictional pressure drop around the system. However this analysis does not take these into account because of the complexity of adding these mechanisms while the focus of this thesis is to size the phase separator based on the vapor separation rate needed to drive a turbine at a specific power level. The code developed for the high vapor flow separator model is listed in Appendix B.

CHAPTER III

EXPERIMENTAL PROCEDURE

Experiments were performed on the NASA C-9 reduced gravity aircraft and on the ground which included the MVS operating at saturated conditions. The goal was to demonstrate the MVS's ability to operate in a saturated state as it would in the Rankine cycle. The following sections discuss the experiments in detail and provide the test matrix from the flights.

Flight and Ground Testing

The performance of a saturated MVS had not been characterized in previous phase separator ground or flight experiments. Prior experiments with the MVS used nitrogen and water as the working fluids to determine the operating envelope for proper vortex formation in a sub-cooled state.[1,2,26,28)] Saturated systems are difficult to pump because any pressure drop will cause liquid flashing to occur. Liquid flashing will lead to pump failures because the 'dryout' condition which exists at the pump inlet will not provide net positive suction head (NPSH) for the pump to properly operate. Pumped two-phase saturated systems, such as a boiling water reactor pressure vessel seen in Fig. 34, utilize jet pumps to pump saturated liquid. Recirculation flow provides sub-cooled liquid at the jet pump inlet which will raise the pressure of the saturated liquid prior to entering the pump.

In order to operate a saturated MVS system, a liquid eductor, which is similar to a jet pump, is used in the system to provide the necessary NPSH to pump the working fluid. A test bed was designed and fabricated by the ITP group which utilizes the MVS to simulate an element of the secondary side of a Rankine cycle. The goal of the

experiment was to demonstrate the ability of the MVS to operate in a saturated state as it would in the Rankine cycle boiler exit and condenser locations. A detailed drawing of the liquid eductor used in the experiment can be seen in Fig. 35. The recirculation flow to the pressure connection of the eductor raises the pressure of the incoming liquid to prevent liquid flashing at the pump inlet. The suction flow is the saturated fluid exiting the MVS. The performance of the eductor is principally dependent on its geometry. Although this thesis concentrates on integrating MVS technology with space Rankine cycles, eductor performance and design is being further investigated by the ITP to characterize saturated two-phase systems.[33)]

The experiment loop schematic can be seen in Fig. 36. The MVS used in the experiment loop has a diameter of 5.5 inches and a maximum liquid volume of 2.1 liters. The nozzle exit geometry is 0.0159 inches wide and 0.489 inches tall. A single gear pump provided the necessary flow rate and pressure rise to operate the system. The pump suction removes liquid from the separator and into a liquid eductor where the pressure of the fluid is raised in the eductor to prevent pump cavitations. This fluid then passes through the pump where it is delivered to four different lines at different flow rates by using metering valves. These lines are the recirculation flow to the liquid eductor, the separator drive line, the spray condenser line and the two-phase line. The two most important lines in the system are the separator drive line and the liquid eductor recirculation line.

The separator drive line provides the inlet momentum needed to generate a liquid vortex within the MVS. The recirculation line provides the necessary pressure rise of the fluid through the liquid eductor to prevent pump cavitations. In order to directly condense vapor within the separator a spray line near the gas outlet sends sub-cooled fluid into the separator. The fluid sub-cools from a saturated state by using an ice chest heat exchanger. The condenser spray line is used to reduce separator pressure by reducing the amount of vapor within the separation volume.

Separator pressure can be increased by increasing the amount of vapor within the separation volume. Saturated liquid which passes through the two-phase line is changed to a two-phase mixture by adding thermal energy to the fluid from heating tapes. The two-phase line delivers liquid and vapor to the MVS to be separated. The amount of vapor provided by the two-phase line was measured by a Creare void fraction sensor. This sensor and the Lockhart-Martinelli correlation allows the flowing quality delivered to the separator to be calculated. Ground testing was performed to verify the integrity of the system and to collect 1-g data. However, the size of the separator does not allow a vortex to form in a 1-g environment so the experiment relied on the reduced gravity conditions provided by the NASA C-9 aircraft.

The working fluid of this system is HFE-7000 which is a low toxicity fluorocarbon manufactured by 3M Corporation. This fluid was chosen because it is relatively benign and has a low boiling temperature for use on the NASA C-9 reduced gravity aircraft. HFE-7000 has a much larger liquid and vapor density difference than saturated liquid metal systems. The HFE-7000 density difference from the flight conditions is around 1400 kg/m^3 while liquid metals such as potassium, lithium, and sodium have density differences between 800 and 400 kg/m^3. As indicated by Eq. (2.10), the difference in density between the liquid and gas phases affects the vortex stability criterion. Due to the complexity of acquiring RPM data from the separator, a stability analysis cannot be conducted from this flight because the experiment lacked the instrumentation needed to acquire the data. The flight experiment did not concentrate on collecting RPM data because the purpose of the test was to operate a MVS at saturated conditions while controlling separator pressure.

Vortex stability was visually noted on every parabola. However, the ITP has determined that vortex stability can be attained under normal operating conditions for any working fluid as long as the Weber number is at least 100. Fig. 37 displays the normalized gas core diameter versus separator diameter of different working fluids at a Weber number of 100. Using HFE-7000 as the working fluid allows a liquid vortex to

form at much lower rotational speeds. These calculations show that stability tests with HFE-7000 are actually more liberal in terms for vortex formation than air/water and liquid metal system. Fig. 37 shows that liquid metal systems will behave in a similar manner to air/water systems for which the stability criterion was established.

Even though the stability analysis of this flight can only be performed visually, the air/water data which has been collected on previous flights allows the ITP to create separator design models for liquid metal systems which have similar thermophysical properties.

Flight Test Matrix

The simulated Rankine cycle test bed was flown aboard NASA's reduced gravity aircraft in June 2006. Pressure within the separator was controlled by managing liquid and vapor inventories within the device. The condensing and evaporating lines send sub-cooled and saturated two-phase fluid to the separator to control the amount of liquid in the buffer volume. The condensing line injected sub-cooled fluid into the vortex by a spray nozzle to directly condense vapor within the separator and vapor was added to the separator through the two-phase line. Thermal energy was added to the two-phase line by a heater tape and energy was removed in the condensing line by the ice chest heat exchanger.

The separator was operated at a range of flow rates through the drive, two-phase and condensing lines. The eductor and separator flow rates were adjusted during flight in order to determine the operating envelope needed for stable vortex formation. The sight glasses shown in Fig. 36 were used to visually indicate the quality of the working fluid entering the eductor and pump in order to prevent pump cavitations. A complete test matrix of the flight operating states can be found in Appendix A. Table 5 gives a summary of the operating states seen in each flight.

Fig. 38 shows a picture of the separator operating during a microgravity period aboard the NASA C-9. A stable vortex and the liquid/vapor interface can be seen in the photograph. The liquid eductor location is also noted in Fig. 38.

CHAPTER IV

RESULTS AND CALCULATIONS

The results from the data acquired during the saturated separator flight, the calculations from ALKASYS-SRPS, and the separator sizing models at the locations in the Rankine cycle are presented in this chapter. Each model is separated into sections in the order of: the saturated separator experiment, boiler exit separator, condenser separator, turbine separator, and an overall system schematic.

Saturated Separator Flight Results

The vortex phase separator was successfully operated in a saturated state by utilizing the eductor and by maintaining liquid and vapor inventories. The data acquired from the flight was used to create an energy balance model for separator operation. The separator was run in three main modes: steady-state, net energy in, and net energy out. The steady-state energy balance, Eq. (4.1), was achieved in flight by holding the pressure in the separator at a given level by adjusting the mass flow through the two-phase and condenser lines. From the flight data it was determined that thermal energy from the pump was balanced by the ambient losses from cabin air convection. Fig. 39 represents a schematic flow loop used for the energy balance calculations. The components which are colored red add thermal energy to the system and the components in blue remove thermal energy from the system. Air convection also removes thermal energy but it not shown in Fig. 39.

$$\dot{Q}_{pump} + \dot{Q}_{2\varphi} - \dot{Q}_{spray\,condenser} - \dot{Q}_{ambient\,loss} = \dot{Q}_{gain} \tag{4.1}$$

The energy input by the two-phase line was determined by Eq. (4.2). It is assumed that the quality, x, can be calculated using the Lockhart-Martinelli correlation, (Eq. 4.3)

which relates void fraction to flowing quality by the physical properties of the fluid. Lockhart-Martinelli is used in the calculations because it has been demonstrated to be reasonably accurate for two-phase flow experiments flown aboard reduced gravity aircraft.[34] Sensible heat transfer was calculated by Eq. (4.4) which determines the amount of thermal energy removed by the condensing line.

$$\dot{Q} = \dot{m} x h_{fg} \tag{4.2}$$

$$\alpha = \left[1 + 0.28 \left(\frac{1-x}{x} \right)^{0.64} \left(\frac{\rho_g}{\rho_l} \right)^{0.36} \left(\frac{\mu_l}{\mu_g} \right)^{0.07} \right]^{-1} \tag{4.3}$$

$$\dot{Q} = \dot{m} \left(h_{out} - h_{in} \right) \tag{4.4}$$

For several parabolas, the separator was operated at steady-state where the energy input from the two-phase line is balanced with the energy removed by the condensing line. Fig. 40 is a plot representing the energy balance of the steady-state parabolas. Because it was determined that the calculated quality in the two-phase line has a large effect on the amount of energy added to the separator, the energy balance was relaxed to eight watts to account for the error inherent in the Lockhart-Martinelli correlation.

During a five parabola period, the two-phase line was turned off and the condensing line was adjusted to decrease separator pressure. Separator pressure was reduced by condensing vapor within the separator. Fig. 41 displays a pressure trace of the vortex phase separator during this time period with an overlay of the plane's vertical acceleration. The pressure of the separator was reduced by 0.5 PSI over a 300 second period with an average condensing line flow rate of 3 grams per second. This flow rate equates to an average thermal energy removal rate of 50 watts from the separator. As indicated by Fig. 41, the condensing transient has no visible dependence on the plane's acceleration.

Fig. 42 displays the separator pressure and temperature during the energy removal period when compared to the saturated temperature and pressure. As indicated by Fig. 42, there is a four psi offset between the flight data and the saturation curve. This offset suggests the presence of non-condensable vapor within the separator because the slope between these two curves is approximately the same. Future experiments will need to concentrate on removing this non-condensable gas from the system to get more accurate results during a pressure and temperature trace.

The opposite experiment was performed over a four parabola period where the two-phase line was used to increase separator pressure by increasing the amount of vapor within the device. The average mass flow through the two-phase line was 18 grams per second. This mass flow rate equates to an average thermal power input to the separator of 60 watts. Fig. 43 displays the pressure trace of the separator during the energy addition period and again shows the transient is independent of the plane's vertical acceleration. Fig. 43 shows that the pressure during this transient increased by approximately 0.9 PSI.

Figure 44 shows the separator pressure and temperature during the energy addition transient to the separator. Figure 44 also shows the pressure offset between the flight data and the saturation curve due to the non condensable gases present in the separator. This offset is similarly around four PSI.

From Fig. 41 and Fig. 43, the microgravity time between the 1.8 g periods and the transition between these accelerations on the plane are not clear because the timescale at which the plot is presented. The typical transition times for this experiment between the 1.8g and microgravity periods are approximately five seconds. The microgravity periods are between 15 and 20 seconds. Two-phase experiments which operate aboard the aircraft must be designed so the transition period and the limited time in microgravity do not significantly affect the performance of the system. The MVS in this

simulated Rankine loop operates with wall velocities on the order of 1 to 13 meters per second.[26] These wall velocities allow the separator to transition from a 1.8 g stratified state to a microgravity liquid/vapor vortex condition almost instantaneously so the separator can operate normally during the full length of the microgravity period.

The transition and microgravity time in the aircraft does not significantly affect single phase lines in the system. However, flow regimes of two-phase lines have been demonstrated to be gravity dependent.[35] The transit time of the fluid through the two-phase line, which was about one meter in length, is important to note when investigating acceleration effects on flow regime. Two-phase velocities were calculated using the instrumentation from the flight and the Lockhart-Martinelli correlation (Eq. 4.3). Two-phase flow regimes in the experiment would not reach steady-state conditions if the fluid transit time through the line is significant when compared to the microgravity time period. The lowest velocity calculated for the two-phase line through out the experiment was a liquid velocity of 0.22 meters per second. With a meter long two-phase section, this velocity corresponds to a transit time of 4.5 seconds. Because each microgravity period is at least 15 seconds long, it is assumed that a steady-state flow regime in the two-phase line is attained for all the parabolas. However, it is recognized that the transition periods will affect the flow regimes in the pressure increase transient presented in Fig. 41 and Fig. 43 because the data is presented over the entire time period. Because the flow rates through the two-phase line are small, the changes in flow regime will only marginally affect the overall pressure transient of the separator.

Boiler Exit Separator

The main advantage of the liquid metal space Rankine cycle is the power to weight ratio of the system when compared to other power conversion systems. Table 6 displays the minimum masses of the 100 kW(e) Rankine cycle ALKASYS-SRPS output for the major components needed to operate the cycle. A primary factor when integrating a

MVS with the Rankine cycle is minimizing separator mass. The high temperatures which are present at the boiler exit in liquid metal Rankine cycles require using materials which are temperature tolerant such as the niobium and tantalum alloys presented in Table 4.

However these materials are denser than stainless steel and will result in a large separator mass as the separator radius increases. Their yield stresses also reduce significantly at the high temperatures experienced on the hot side of the system. The separator mass for the boiler exit can be estimated using the assumptions outlined in the separator mass model which was previously presented. Fig. 45 presents a plot of separator mass versus radius for the boiling saturation temperature and pressure of 1300 K and 110 psia. As expected the mass of the separator increases with the square of the radius. The separator mass almost doubles after 20 to 25 cm. Therefore minimizing the size of the separator and the radiator is important for reducing the overall mass of the space Rankine cycle.

Fig. 46 presents a plot similar to Fig. 45 using the same values but with a different separator radius scale. Both figures indicate that ASTAR-811C would be the ideal material to use for constructing the separator because of its high yield strength at increased temperature. The Ni-1%Zr was the most common material used in construction of the Rankine cycle but its poor yield strength at increased temperatures yields a much higher separator mass than the underdeveloped ASTAR-811C.

Fig. 47 represents the operation of a boiler exit separator for the Rankine cycle. High quality two-phase flow enters the separator through a low differential pressure (DP) port. The vapor moves through the liquid layer until it coalesces with the vapor core. Upon separation the vapor leaves the separation volume through the gas outlet and is delivered to the turbine. The separator is driven by a mechanical pump which delivers liquid to the separator nozzle. NPSH is provided by a liquid eductor and the mechanical pump is

sized to provide a recirculation flow to the driving side of the eductor. Liquid separated from the two-phase flow injection is sent back to the turbine feed pump where it is returned to the boiler.

To understand the pressure drop associated with the separator and determine the vapor core diameter needed to effectively operate the device, Fig. 48 was made to compare the diameter of the separator needed to separate the 0.27 kg/s of vapor to drive a 100 kW turbine to the total pressure drop of the separator. This plot was made with results from the program using negligible liquid volume in order to determine to magnitude of the pressure drop. As indicated by Fig. 48, the pressure drop of the separator falls significantly as a function of separator diameter. This is because the nozzle size of the separator is scaled linearly with separator size.

Fig. 49 confirms the results of Fig. 48 with a plot of the nozzle volumetric flow rate and pressure drop versus the separator diameter with 90% vapor core diameter. Fig. 49 shows that while separator diameter increases, the increased volumetric flow rate required to drive the separator does not increase the pressure drop of the nozzle because the nozzle area increases with separator diameter. Fig. 48 and Fig. 49 confirm that the separator will operate more effectively with larger vapor core diameters because the momentum needed to drive the separator reduces with smaller liquid volumes.

Because pumping power is a primarily a function of the nozzle flow rate and the pressure drop of the separator, Fig. 50 shows that pumping power increases as separator diameter increases for both the EM and mechanical pumps. This is due to the large liquid volumetric flow rate associated with increasing separator diameter. However EM pumping power increases significantly more than mechanical pumping power with separator diameter because EM pump efficiency is typically less than 10% and decreases with increasing flow rate. It is evident from this study that using an EM pump to drive

the MVS will significantly reduce overall Rankine cycle system efficiency due to its large power requirement.

Fig. 51 was made to investigate the separator mass and pump mass associated with a 100 kW(e) system as a function of separator diameter. Fig. 51 shows that separator mass increases significantly with the diameter but EM pump mass reduces by about 60 kilograms over the range of the separator diameters. However mechanical pump mass increases by about 50 kg over the range of separator diameters. The EM pump mass is estimated from Eq. (2.26) where the flow rate and pressure rise of the pump are raised to a fractional power. Therefore as flow rate increases and pressure drop decreases the pump mass will also decrease. This result does not seem logical because typical terrestrial pumps generally increase in mass with increasing flow rate which is evident by the increase in mechanical pump mass line shown in Fig. 51. Therefore the EM pump will not be chosen to drive the boiler exit separator due to its high power requirement and uncertainty in estimating pump mass. The figure also indicates the difference between the three materials the separator can be constructed from and shows that the alloy ASTAR-811C would require the least amount of mass. Pump mass does not significantly affect the total mass of the separator system, therefore sizing the separator will not be heavily weighted by reducing its mass.

Fig. 52 shows a plot of the pressure drop and mechanical pump power versus separator diameter with 90% vapor core diameters. Fig. 52 indicates that pumping power is minimized at smaller separator diameters because of the reduced liquid flow rate required to separate the two phases. In order to increase Rankine cycle system efficiency, the pumping power required to operate the boiler exit separator will need to be minimized. Fig. 52 shows that the estimated pumping power between 10 cm and 50 cm separator diameters spans 0.75% to 2.75% respectively of the electrical output from the generator of a 100 kW(e) system. Therefore choosing separators between 10 and 30 cm in diameter will require a maximum of 2% of the system power while reducing the separator mass.

Fig. 50 through Fig. 52 suggest that the separator diameter for a 100 kW(e) system should be between 10 and 30 centimeters in order to reduce the mass, pressure drop, and pumping power of the boiler exit separator. Therefore several studies were made to investigate the volumetric flow rate required to drive separators between these diameters while liquid volume fraction (the amount of liquid volume present within the device divided by the total separator volume) and vapor core diameter were varied. Fig. 53 gives the results of this study and indicates that each separator diameter has a range of liquid volume fractions and vapor core diameters which will allow the separator to operate with minimal volumetric flow rate.

Fig. 53 shows that as separator diameter increases from 15 to 40 centimeters, the minimal liquid volumetric flow rate operating region increases. These regions are indicated by the blue to green areas. These minimal operating regions indicate that liquid volumetric flow rate to the separator will change more with the larger separators than with the smaller separators making larger separators more difficult to operate in terms of changing pump flow rate. However smaller diameter separator performance is more unstable than larger separators in terms of system transients and fluid volumetric flow rate changes required to operate the device because of the smaller buffer volume. As separator diameter increases, the minimal liquid volumetric flow rate required to effectively operate increases. The 10 centimeter separator needs less than 40% the volumetric flow rate than the 30 centimeter separator to operate in a 100 kW(e) system. All plots do indicate the dark blue to green area of minimal liquid volumetric flow to operate as a function of liquid volume fraction and vapor core diameter.

Another study was performed to investigate the performance of using multiple smaller separators to manage the vapor volumetric flow rate rather than one large separator. The results from this study can be seen in Fig. 54 and Fig. 55. Fig. 54 represents a plot of a separator diameters with 25% of the vapor volumetric flow rate required to operate a 100 kW(e) system. Thus four separators of the same size would be needed to operate in this

configuration. The performance gain in this configuration is a reduction in liquid volumetric flow rate needed to drive the separator. A 15 cm diameter requires about 40% of the liquid volumetric flow rate of a single 15 cm separator in the 100% vapor flow rate system. However the mass and volume gain of the four separators with smaller pumps does not offset the mass of a single separator with a larger pump. The mass difference between these two configurations is about 130 kilograms. A similar trend is seen for the other separator diameters. Fig. 55 shows comparable results of separator diameters with 50% of the vapor volumetric flow rate required to operate a 100 kW(e) system.. Thus two separators of the same size would be needed to operate in this configuration. The liquid volumetric flow rate is only reduced by about 50% in this configuration. Again the mass and volume gain of the two separators does not offset the mass of a single separator with a larger pump.

Fig. 56 shows the required pumping power to operate the separator for several diameters. The point of this plot is to show the difference in pumping powers between the separator diameters. The normal pumping power to operate the 15 cm separator is about 0.7% of the Rankine cycle electric power. The maximum pumping power is approximately 1% percent of the Rankine system power. The pumping power from this study is slightly larger than the results of Fig. 52 because there is more liquid volume present within the device in this study. More momentum is needed to rotate the liquid layer around the vapor core to increase the buoyancy force present within the device to effectively remove the vapor bubbles within the liquid layer. From this data the maximum pump mass can be estimated for each separator diameter. Table 7 presents the pump mass data.

The main results of this study are shown in Fig. 57 which indicates that a single 15 cm diameter separator has the best performance in the boiler exit configuration in terms of the pumping power, pressure drop, mass and stable region of operation for system transients. The linear relationship of maximum pumping power with separator diameter in Fig. 57 is a result of scaling the nozzle area linearly based on separator diameter and

not including viscous pressure losses in the nozzle or on the separator walls. Fig. 57 shows that the 10 cm separator needs the least amount of liquid flow rate to operate, but the buffer volume is only about a half liter to accommodate system transients and the liquid pressure drop is very large. The range of liquid flow rate in the 10 cm separator also increases more quickly when conforming to system transients due to the small buffer volume. The buffer volume of the 15 cm separator is approximately 1.7 liters. By using the results from Fig. 54 the mass of the 15 cm boiler exit separator system is estimated to be about 70 kg which includes the pump and separator mass. This mass represents about a 3% increase in the system mass presented in Table 6.

An additional study using a 15 cm separator is performed using the same code but with a bubble diameter of 2000 microns. This bubble diameter is not as conservative as the 1000 microns which Fig. 53 through Fig. 56 used to determine the liquid flow rate but the value is still realistic. With this model the maximum separator pumping power is reduced from 1% to 0.73% of the total electrical output of the cycle. The total boiler exit separator mass is reduced from 70 kg to 64 kg. This result does not represent a significant improvement in operating performance.

Separator mass increases significantly with radius at higher temperatures because of the reduction in yield stress. As the operating temperature decreases the estimated allowable stress increases. An investigation is made into the effect that turbine inlet temperature has on separator and radiator mass. Fig. 58 shows the results from this study. From the design temperature of 1300 K to 1100 K the radiator mass increases by 500 kg. However the separator mass only decreases by 200 to 350 kg with the ASTAR-811C and T-111 materials respectively. The results from this plot show that decreasing turbine inlet temperature will not reduce separator mass enough to justify the increase in radiator mass. This study also does not take into account the increase in vapor mass flow rate which the separator would have to deliver to the turbine. The ALKASYS-SRPS outputs show decreasing the turbine inlet temperature must result in an increase in the vapor

mass flow rate because of the vapor density difference. Therefore larger separators and more pumping power are required to effectively separate the two phases as turbine operating temperature decreases.

Although it is not investigated in this thesis, it has been proposed by the ITP to combine the boiler and separator within a Rankine cycle into one component. If a heat flux was applied at the outer wall of the device then nucleation sites would form on the inner wall and be sheared off by the rotating liquid layer. The forced convection at the inner wall of the separator should increase the heat transfer coefficient significantly. Fig. 59 shows the boiling separator hardware brass board. The copper plate will have imbedded heating elements to provide a heat flux at the wall. The white plastic has a coefficient of linear expansion similar to that of copper and should not pose any sealing issues. The goal of the experiment is to characterize the overall heat transfer coefficient of the separator by varying the separator operating parameters.

This combined design is promising for the Rankine cycle because it can potentially reduce the mass of the system while always delivering 100% vapor to the turbine. A space Rankine cycle system using the MVS as the boiler could operate by removing thermal energy from the reactor by passing the lithium coolant through the walls of the separator in a series of tubes. This would result in an increase in boiler separator mass by thickening the walls, but would probably have less combined mass than the twisted-tape boiler and separator system. The wall heat exchanger would provide a heat flux at the separator inner wall which can cause nucleation in a saturated system. The boiler separator would need to be sized by maximizing the thermal energy removed from the lithium coolant while minimizing separator mass. Further publications by the ITP will include the results of the boiler separator experiments.

Condenser Separator

The condenser separator operates at a pressure and temperature significantly lower than the boiler exit separator and will only be required to remove excess vapor bubbles leaving the condenser. The separator will need to remove bubbles from a 23 LPM liquid flow sent to the device. The mass of the condenser separator is significantly less than the mass of the boiler exit separator because of the difference in operating pressure and temperature. Fig. 60 resents a plot of the condenser separator mass versus separator radius at 900 K and 3 psia. The plot indicates that the stainless steel and Niobium-Zirconium alloys yield less mass than the tantalum alloys. This is due to the density difference between the two materials and the yield strength at the lower operating temperatures. The ASTAR-811C and T-100 alloys yield similar separator masses because these materials are principally tantalum based. The significant difference in separator mass between the boiler exit separator and the condenser separator indicate that the condenser separator will not drastically affect the final system mass like the boiler exit separator.

Even though the condenser separator will have much less mass than the boiler exit separator, it still must be driven with a pump which will increase the mass added to the cycle. The condenser separator will be operating with a liquid eductor to provide the turbine feed pump with net positive suction head. However, instead of using another EM or mechanical pump to drive the separator, the turbine feed pump can be used to provide the necessary momentum for phase separation by increasing its liquid flow rate. Fig. 61 presents the condenser separator configuration using the feed pump turbine to provide the necessary flow rate to drive the separator. The vapor which is separated from the condenser exit will be at a slightly lower pressure than the condenser inlet. Therefore returning it to the condenser inlet will require a slight pressure increase by using a gas eductor. This configuration is shown in the system summary section of this

thesis and will be omitted from this investigation because the pressure rise required is small.

ALKSYS-SRPS was used to estimate the performance increase of the feed pump turbine to determine the increase in vapor bleed flow necessary to increase liquid flow rate of the device. The results of this study are given in Table 8. A negligible vapor bleed flow rate increase of about 70 LPM to the turbine can provide an additional 10 LPM for driving the phase separator. It is assumed in this study that the condenser separator will be sized primarily by minimizing the pump power increase of the feed pump turbine to drive the separator and maximizing the available buffer volume within the separator.

Fig. 62 shows a plot of buffer volume versus separator diameter assuming that the maximum vapor core diameter is 90% of the separator diameter and the minimum varies between 50% and 80% of the separator diameter. The scale of 10 to 25 cm is chosen to match the scale of Fig. 60 and to appropriately size the separator to match other components sizes in the system. It is no surprise that the maximum available buffer volume comes from larger separators and smaller vapor core diameters. However the point of this plot is to provide a magnitude of the available buffer volume as a function of separator diameter. Fig. 62 shows a 25 cm separator can provide a buffer volume between two and seven liters. It is important to note that separator stability increases with increasing vapor core diameters and that minimizing the vapor core diameter and maximizing separator diameter will require more pumping power to form stable vortices.

Choosing a separator diameter for the condenser is principally dependent on the available buffer volume and the pumping power required operating the system. A study is performed using a module of the code developed for the high vapor flow separator model to determine the feed pump power required to operate the condenser separator at a Weber number of 100 for various separator and vapor core diameters. The maximum vapor core diameter is assumed to be 90% of the separator diameter. If the liquid flow

to the separator is constant, the limiting condition for separator stability is at the smaller vapor core diameters. Therefore a separator at a Weber number of 100 at a specific vapor core diameter will become more stable as vapor core diameter increases and requires less pumping power. This study concentrated on keeping the feed pump power below 1% of the total system power production.

Fig. 63 shows a plot of Weber versus separator diameter at various vapor core diameters for a feed pump power of 1 kW. For this pump power a 50% vapor core diameter at a Weber number of 100 can only be obtained in the 10 cm separator diameter. This equates to a buffer volume of approximately half a liter. At 80% vapor core diameter a separator of 17 cm can attain a Weber number of 100. This 17 cm separator will have a buffer volume of about 0.7 liters.

Fig. 64 shows a similar study of Weber number versus separator diameter for a pump power of 1.05 kW. At this increased pump power a 18.5 cm separator at 50% vapor core and a 25 cm separation at 70% vapor core can obtain a Weber number of 100. Fig. 65 shows that an increase in pump power allows for greater separator stability because more momentum can be added to the liquid layer to increase the liquid rotational speed.

By combining the results of Fig. 62 through Fig. 64 a plot can be made which investigates separator performance as a function of the available buffer volume and pumping power. Fig. 65 presents the outcome of this study. Each of the power levels presents an asymptotic plot of available buffer volume versus separator diameter. At 1 kW feed pump power the maximum available buffer volume is approximately 0.75 liters between 13 and 14 cm separator diameters. As expected a larger buffer volume can be attained at higher pumping power. The available buffer volume at the 1.05 kW and 1.1 kW levels is approximately 2 and 4.25 liters respectively. Minimizing turbine bleed flow to drive the feed pump turbine is a design condition which must be met. An increase from 1 kW to 1.1 kW requires an additional 30 LPM of turbine bleed flow to

yield a final liquid flow rate of 40 LPM. Increasing the turbine bleed flow will increase the mass flow through the boiler which feedbacks into the boiler exit separator model. But to keep the argument conservative, the separator size will be chosen based on a turbine feed pump power of 1 kW.

Choosing a separator size of 14 cm for the condenser will provide a buffer volume of approximately 0.75 liters. This separator diameter yields a separator mass of 6 to 14 kg depending on the material and fittings which connect to the device. The feed pump turbine will be sized to account for the increase of 10 LPM liquid flow for driving the separator and will result in a negligible mass increase. Therefore the mass of the condensing separator system will be approximately 20 kg to account for the eductor, extra pipe runs, and feed pump turbine size.

The ITP normally operates the MVS in a sub-cooled condition where an eductor is not needed to provide NPSH to the pump. Several investigations for using the separator as a direct contact heat exchanger have been made to reduce the temperature and humidity of "hot" humid nitrogen by passing it through a "cold" liquid volume within the separator. This concept could be applied in the Rankine cycle to eliminate the need for a condenser and eductor. Fig. 66 presents the sub-cooled separator concept.

Turbine potassium exhaust at 900 K enters the separator and is condensed within the separation volume. Once the vapor is condensed it is returned to the boiler. Keeping the separator in a sub-cooled state requires that the liquid potassium must exchange energy through a radiator. For a 100 kW(e) system, approximately 460 kW of waste thermal energy much be removed from the vapor at the exit of the turbine. A single separator most likely would not be able to handle this magnitude of energy exchange. This approach also results in a heavier radiator mass because the temperature of the working fluid decreases with position through the radiator as opposed to the current condenser radiator design. Also designing a separator to handle the volumetric flow rate alone would be challenging. The condensing power of the separator has not been

previously evaluated and will therefore not be included in this analysis. Current research projects within the ITP have been investigating the direct contact heat exchanger characteristics of the MVS.

External Turbine Separator

The ALKASYS-SRPS model for turbine separation includes an external turbine separator and an inter-stage turbine separator for removing moisture which evolves from vapor expansion. The code is designed so the separators keep the moisture level within the turbine to below 12%. The default performance for the external separator is that it can remove 90% of the liquid sent to the device but has an associated penalty of removing 0.1 pounds of vapor for every pound of liquid removed. Additionally the inter-stage separator can remove 25% of the liquid sent to the device but removes 0.25 pounds of vapor for every pound of liquid removed. Because the inter-stage separator is built into the turbine, a study will not be performed to examine performance gains by using a MVS. However the external separator performance is varied to study the effect that it has on overall system mass. Fig. 67 represents the total Rankine cycle system mass versus separator moisture removal efficiency for various separator penalties at 100 kW(e).

Fig. 67 shows for a separator efficiency increasing from 90% to 100% with a penalty of removing 0.001 pounds of vapor for every pound of liquid removed the total system mass of the Rankine cycle is reduced by only 6 kg. Most of the mass reduction occurs in the radiator size. Each of the other penalties has similar mass reductions. It is evident from this data that external separator does not play a key role in reducing the system mass and that more development should be made in increasing the efficiency of the interstage separators. The external separator will be operating at conditions similar to the boiler exit separator with high volumetric vapor flow rates. A thermodynamic change between the turbine inlet and the external separator location is the reduction of

vapor density from 3 kg/m^3 to 0.4 kg/m^3. This reduction in density significantly increases the vapor volumetric flow rate through the separator. Therefore the use of a MVS at this location will add a significant amount of mass for an unnecessary performance gain of the entire system.

The total system mass change for using inter-stage turbine separators is examined further by modifying ALKASYS-SRPS to remove external turbine separation. With the inter-stage turbine performance set to the default value and the external separation set to minimal conditions the system mass increased by 46 kg. This mass increase comes from increasing the reactor and shield mass to accommodate an increase in potassium flow rate by 10 grams per second. The potassium flow rate increase is a result of reducing turbine stage efficiency by not having external moisture separation. There is also a small increase in radiator mass to accommodate the potassium flow rate increase.

Fig. 68 shows the results of removing the external separator and varying the interstage separator moisture removal efficiency. This plot shows that there is a near linear relationship with increasing the separator efficiency while reducing the total system mass. However relying on increasing the inter-stage separation efficiency may not be a good assumption for estimating the total system mass because terrestrial interstage separator efficiency has never been tested for reduced gravity Rankine cycles. Therefore using an additional interstage separator in the turbine is investigated with ALKASYS-SRPS. Both interstage separators are assumed to have an efficiency of 25% and the results show that system mass only increases by 35 kg.

It is suggested with this analysis that interstage separators be used in multiple turbine locations to increase turbine efficiency and lifetime. Using an external MVS at this location would increase system mass significantly more than the boiler exit separator because of the reduction in vapor density, the additional pump mass, and the piping required operating the system. However optimizing nozzle design and minimizing

separator size might yield results to be able to use a MVS at the external turbine location because of the small amount of liquid which would be removed. This analysis should be further investigated in future Rankine cycle experiments and studies.

System Summary

This section provides a summary of the performance changes which result from integrating vortex phase separation into the 100 kW(e) Rankine cycle. These results presented in this section assume that the Rankine cycle designed by ORNL will function properly by delivering vapor only to the turbine and providing NPSH to the boiler feed pump by using the RFMD at the boiler and condenser exit. Delivering vapor only to the turbine and providing NPSH to the turbine feed pump are characteristic problems of the ORNL Rankine cycle design and represent untested areas for the RFMD. However it is recognized that the goal of this thesis was to modify the Rankine cycle to manage the two-phase flows with the MVS.

Fig. 69 represents a schematic of how the MVS would integrate with the ORNL Rankine cycle to make the cycle work in reduced gravity conditions. Liquid from the feed pump turbine is sent to the boiler where it is vaporized and delivered to the boiler exit separator. The boiler exit separator removes any excess moisture from the mostly vapor flow and delivers the liquid back to the feed pump and sends vapor only to the turbine. The turbine has two interstage separators for removing excess moisture which occurs from vapor expansion within the device and this flow is sent directly to the condenser. Turbine exhaust is delivered to the condenser and the condenser exit separator removes any vapor from the flow and delivers it back to the condenser by using an eductor. The condenser separator provides NPSH to the feed pump to complete the cycle. The eductor present on the turbine exhaust to the condenser is needed to pump vapor from the condenser separator and send it back to the condenser because the vapor will be at a slightly lower pressure than the two-phase mixture going into the condenser. This

eductor can be sized to have negligible mass and pressure drop associated with its operation using procedures developed by the ITP group.[33] The schematic also presents the predicted mass flow at different points within the cycle assuming that the boiler delivers at least 90% quality flow to the boiler exit separator and the condenser delivers at most 5% quality flow to the condenser separator. The quality at the boiler and condenser exits are conservative estimates used in this analysis to obtain the magnitude of the maximum liquid and vapor return lines for the boiler and condenser separators. Even with these conservative exit qualities, the liquid return from the boiler exit separator and the vapor return from the condenser separator have negligible mass flow rates when compared to the major lines within the cycle and should have little effect on system efficiency.

Table 9 gives the mass and power requirements of adding the boiler exit separator, condenser separator and extra interstage turbine separator. The boiler exit separator system impacts the system performance significantly more than the condenser or interstage turbine separators. The thermal power required is a result of slightly increasing the original working fluid mass flow rate by about 60 grams per second to account for additional turbine bleed flow and the removal of the external turbine separator. The increase in working fluid flow rate results in a 1.5 LPM increase in the volumetric flow rate required by the boiler exit separator to effectively separate the two phases. This change in pump power is accounted for in Table 9.

Table 10 gives the change in efficiency and specific mass of the Rankine cycle by adding vortex phase separation. This table is completed using the results from ALKASYS-SRPS to investigate the changes in thermal requirements by adding the separators. The plant efficiency is the ratio of the generator power output to the cycle thermal power requirement. The thermal to electric efficiency is a ratio of the net electrical production of the system to the required reactor thermal power. The specific mass is the gross system mass divided by the net electrical output. Minimizing specific mass is the most important term for Rankine cycle systems because of their power to

weight ratio is considered the most favorable of all the power conversion systems. The ORNL 100 kW(e) base case has been modified to account for the estimated RFMD mass gain of 200 kg and power requirement of 2 kW(e) for both the boiler exit and the condenser exit.

The max integrated case is the result of the separators operating at their maximum electrical and thermal power requirements. This case is the most conservative estimate for the reduction in efficiency and increase in specific mass. The plant efficiency decreases by about 0.5% due to the increased thermal power requirement of the condenser and interstage separators. The thermal to electric efficiency remains about the same when compared to the base case. The specific mass decreases by 1.3 kg/kW(e) principally because of boiler exit and condenser separators total only 25% of the combined RFMD masses. The average integrated case shows that plant efficiency decreases by 0.2% and thermal to electric efficiency improves by about 0.1% over the base case. However the specific mass does not improve much because it is primarily a function of the mass of the additional components.

This performance data shows promising results for the integration of the MVS with the reduced gravity Rankine cycles and eliminating the need for the RFMD. There is only a slight reduction in thermal performance by adding the additional components to the ORNL design which had two-phase flow management problems.

To further investigate the integration of the MVS with the Rankine cycle ground and flight tests are needed for determining the performance characteristics of the high vapor flow separator. Reducing the mass and power requirements of this separator will significantly enhance the specific mass of the system. Future phase separator development should concentrate on optimizing nozzle area to the geometry of the separator. Reducing the pressure drop of the nozzle would result in a significant reduction in the pumping power and mass.

Using the separator as a boiler is an ideal method for reducing the mass and increasing the turbine lifetime of the Rankine cycle. Another possible way of decreasing the specific mass of the cycle is to investigate the use of a separator as the condenser. The ITP will further investigate these technologies in future Rankine cycle experiments.

CHAPTER V

CONCLUSIONS

The Vision for Space Exploration set forth by President Bush in 2003 to further explore the lunar surface and establish a human presence through out the solar system has provided the need for more efficient and larger power sources for space missions. Liquid-metal Rankine PCS coupled with a fission reactor remain an attractive option for space power applications when compared to other PCS such as Brayton, Stirling, thermionic and thermoelectric. Rankine PCS specific power is very favorable for plant designs of 100 kW(e) or higher from the viewpoint of power to weight ratio and high thermodynamic efficiency. Rankine cycle power conversion is used in most commercial power reactors on Earth and is well understood in a 1-g environment. However potential drawbacks to the technology in a reduced gravity environment include two-phase fluid management processes such as liquid-vapor phase separation.

Several investigations of Rankine cycle performance and design have been done in past programs since the late 1950's. Most work was completed in characterizing liquid metal flows and heat transfer. Additional experiments investigated turbine lifetime as a function of the amount moisture which passed through the device. In 2005 Project Prometheus was effectively terminated because of budget concerns but ORNL had made several designs for a 100 kW(e) liquid metal Rankine cycle system for the mission. ORNL also scaled and planned many experiments for investigating the performance of the boiler, condenser and other system components prior to its end.

Rankine cycle systems require vapor separation from a two-phase mixture at many locations in the power plant. These locations include: the boiler exit, turbine, and condenser. The most critical location is at the boiler exit where only vapor must be sent to the turbine because blade erosion occurs from high velocity liquid droplets entrained

by vapor flow. Space Rankine cycle boilers have been designed to provide the vapor necessary for power production but little reduced gravity testing has been completed with these devices. Ground studies indicate exit quality from the boiler with a reasonable body length may not be sufficient to effectively operate the turbine. ORNL anticipated using a RFMD to manage two-phase flows within the Rankine cycle, but this device needs a significant amount of power to operate, has complex turbo machinery and seals and is relatively untested for use in the cycle. Therefore the need exists for low power, passive and reliable phase separation at the boiler exit and other plant locations.

The ITP laboratory has developed a passive microgravity vortex phase separator which has already proven to be an essential component of two-phase systems operating in low gravity environments. The vortex phase separator uses the fluid's intrinsic momentum to produce a radial acceleration field within the device to generate separation through buoyancy. This phase separator design has been flight tested on thousands of parabolas aboard NASA reduced gravity aircraft and has achieved a NASA TRL of 6. Along with its ability to separate liquid and vapor in zero gravity, the separator can also act as an accumulator for inventory control and as a direct contact heat exchanger.

The microgravity vortex phase separator developed by the ITP was successfully operated under saturated conditions as it would in a reduced gravity Rankine cycle aboard the NASA C-9 reduced gravity aircraft. The flight data presented in this thesis indicates the separator has the ability to operate at steady-state and conform to system transients by adjusting the amount of liquid and vapor inventories within the device. Managing the pressure and temperature within the separator is an important part of using the device for the Rankine cycle.

The flight results demonstrate that the vortex separator can be a vital component in space Rankine cycles by making the cycle effectively work in reduced gravity. From the results in this thesis it is proposed the vortex phase separator be utilized within a space

Rankine cycle PCS to separate two-phase flow at the boiler exit and condenser exit. A new model is developed for the MVS to predict performance for phase separation at high vapor flow conditions. Using the high vapor flow and current MVS design parameters a sizing model is developed for the vortex phase separator at the boiler exit and condenser locations within the cycle. Turbine moisture removal performance is investigated by using the MVS and interstage separators. Schematics of the Rankine cycle with the integration of passive vortex phase separation were also presented.

The separator works at the boiler exit to deliver only vapor to the turbine to reduce turbine blade erosion. The boiler exit separator was sized primarily by reducing the mass of the separator system. The condenser exit separator removes vapor from the condenser exit flow and provides NPSH to the turbine feed pump eliminating the need for the RFMD. The condenser separator was sized primarily to maximize the available buffer volume while minimizing pump power. At the turbine, moisture is removed by interstage separators and not by external separators. The removal of the external separators is necessary because the vapor density in the turbine increases the vapor flow rate significantly more than the boiler exit which results in difficulty sizing a MVS with low mass and power. Additional separation in the turbine is provided by adding a second interstage separator. Increasing the efficiency of moisture removal in the turbine improves overall system mass and efficiency.

The study is concluded with overall system efficiency and performance changes due to adding vortex phase separation rather than using the RFMD. A minor reduction in plant efficiency of approximately 0.5% occurs from integrating the MVS with the Rankine cycle. This change is a result of the additional mass and thermal power requirements of operating the separators in the cycle. A slight increase in thermal to electric efficiency of about 0.1% occurs because the power requirement for the MVS is significantly less than the RFMD. A significant improvement over the RFMD is a 1.5 kg/kW(e) reduction of the specific mass of the cycle from using the MVS. The total MVS mass is much less

than the predicted RFMD mass. Even though the plant efficiency slightly decreases, the addition of these components allows the cycle to operate in a reduce gravity environment by properly managing two-phase flows within the system and eliminating the need for the RFMD.

Future phase separator development should concentrate on optimizing nozzle area to the geometry of the separator. Reducing the pressure drop of the nozzle would result in a significant reduction in the pumping power and mass. Other work and experiments conducted by the ITP will further investigate the integration of vortex phase separation with space Rankine cycles by testing high vapor flow separators, using the separator as a boiler, and using the separator as a condenser in order to increase the performance of the cycle.

REFERENCES

1) R. C. Kurwitz, K. Marsden, M. C. Ellis, F. R. Best, "Vortex Separator for Use in Microgravity Nuclear Power Systems," *American Nuclear Society Embedded Topical Meeting - Space Nuclear Conference*, San Diego, California, June 5-9, 2005, **1130**, 346-355 (2005).

2) M. Ghrist, M. C. Ellis, D. C. Bean, R. C. Kurwitz, F. R. Best, "Microgravity Phase Separation for the Rankine Cycle," *Nuclear Technology*, **156**, 282-288 (2006).

3) R. Oinuma, D. C. Bean, C. Neill, R. C. Kurwitz, F. R. Best, "Two-phase Flow Issues in Space Nuclear Reactor and Nuclear Propulsion Systems," *American Nuclear Society Embedded Topical Meeting - Space Nuclear Conference*, San Diego, California, June 5-9, 2005, **1135**, 213-222 (2005).

4) R. T. Lahey, V. Dhir, "Research in support of the use of Rankine Cycle Energy Conversion Systems for Space Power and Propulsion," National Aeronautics and Space Administration, Internal Document, NASA/CR-2004-213142 (2004).

5) L. S. Mason, "Power Technology Options for Nuclear Electric Propulsion," *Proceedings of the 37th Intersociety Energy Conversion Engineering Conference - IECEC*, Washington, DC, July 29-31, 2002, **20159**, 114-121 (2002).

6) G. L. Yoder, J. J. Carbajo, R. W. Murphy, A. L. Qualls, J. Hojnicki, M. P. Moriarty, F. J. Widman, K. J. Metcalf, M. Nikitkin, "Potassium Rankine Cycle System Design Study for Space Nuclear Electric Propulsion," *3rd International Energy Conversion Engineering Conference*, San Francisco, California, Aug. 15-18, **2**, 1123-1133 (2005).

7) H. M. Dieckamp, *Nuclear Space Power Systems*, Atomics International Technical Report, Canoga Park, CA (1967).

8) B. B. Bevard, G. L. Yoder, "Technology Development Program for an Advanced Potassium Rankine Power Conversion System Compatible with Several Space Reactor Designs," *AIP Conference Proceedings*, Albuquerque, New Mexico, Feb. 2-5, 2003, **654**, 629-634 (2003).

9) C. D. Sulfredge, G. L. Yoder, "Scaling of Thermal-Hydraulic Experiments for a Space Rankine Cycle and Selection of a Preconceptual Scaled Experiment Design," Oak Ridge National Laboratory, Internal Document, ONRL/TM-2005/213 (2005).

10) J. A. Angelo, D. Buden, *Space Nuclear Power*, Orbit Book Company, Malabar, FL (1985).

11) R. S. Holocomb, "Potassium Rankine Cycle Power Conversion Systems for Lunar-Mars Surface Power," *Proceedings of the 27th Intersociety Energy Conversion Engineering Conference*, San Diego, California, Aug. 3-7, 1992, **2**, 233-237 (1992).

12) R. Oinuma, D. C. Bean, C. Neill, K. R. Supak, F. R. Best, "Two-Phase Pressure Drop in a Twisted Tape Boiler for a Microgravity Rankine Cycle Power System," *AIP Conference Proceedings*, Albuquerque, New Mexico, Feb. 12-16, 2006, **813**, 35-42 (2006).

13) C. Liao, R. Oinuma, R. C. Kurwitz, "Heat Transfer Coefficient Computational Model for Tube Boiler with Twisted-Tape," *Transactions of the American Nuclear Society*, Albuquerque, New Mexico, November, 2006, **95**, 808-809 (2006).

14) T. T. Robin, "Design of Boiler-Superheater Units for Representative Cesium and Potassium Space Power Plants," Oak Ridge National Laboratory, Internal Document, ORNL-TM-2080 (1968).

15) J. F. Mondt, V. C. Truscello, "SP-100 Power Program," *AIP Conference Proceedings*, Albuquerque, New Mexico, Jan. 9-13, 1994, **301**, 143-155 (1994).

16) J. C. Moyers, J. P. Nichols, "ALKASYS, A Computer Program for Studies of Rankine Cycle Space Nuclear Power Systems," Oak Ridge National Laboratory, Internal Document, ORNL/TM-10427 (1987).

17) J. J. Carbajo, G. L. Yoder, "Optimization of Rankine Space Power Conversion Systems with the codes ALKASYS-SRPS and DAKOTA," *American Nuclear Society Embedded Topical Meeting - Space Nuclear Conference*, San Diego, California, June 5-9, 2005, 376-380 (2005).

18) J. J. Carbajo, G. L. Yoder, "Optimization of Small Rankine Space Power Conversion Systems," *Proceedings of the 2004 International Congress on Advances in Nuclear Power Plants* - ICAPP'04, Pittsburgh, PA, June 13-17, 2229-2233 (2004).

19) T. J. Bland, R. S. Downing, D. P. Rogers, "A Two-Phase Thermal Management System for Large Spacecraft," *SAE Technical Paper Series*, **SAE 851351** (1985).

20) J. McQuillen, J. Sankovic, N. R. Hall, "Multiphase Flow Separators in Reduced Gravity," *ASME International Mechanical Engineering Congress and Exposition*, Orlando, Florida, Nov. 5-11, 2005, **261**, 737-743 (2005).

21) G. L. Yoder, J. J. Carbajo, R. W. Murphy, A. L. Qualls, C. D. Sulfredge, "Technology Development Program for an Advanced Potassium Rankine Power Conversion System Compatible with Several Space Reactor Designs," Oak Ridge National Laboratory, Internal Document, ORNL/TM-2004/214 (2004).

22) D. F. Chao, J. F. Lekan, J. B. McQuillen, J. M. Sankovic, N. Zhang, "On Analog Simulation of Liquid-Metal Flows in Space Rankine Cycle Power Systems," *ASME International Mechanical Engineering Congress and Exposition*, Orlando, Florida, Nov. 5-11, 2005, **261**, 755-761 (2005).

23) R. M. Manglik, A. E. Bergles, "Heat Transfer and Pressure Drop Correlations for Twisted-tape Inserts in Isothermal Tube: Part I-Laminar Flows," *Journal of Heat Transfer*, **115**, 881-889 (1993).

24) R. M. Manglik, A. E. Bergles, "Heat Transfer and Pressure Drop Correlations for Twisted-tape Inserts in Isothermal Tube: Part II-Transitions and Turbulent Flows," *Journal of Heat Transfer*, **115**, 890-896 (1993).

25) M. K. Jensen, M. Pourdashti, H. P. Bensler, "Two Phase Pressure Drop with Twisted-Tape Swirl Generators," *International Journal of Multiphase Flow*, **11**, 201-211 (1985).

26) M. C. Ellis, *The Tangential Velocity Profile and Momentum Transfer Within a Microgravity Vortex Separator*, M. S. Thesis, Texas A&M University (2006).

27) N. E. Todreas, M. S. Kazimi, *Nuclear Systems I Thermal Hydraulic Fundamentals*, Hemisphere Publishing Corporation, New York (1990).

28) M. Ellis, R. C. Kurwitz, F. R. Best, "Development of a Unique, Passive, Microgravity Vortex Separator," *ASME – Fluids Engineering Division*, **261**, 763-770 (2005).

29) F. P. Beer, E. R. Johnston, *Mechanics of Materials*, McGraw-Hill, Inc., New York (1981).

30) P. M. Clark, "Mechanical Pumps for High-Temperature Liquid Metal," *American Society of Naval Engineers*, **66**, 246-252 (1954).

31) M. S. Smith, D. H. Wood, "An Assessment of Liquid-Metal Centrifugal Pumps at Three Fast Reactors," *Nuclear Technology*, **104**, 118-127 (1993).

32) R. Fox, A. McDonald, *Introduction to Fluid Mechanics,* Fifth Edition, John Wiley & Sons, New York, 362-365 (1998).

33) C. Liao, *Two Phase Flow Ejector Modeling for Design and Analysis*, In-progress, Ph. D Dissertation, Texas A&M University (2007).

34) I. Chen, R. Downing, E. G. Keschock, M. Al-Sharif, "Measurements and Correlation of Two-Phase Pressure Drop under Microgravity Conditions," *Journal of Thermophysics and Heat Transfer*, **5**, 514-523 (1991).

35) K. M. Hurlbert, L. C. White, F. R. Best, and R. C. Kurwitz, "Scaling two-phase flows to Mars and Moon Gravity Conditions," *International Journal of Multiphase Flow*, **30**, 351-368 (2004).

APPENDIX A

Table 1 SNAP reactor power plants summary[14)]

	SNAP -2	SNAP-10A	SNAP-8
Power (kW(e))	3	0.5	35
Design Lifetime (yr)	1	1	1
Reactor power (kW(t))	55	30	600
Efficiency (%)	9	1.6	8
Reacotr outlet temperature (K)	920	810	975
Reactor type	U-ZrHx thermal	U-ZrHx thermal	U-ZrHx thermal
Primary coolant	NaK-78	NaK-78	NaK-78
Power Conversion	Rankine (Hg)	Thermoelectrics (SiGe)	Rankine (Hg)
Boiling Temperature (K)	770	-	850
Turbine Inlet Temperature (K)	895	-	950
Condenser Temperature (K)	590	-	645
Radiator Temperature (K)	590	595	575
Radiator Area (m^2)	11.1	5.8	167.2
System unshielded weight (kg)	545	295	4545
Specific weight (kg/kW)	182	590	130

Table 2 Operation of turbines with potassium working fluid[7)]

Installation	Function	Number of Stages and Turbine Type	Blade Tip Speed (ft/sec)	Blade Material	Operating Hours	Nozzle Inlet Temperature (°F)	Exhuast Temperature (°F)	Outlet Vapor Quality (%)	Remarks
Aeronutronic	Small erosion test facility	1-Impulse	350	TZM	100	1250	~960	~95-97	Erosion on all turbine blades- mass transfer deposit in one nozzle- attributed to high con tent in potassium
AiResearch									
Turbo dynamic bearing test rig	Driver for potassium-lubricated test bearing	1-Impulse	760	Inconel X	3000	1350	1076	~95-97	No erosion-- mass transfer for deposit in one nozzle
Turbine test rig	Space power turbine	1-50% Reaction	670	Waspalloy	50				
General Electric	Space power turbine	2-Reaction	750 750	Udimet 700 w/ several TZN and TZC blades	5100	1500	1240	~92	Negligible erosion during the 5100-hr test
General Electric	Space power turbine	3-Reaction	838	TZM	5000	1450 1550		93	Negligible erosion
Oak Ridge National Laboratory									
ORNL Turbine Pump	Boiler feed pump	1-Impulse	220	TZM	360	1400	1040	~95-97	No erosion
Aeronutronic MK-1	Boiler feed pump	1-Impulse	220	TZM	2600	1250	1040	~95-97	No erosion
Aeronutronic MK-1	Boiler feed pump	1-Impulse	220	TZM	1020	1250	1040	~95-97	Scheduled shutdown; turbine not inspected
Aeronutronic MK-2	Boiler feed pump	1-Impulse	185	TZM	3970	1250	1040	~95-97	No erosion
Rocketdyne	In-house test turbine	1-Impulse	750	Waspalloy	100	1600	1210	~95-97	No erosion

Table 3 Boiler design for two 100 kW(e) units[23)]

Number of tubes	24
Tube diameter (cm)	1
Tube length (cm)	250
Tube pitch (cm)	1.74
Tube wall thickness (cm)	0.08
Twisted tape pitch	2
Boiler dimensions (cm)	7.6 x 11
Boiler wall thickness (cm)	0.12
Number of inlet nozzles	2
Inlet nozzle diameter (cm)	2
Number of outlet nozzles	2
Outlet nozzle diameter (cm)	2.8
Potassium flow rate (kg/s—1 unit)	0.27
Lithium flow rate (kg/s)	1.37

Table 4 Yield stresses of space Rankine cycle materials at various temperatures

Material	**Temperature (K)**	**Yield Stress (MPa)**	**Yield Stress (PSI)**	**Density** (g / cm^3)
Nb-1%Zr	1300	20	2900	8.58
T-111	1300	70	10152	16.7
ASTAR-811C	1300	160	23206	16.7
Nb-1%Zr	800	70	10152	8.58
T-111	800	300	43511	16.7
ASTAR-811C	800	200	29007	16.7
SS-316FR	800	130	18854	7.9

Table 5 Flight test matrix summary

Day	Recirculation Flow [LPM]	Separator Flow [LPM]	Condensing Flow [LPM]	Two-Phase Flow [LPM]	Vortex Quality & Comments
1	1 to 5	0 to 2	0 to 1.5	0	Bad vortices without condensing flow. Once condensing flow was turned on the vortex quality improved.
2	2.8 to 5.6	1.6 to 2	0.8 to 1.25	0	Vortices mostly good. Learned from first flight that condensing flow helps vortex formation.
3	3.4 to 6	1.5 to 3.6	0.02 to 0.03	0.3 to 0.45	Used heaters to send two-phase flow to separator. Had mostly bad vortices with this flight. Flashing in the eductor and pump inlet occurred.
4	4.5 to 6	1.4 to 2	0.06 to 1	1 to 2	Increased pump speed to produce more recirculation flow. Increased pump speed helped produce more stable vortices and increased flow rates through the condensing and two-phase lines.

Table 6 100 kW(e) system mass summary

SYSTEM WEIGHT SUMMARY	KG
REACTOR	236
SHIELD	839
TURBINE CYCLE PIPING, HEATERS,	
AND FEED PUMP WITH DRIVE	16
TURBINES	17
GENERATORS	41
ACCUMULATOR	1.3
RADIATOR	499
CONDENSER	80
POWER CONDITIONING 1/1	599
GRAND TOTAL, KG	2328

WEIGHTS FOR 2x100% PCS

EXTRA BOILER FOR 2/1	10
POWER COND. FOR 2/1	704
GRAND TOTAL FOR 2xPCS UNITS	3115

Table 7 Separator diameter and maximum pump mass

Separator Diameter [cm]	Pump Mass [kg]
10	25
15	31
20	40
30	66
40	100

Table 8 Feed pump turbine power and flow rates from ALKASYS-SRPS

Vapor Bleed Flow [LPM]	**Pump Power [kW]**	**Liquid Flow Rate [LPM]**	**Pump Mass [kg]**
175.95	0.68	24.64	2.56
202.35	0.77	28.07	2.91
228.74	0.88	32.01	3.32
246.33	0.95	34.50	3.57
260.82	1.00	36.50	3.78
273.76	1.05	38.32	3.97
286.69	1.10	40.15	4.15

Table 9 Mass and power requirements of the additional separation components

Additional Components	Mass [kg]	Maximum/Average Electrical Power kW	Maximum/Average Thermal Power kW
Boiler Exit Separator System	71	1.1 / 0.7	-
Condenser Separator System	20	-	0.22 / 0.18
Interstage Turbine Separator System	35	-	12.25 / 5.25

Table 10 Performance changes from the integration of vortex phase separation

	ORNL 100 kW(e)	Max Integrated Case	Average Integrated Case
Plant Efficiency, %	20.23	19.74	20.04
Thermal to Electric Efficiency, %	19.16	19.2	19.27
Specific Mass [kg/kW(e)]	23	21.73	21.65

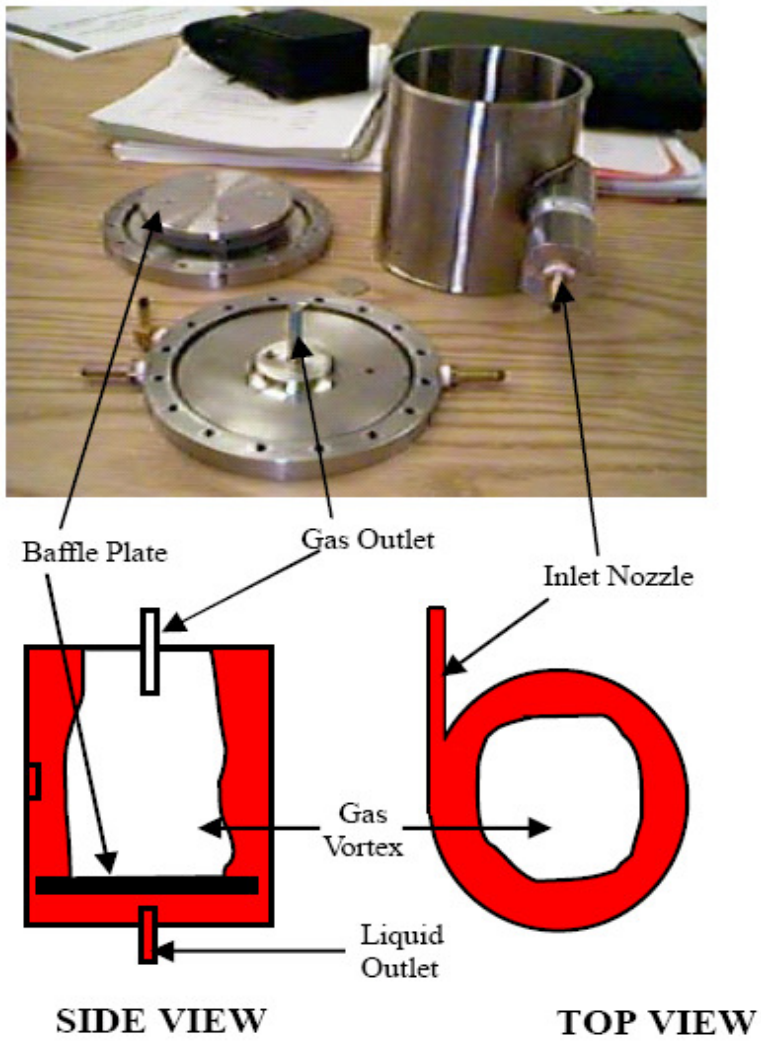

Fig. 1 Texas A&M phase separator

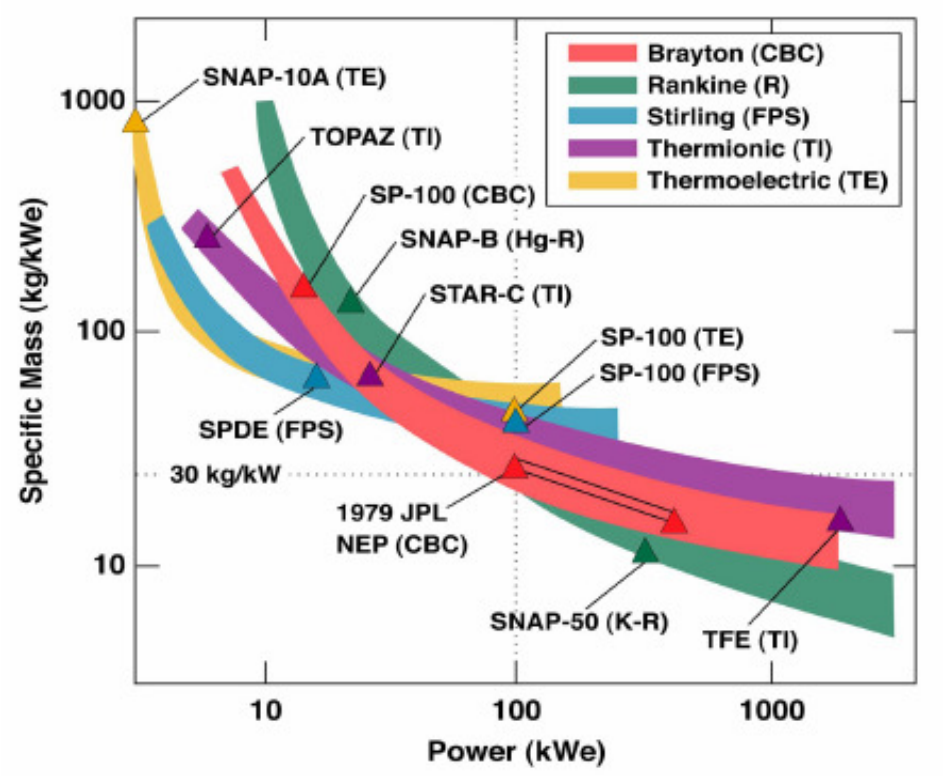

Fig. 2 Reactor Specific Mass (kg/kW(e)) versus power (kW(e))[5)]

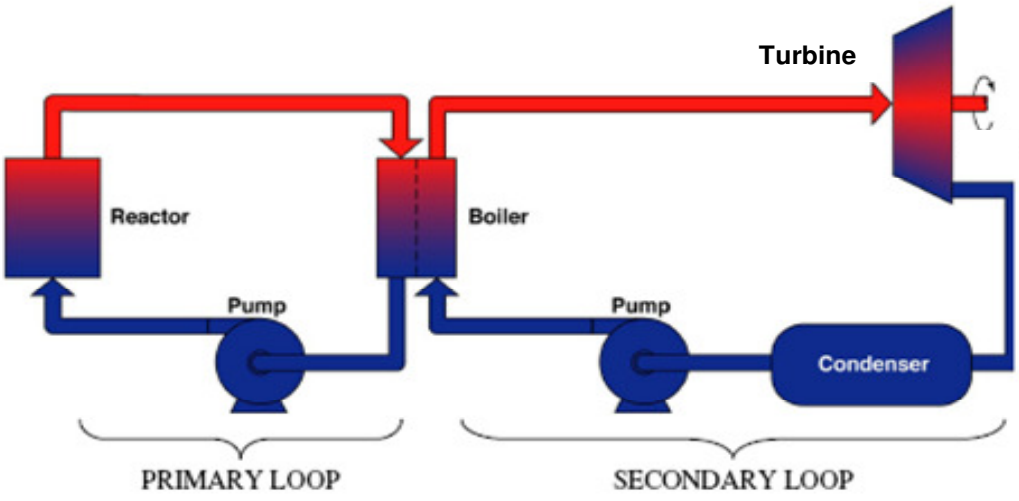

Fig. 3 Simplified schematic of a Rankine cycle power system

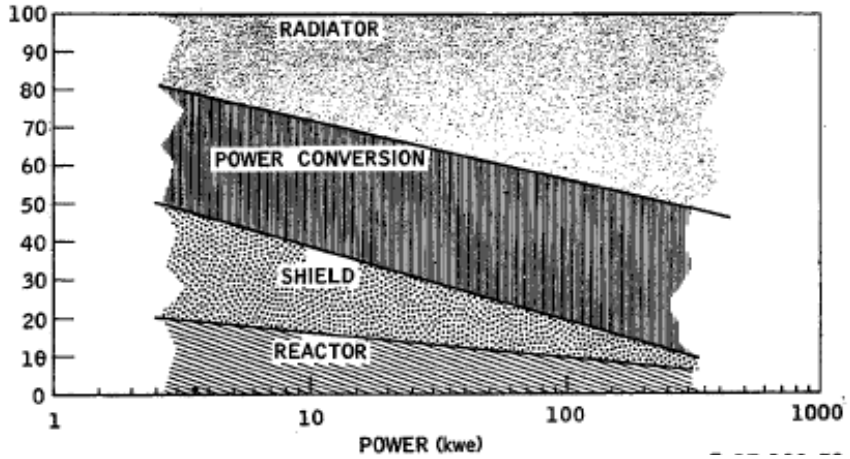

Fig. 4 Component mass fraction versus system power level in turbo-electric power conversion cycles[7)]

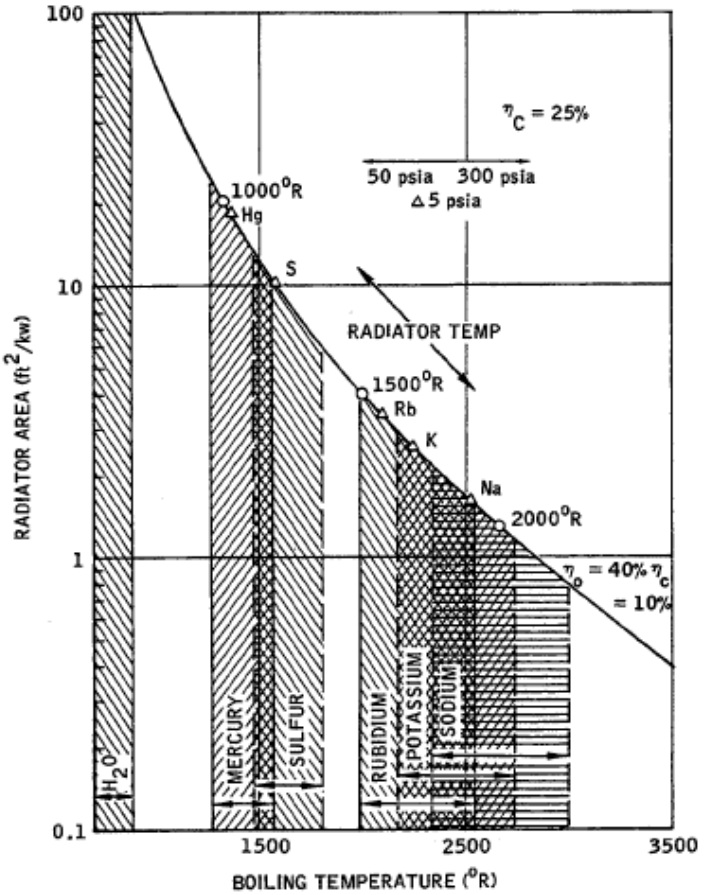

Fig. 5 Radiator area per kilowatt versus system boiling temperature of different Rankine cycle working fluids[7)]

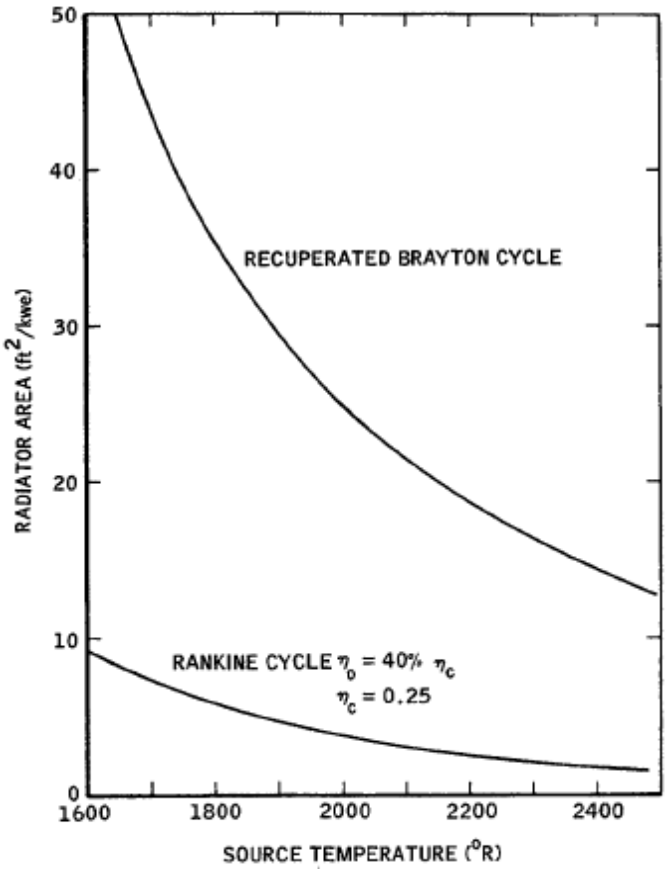

Fig. 6 Radiator area per kilowatt versus system operating temperature of Brayton and Rankine cycles[7)]

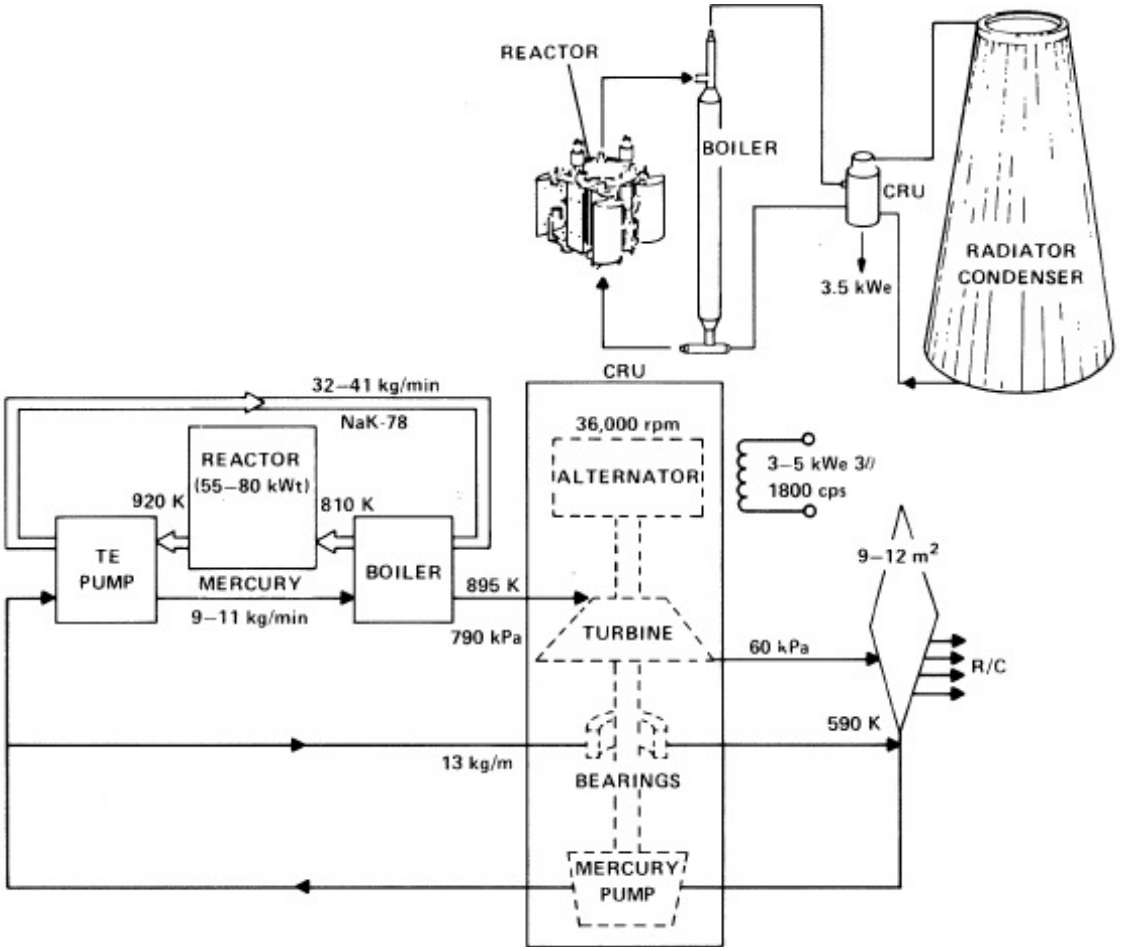

Fig. 7 SNAP-2 mercury Rankine cycle schematic[14)]

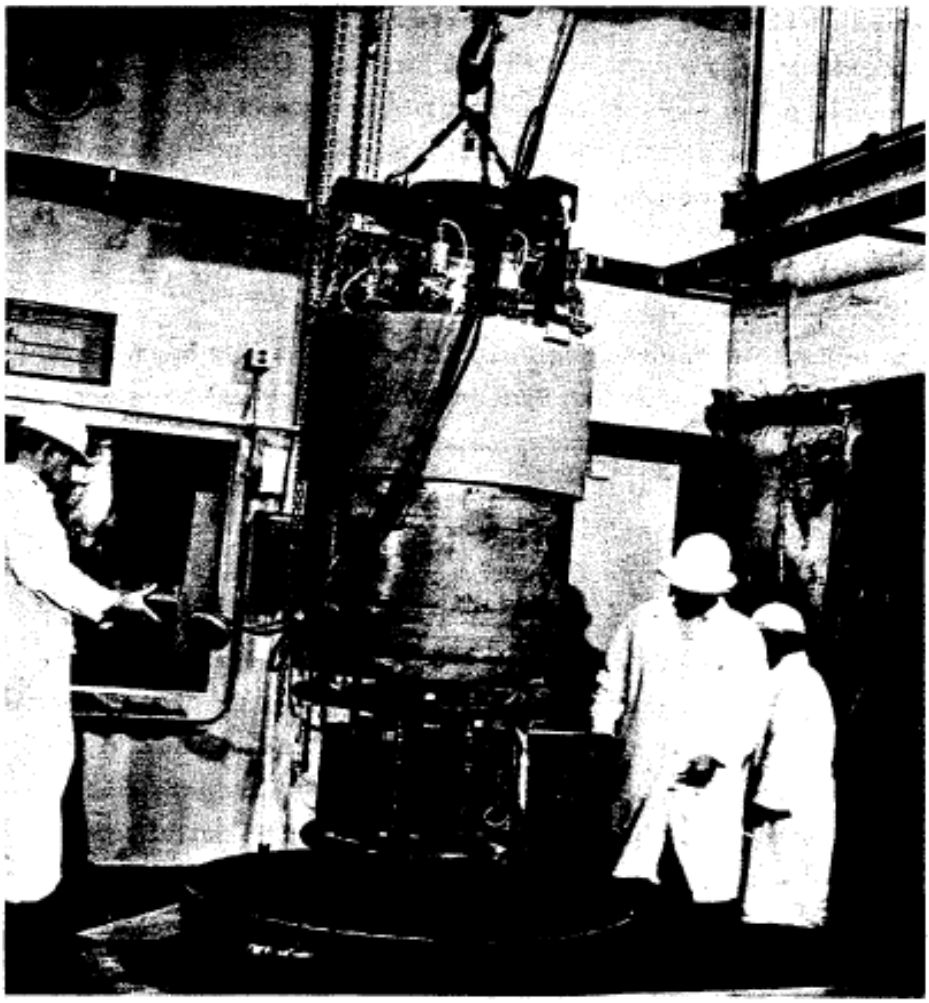

Fig. 8 Complete SNAP-8 reactor test assembly [7)]

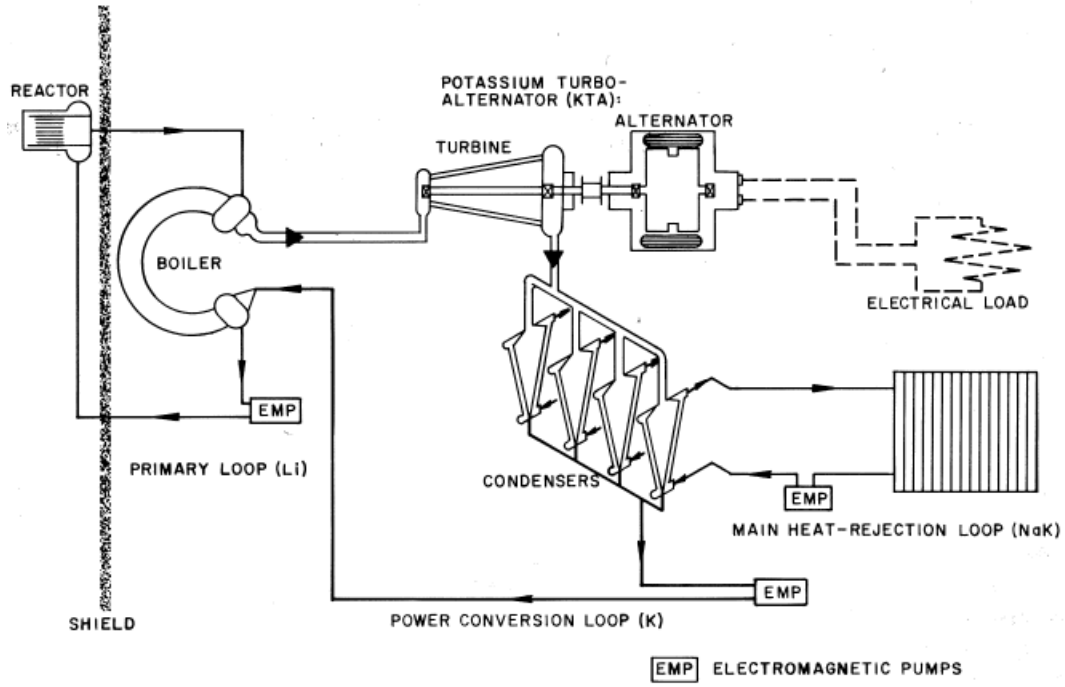

Fig. 9 Rankine cycle schematic for the SNAP-50 space power plant[15)]

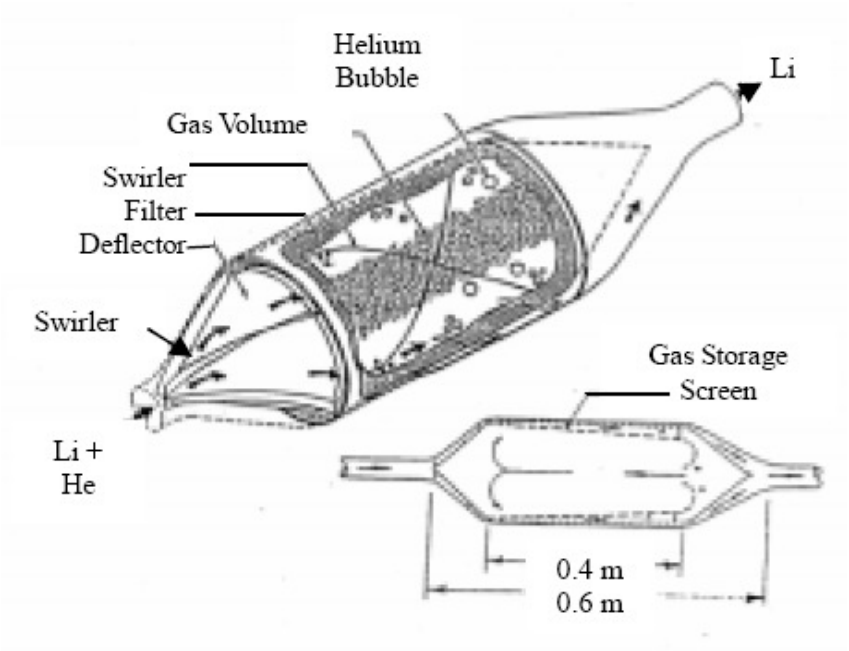

Fig. 10 SP-100 separator/accumulator[17)]

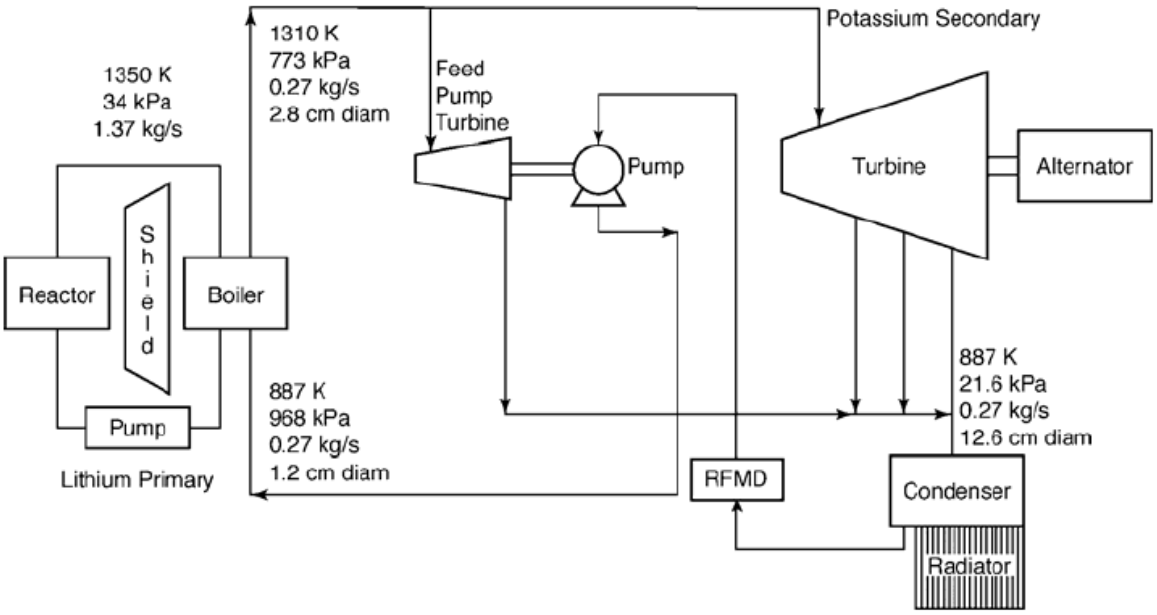

Fig. 11 Baseline Rankine cycle schematic chosen for the ORNL 100 kW(e) system

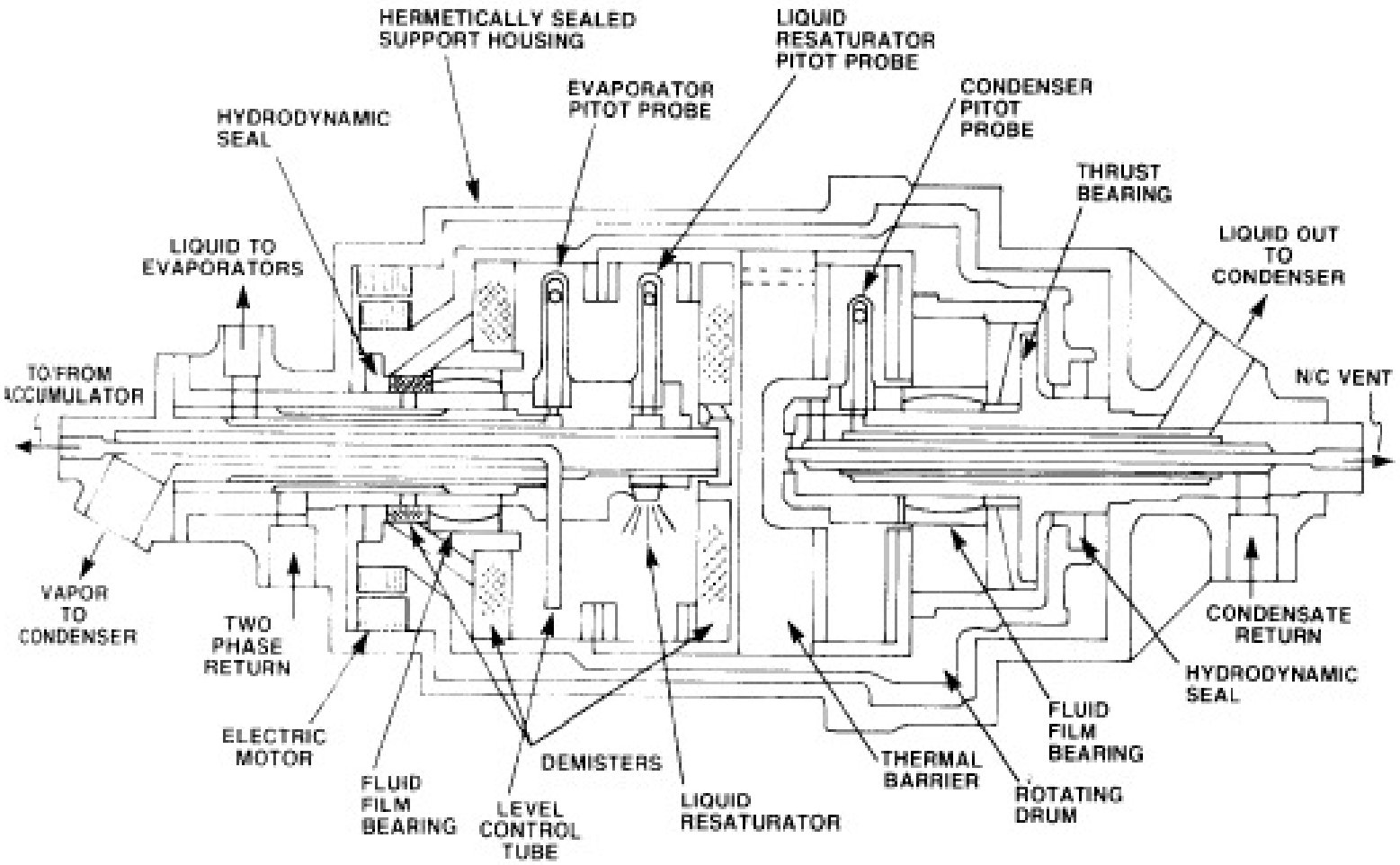

Fig. 12 Flight prototypic RFMD concept[22)]

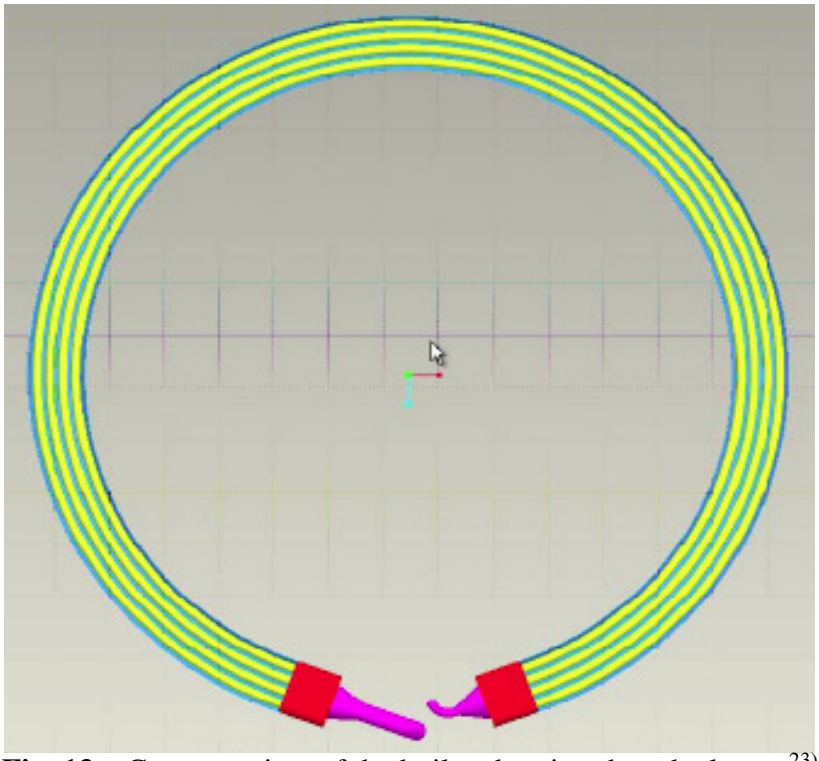

Fig. 13 Cutaway view of the boiler showing the tube layout[23)]

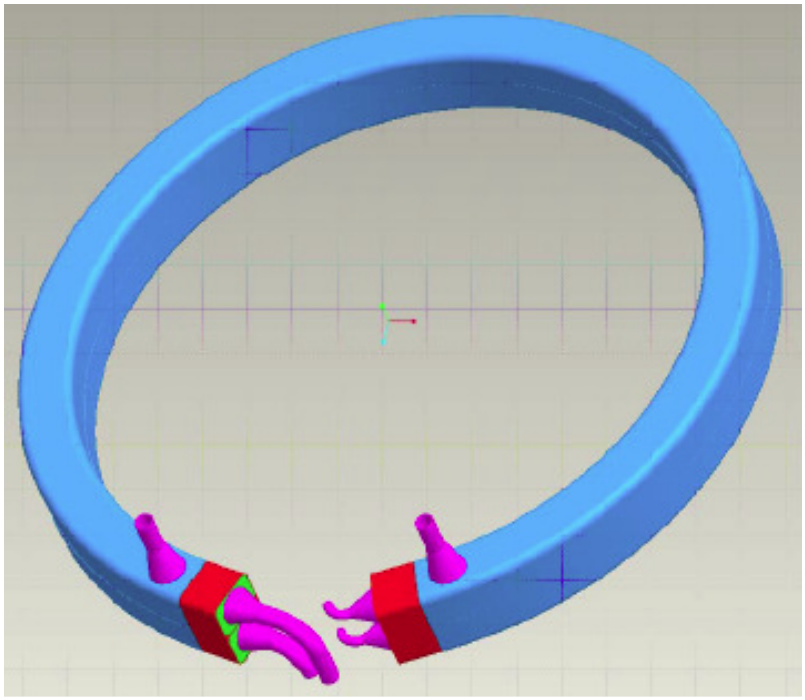

Fig. 14 Boiler isometric view showing the lithium and potassium inlets and outlets[23)]

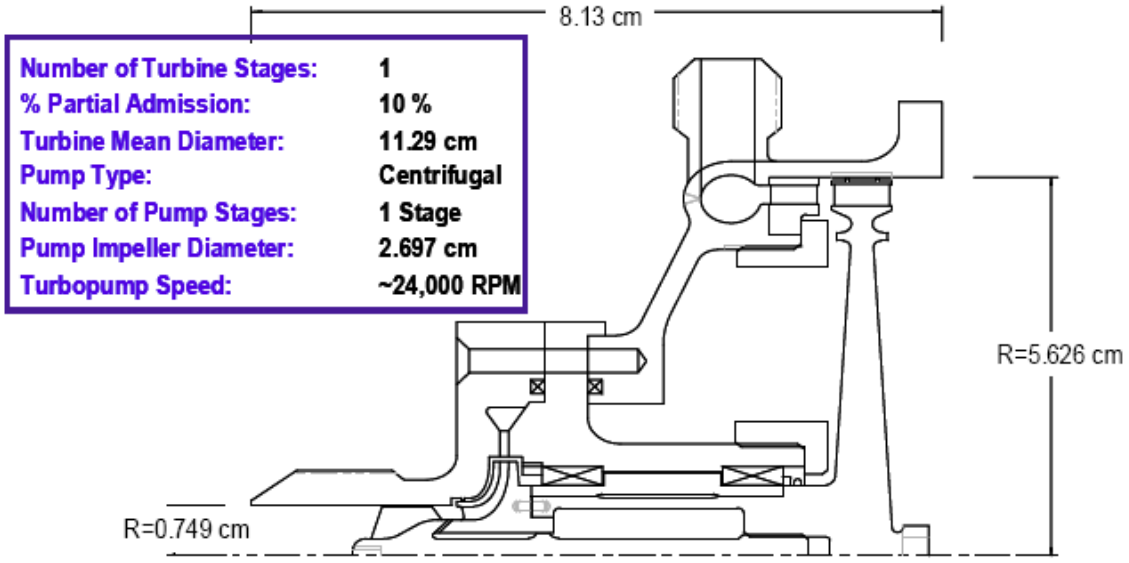

Fig. 15 Feed turbopump design and characteristics[23)]

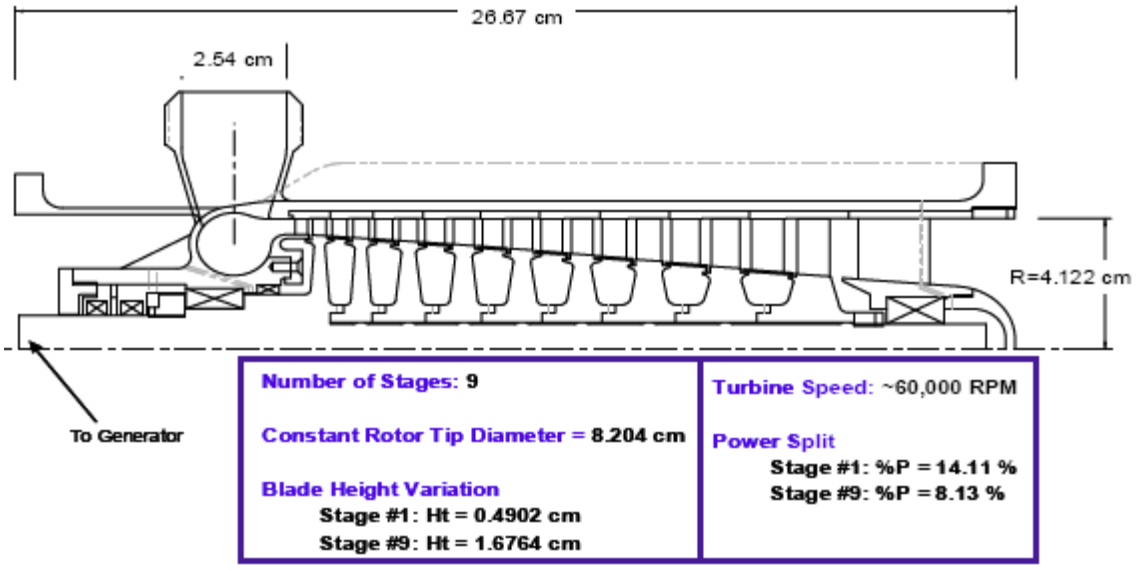

Fig. 16 100 kW(e) turbine design and characteristics[23)]

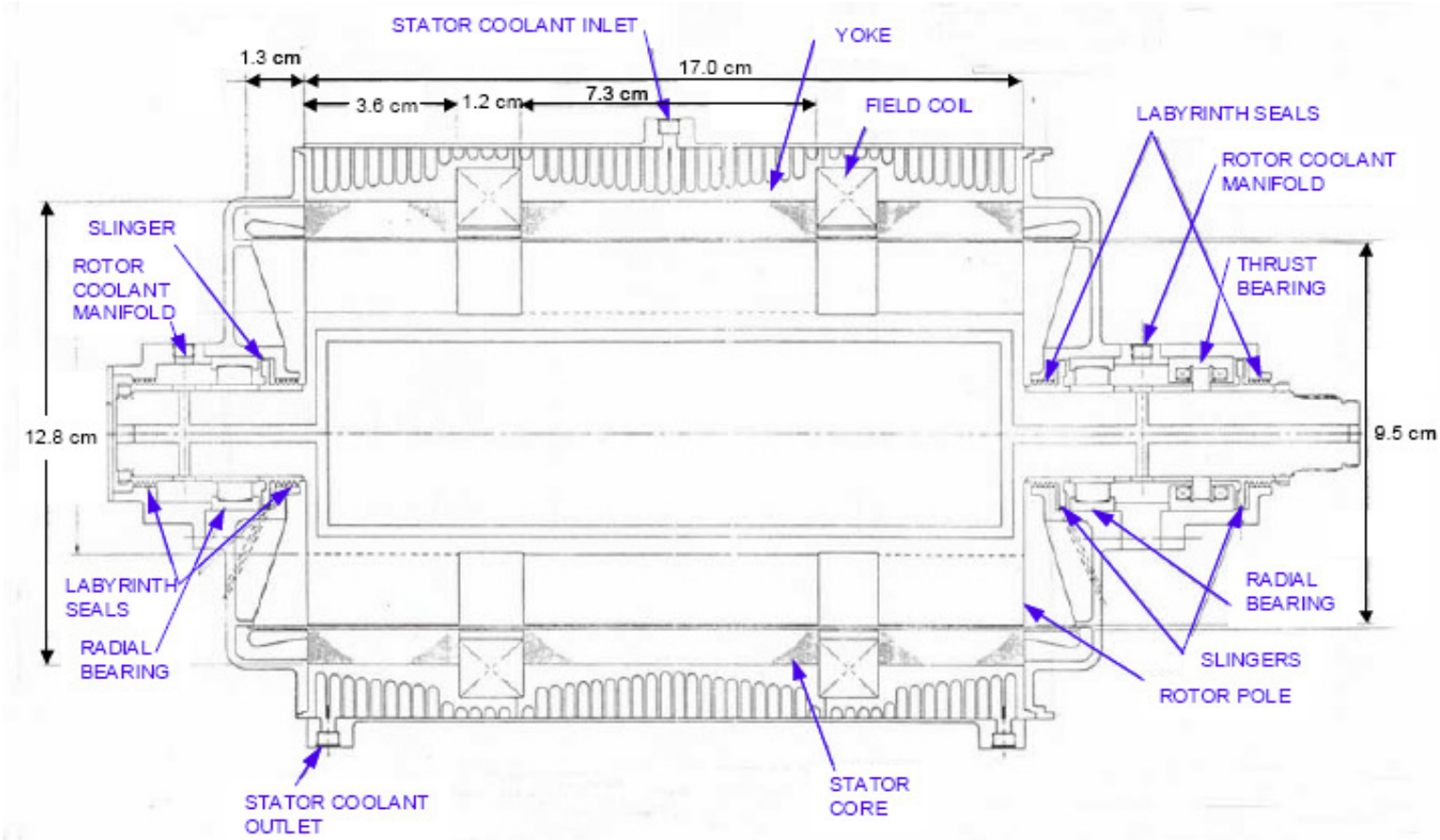

Fig. 17 Homopolar inductor alternator concept for 100 kW(e)[23)]

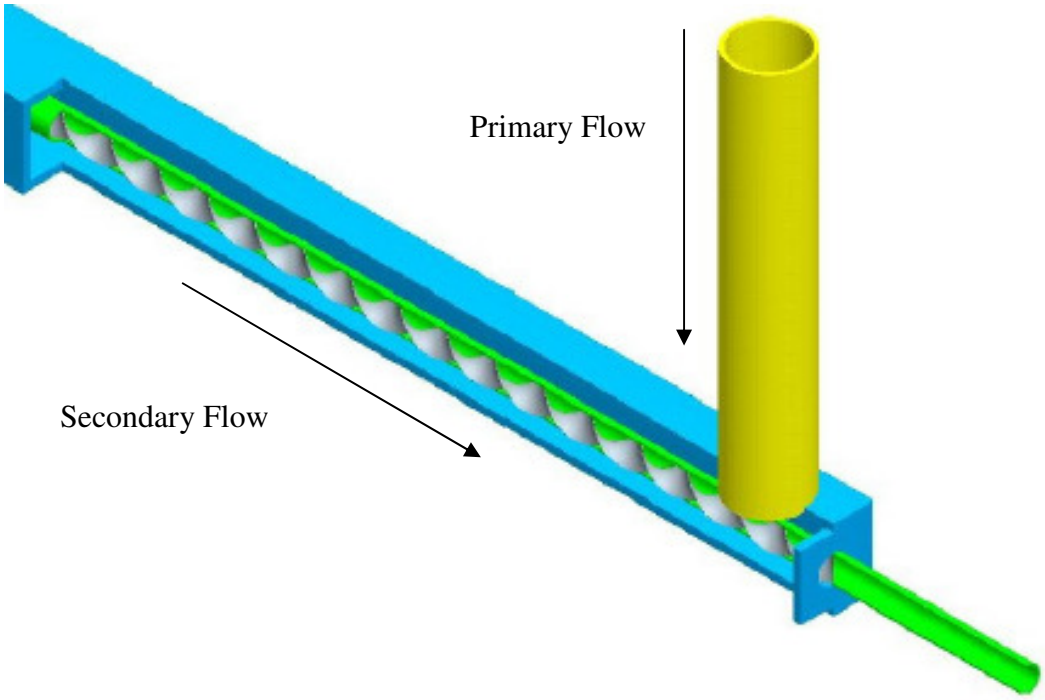

Fig. 18 ORNL scaled twisted tape boiler design[9)]

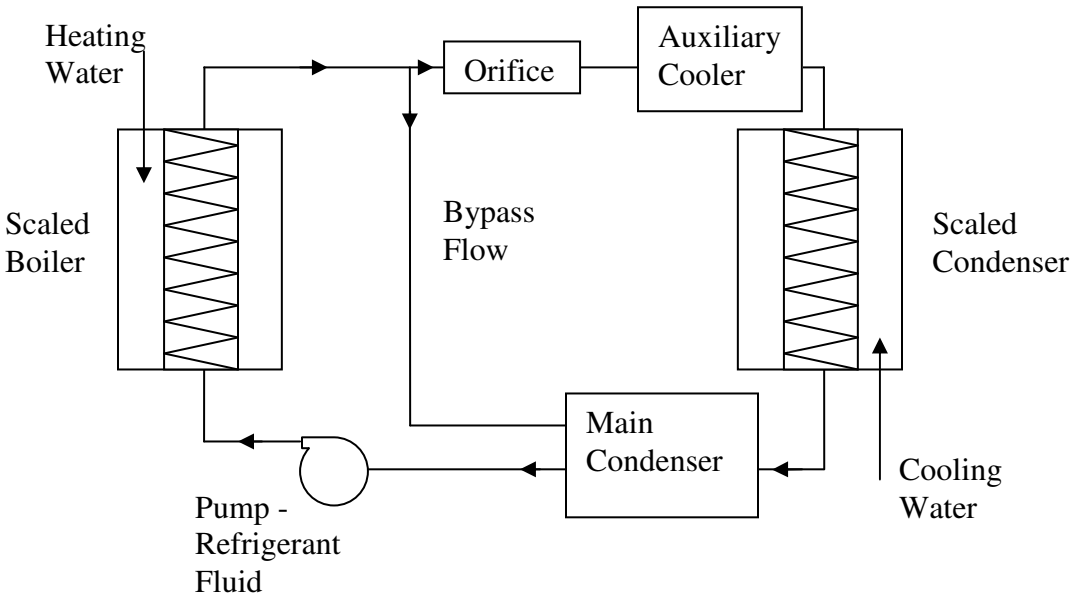

Fig. 19 Complete ORNL scaled refrigerant loop experiment[9)]

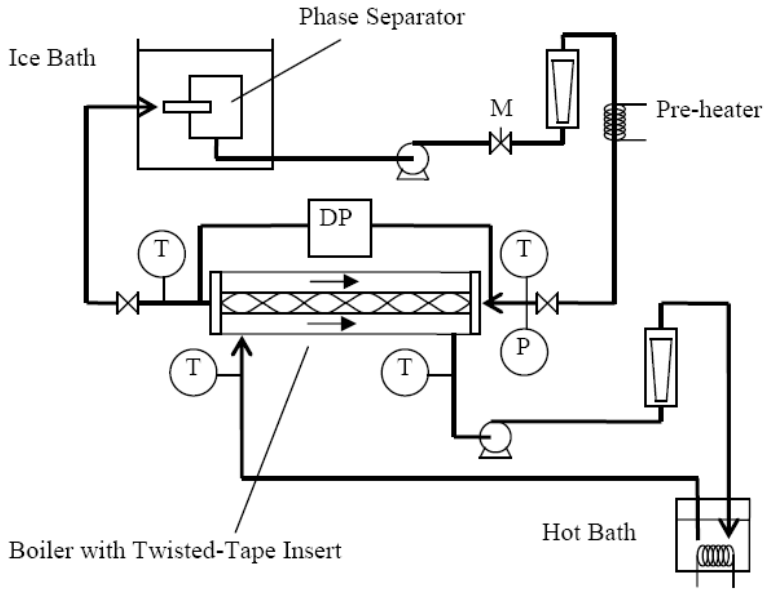

Fig. 20 Schematic of the Rankine cycle experiment at Texas A&M University

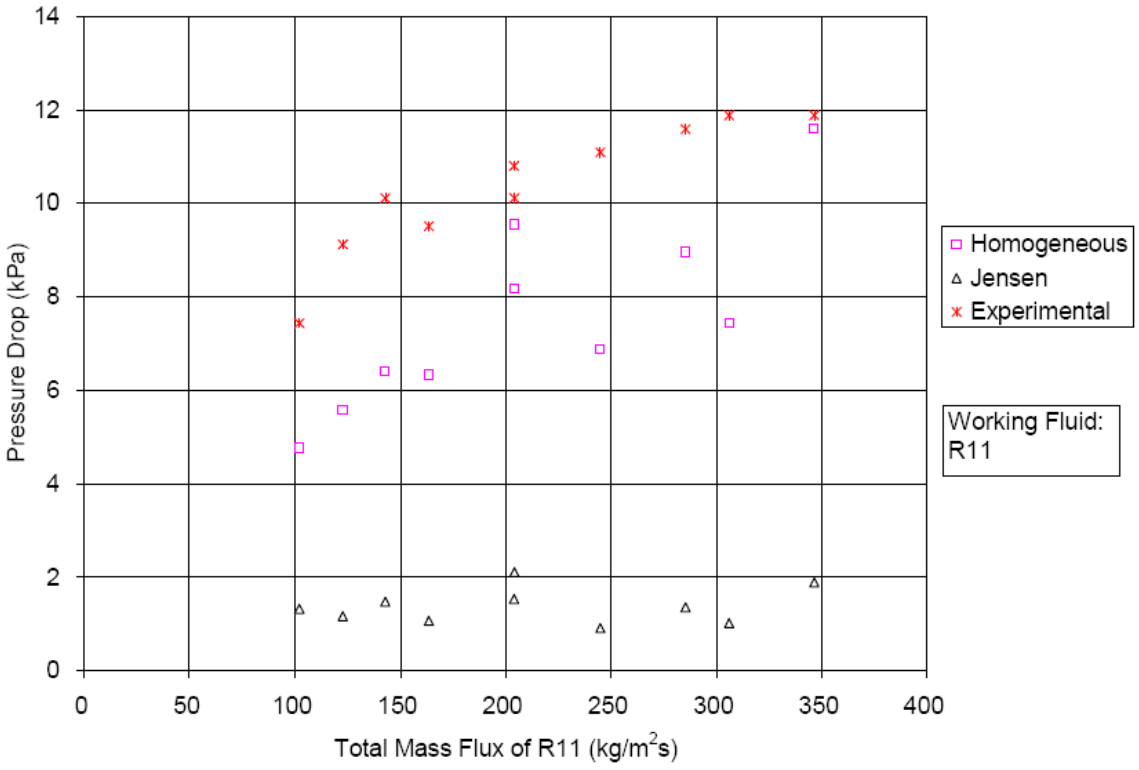

Fig. 21 Adiabatic pressure drop comparison in a once-thru boiler with twisted tape inserts

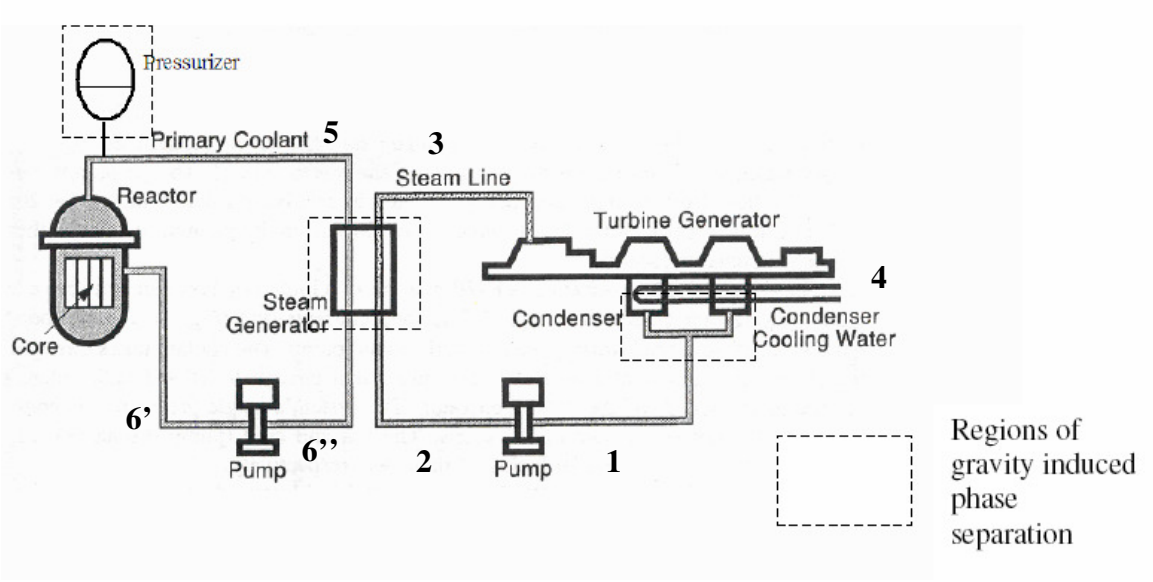

Fig. 22 Schematic of a typical PWR power plant[29)]

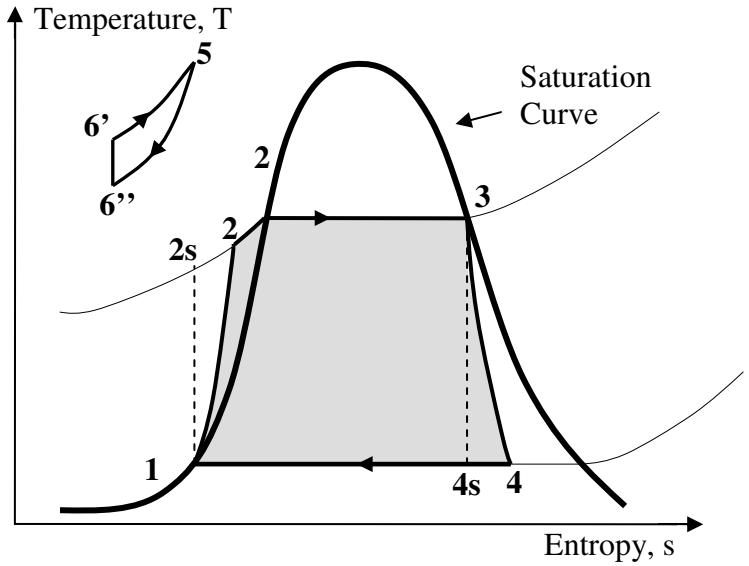

Fig. 23 T-s diagram for a typical Rankine cycle secondary

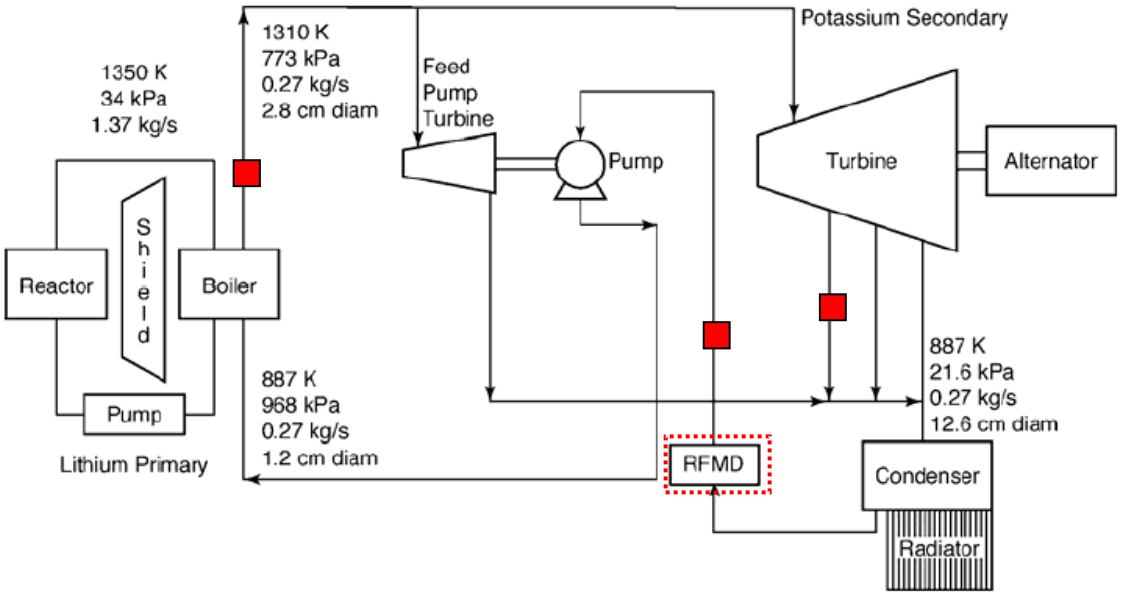

Fig. 24 100 kW(e) ORNL Rankine cycle with state points

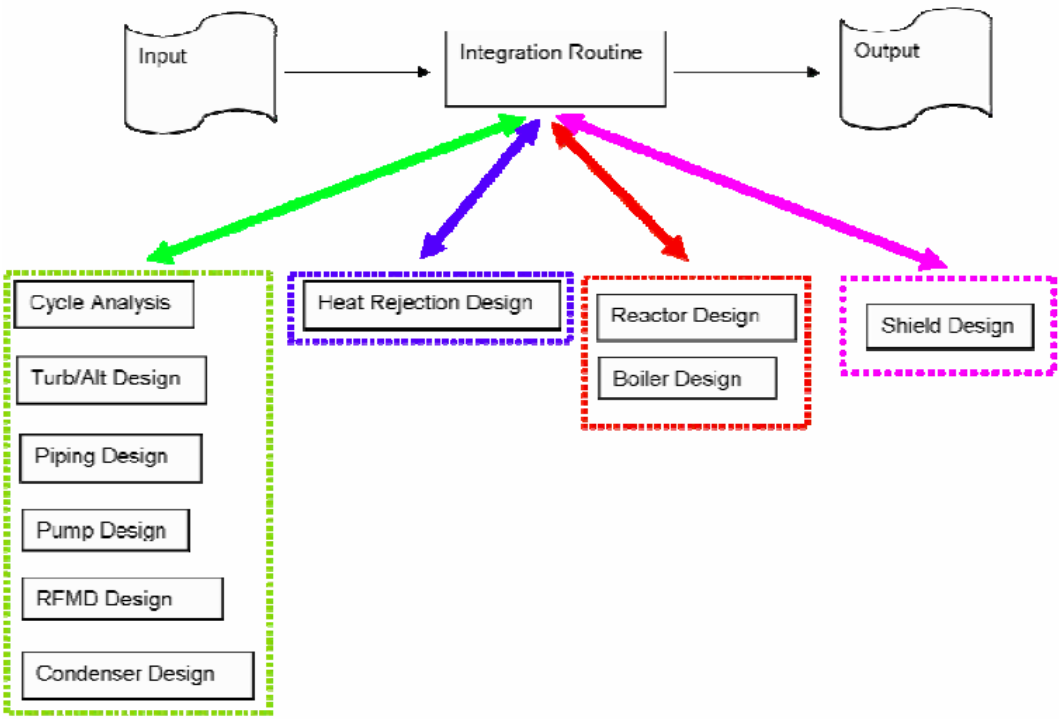

Fig. 25 Diagram showing modular components of ALKASYS-SRPS[23)]

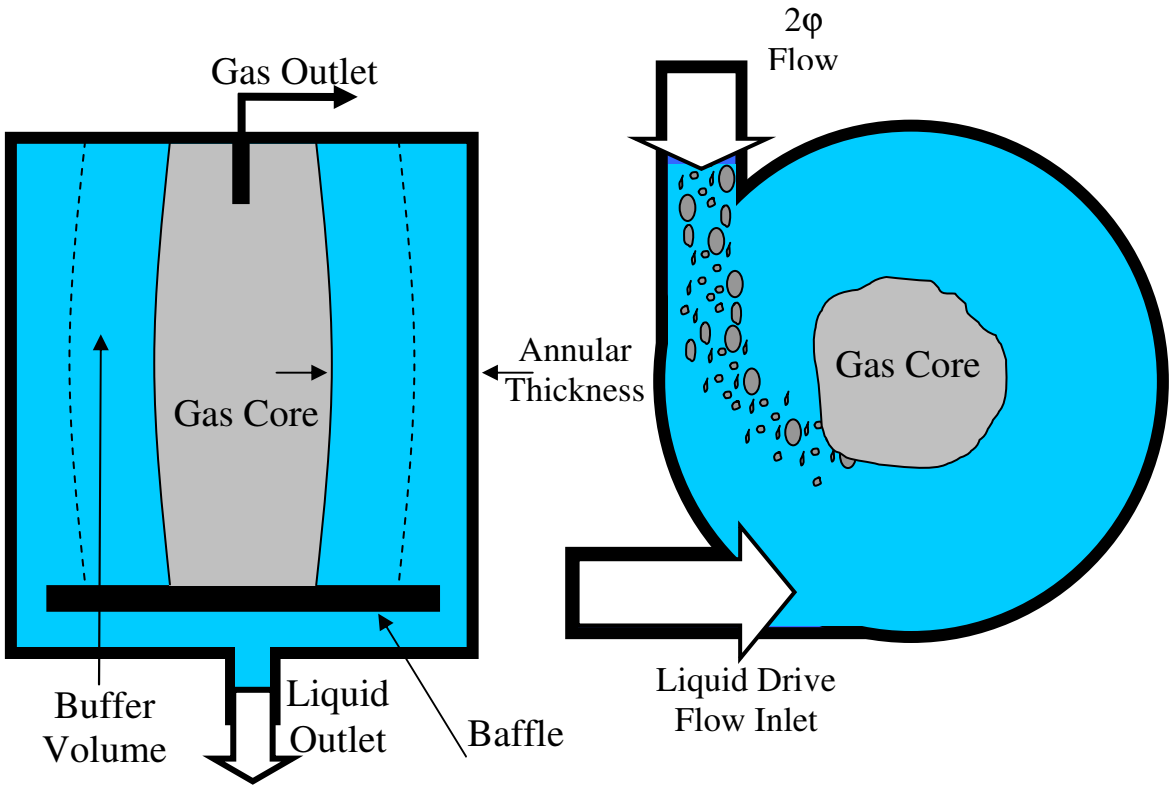

Fig. 26 The Texas A&M University vortex phase separator

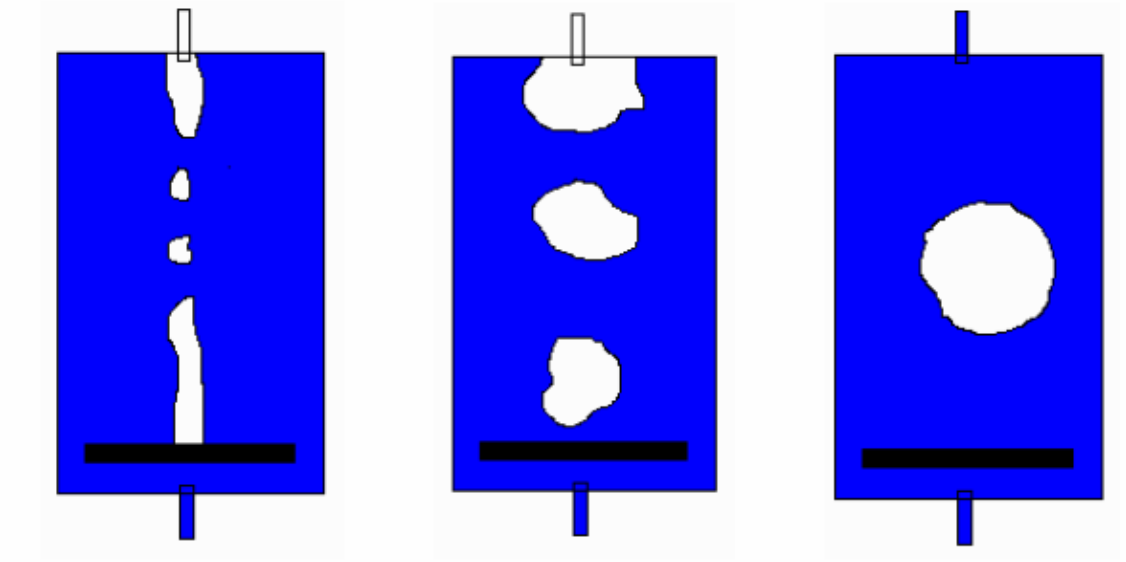

Fig. 27 Various representations of flooding in the MVS

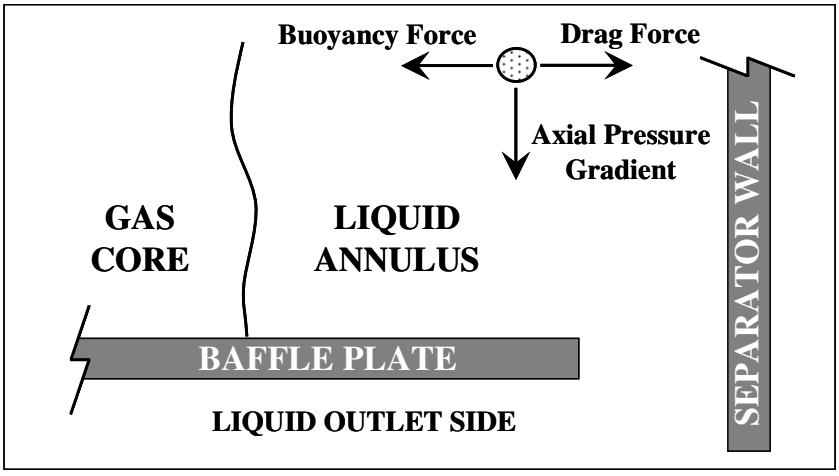

Fig. 28 Forces related to carry under within the MVS

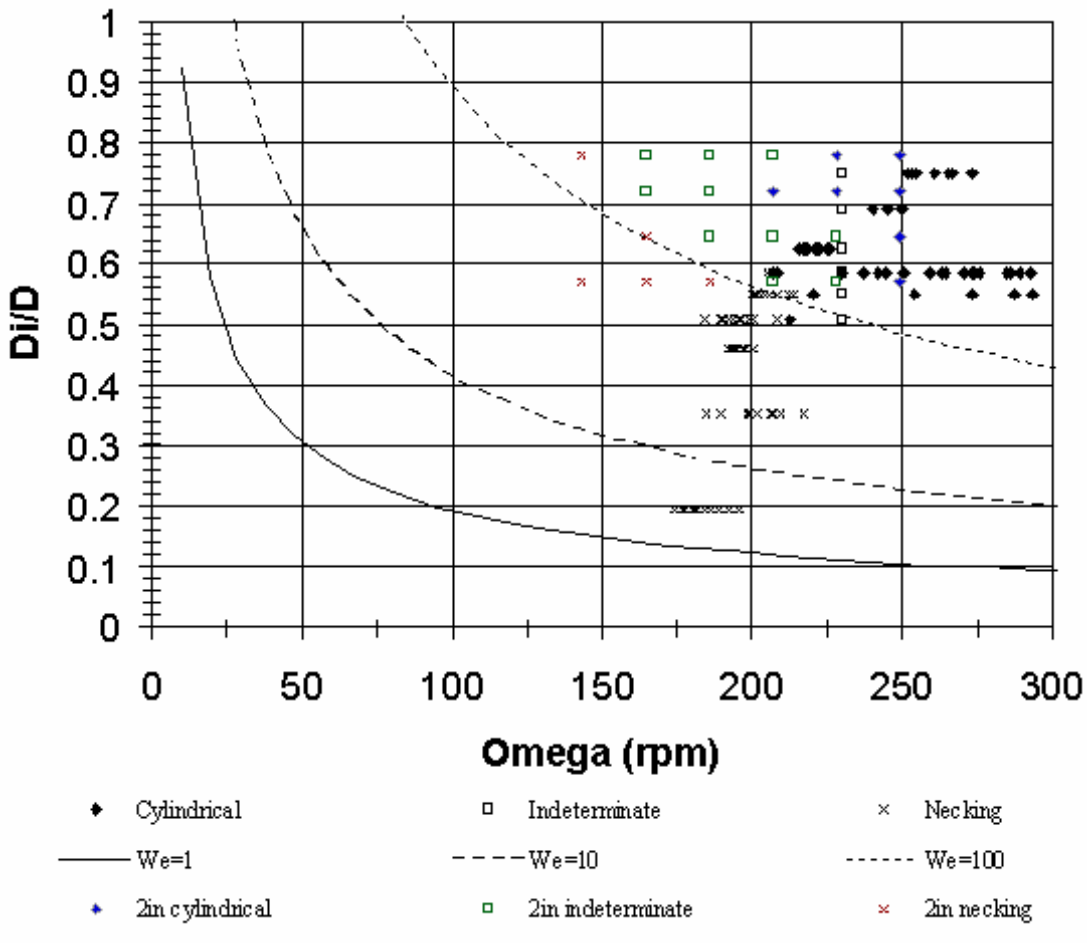

Fig. 29 Hydrodynamic stability of liquid/gas vortices in an air/water system

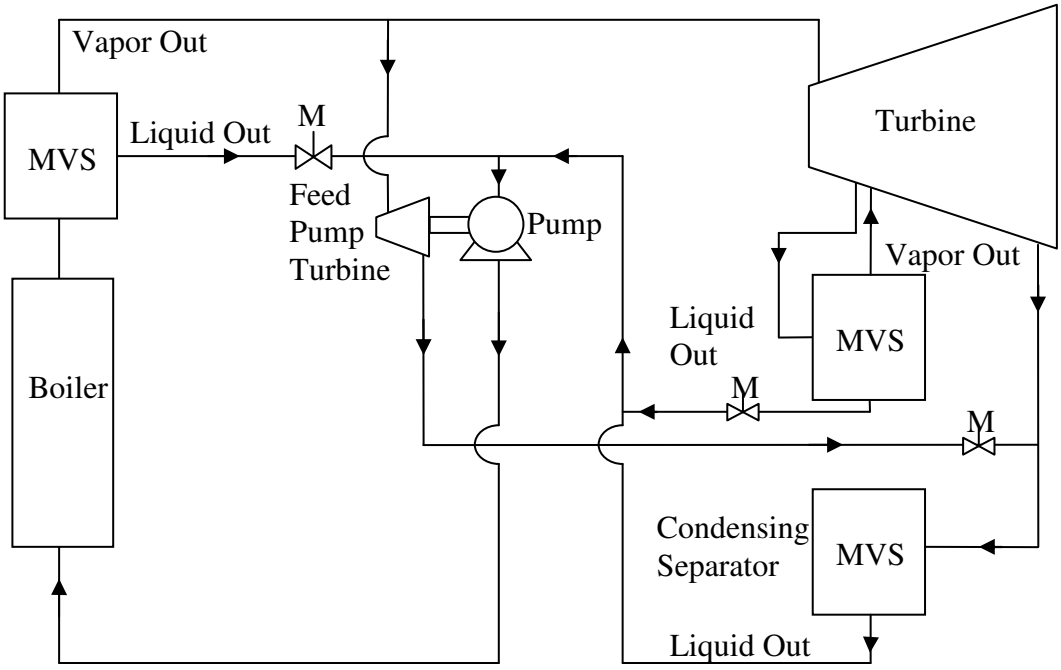

Fig. 30 Proposed MVS locations in a space Rankine cycle

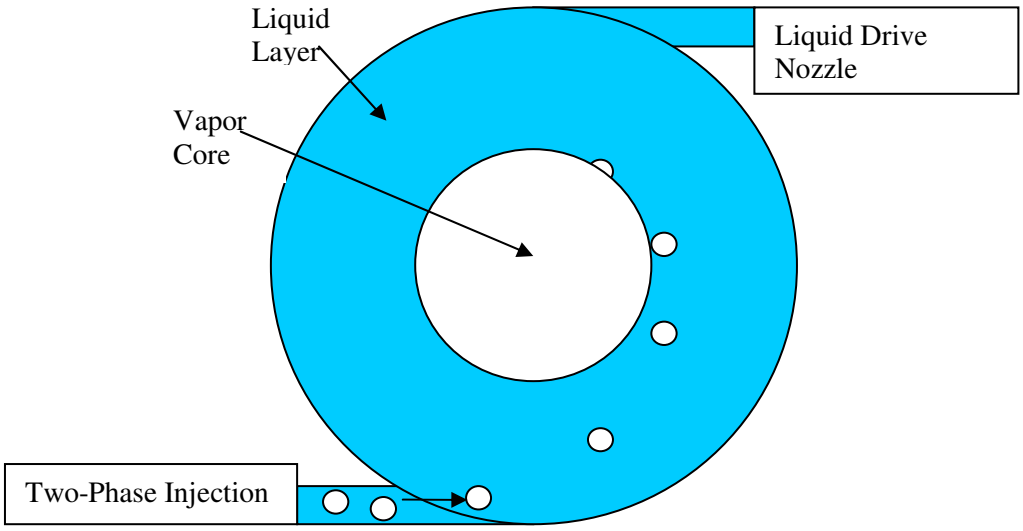

Fig. 31 Conventional TAMU MVS operation

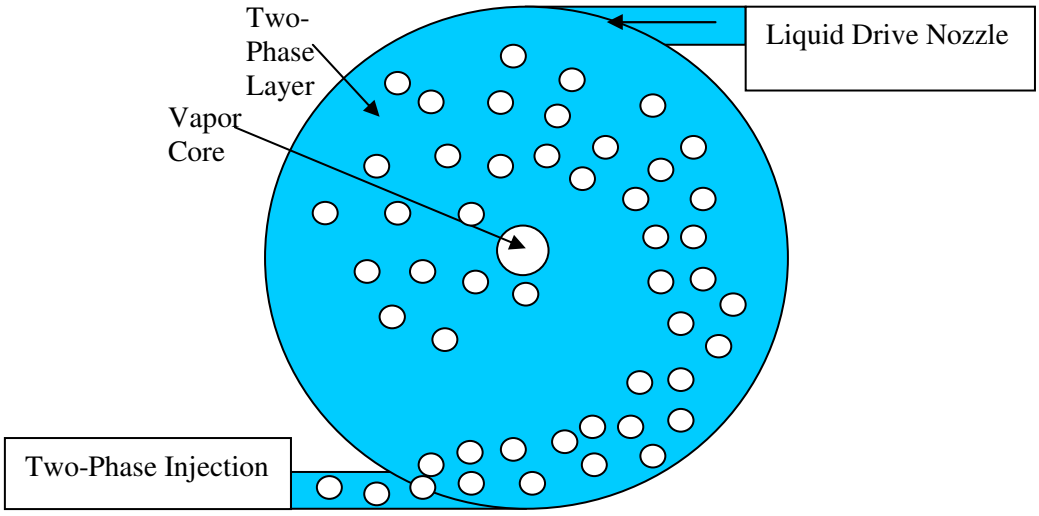

Fig. 32 TAMU MVS separator with high vapor flow rate

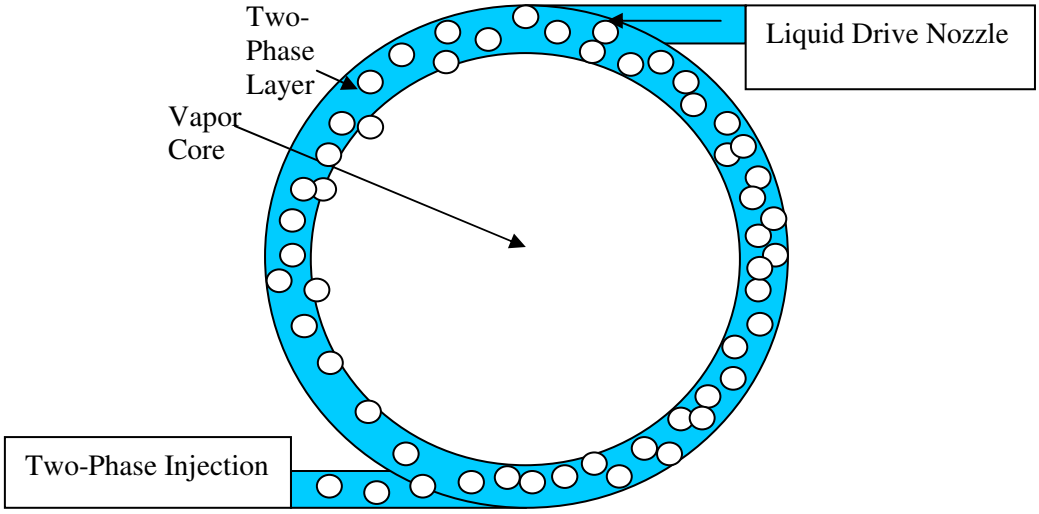

Fig. 33 Effective separator operation with high vapor flow rate

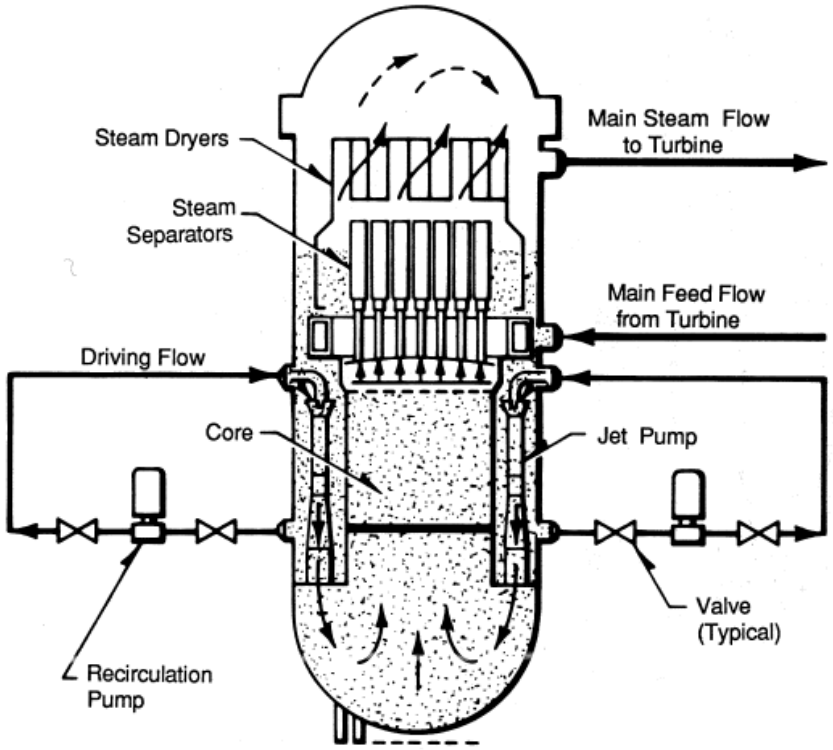

Fig. 34 Steam and recirculation water flow paths in a boiling water reactor[29)]

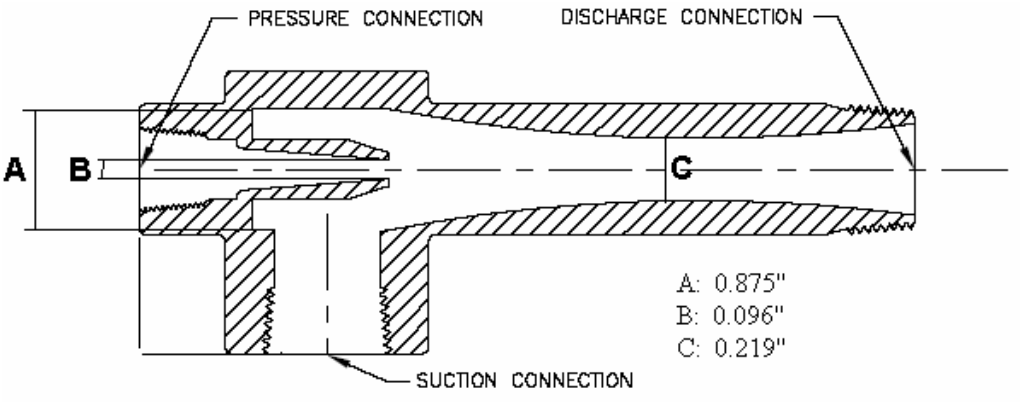

Fig. 35 Liquid eductor dimensions from Rankine test bed

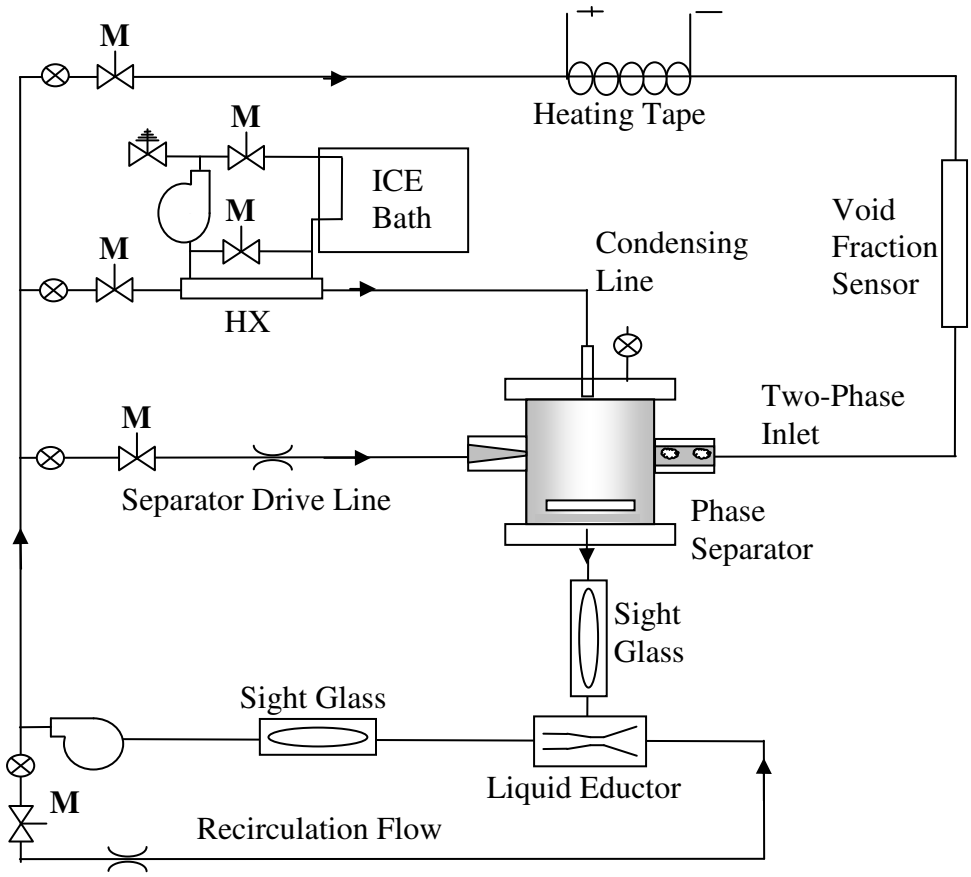

Fig. 36 Simplified schematic of the simulated Rankine cycle test bed

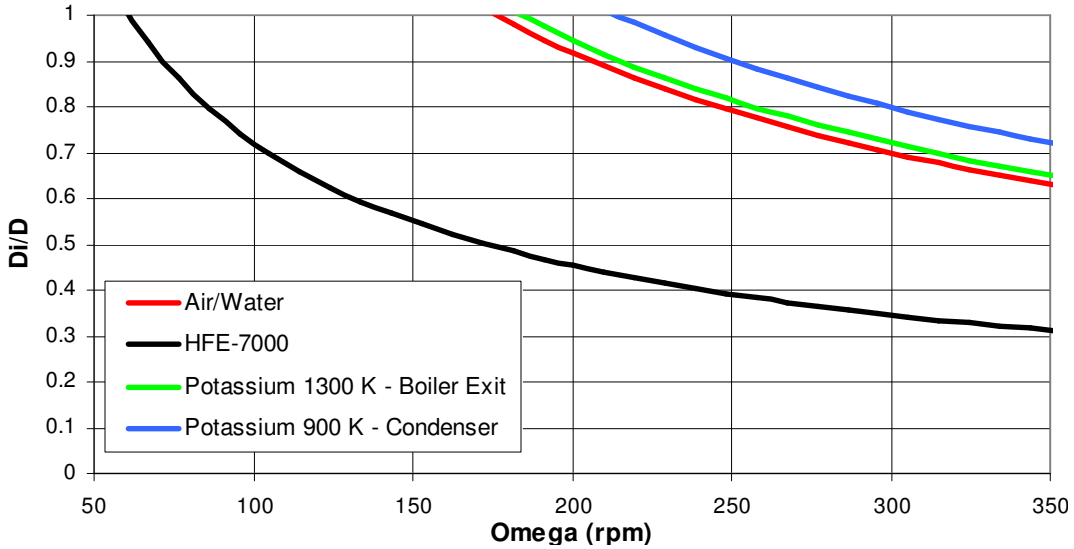

Fig. 37 Weber number contrast for potassium, HFE-7000, and air/water separators

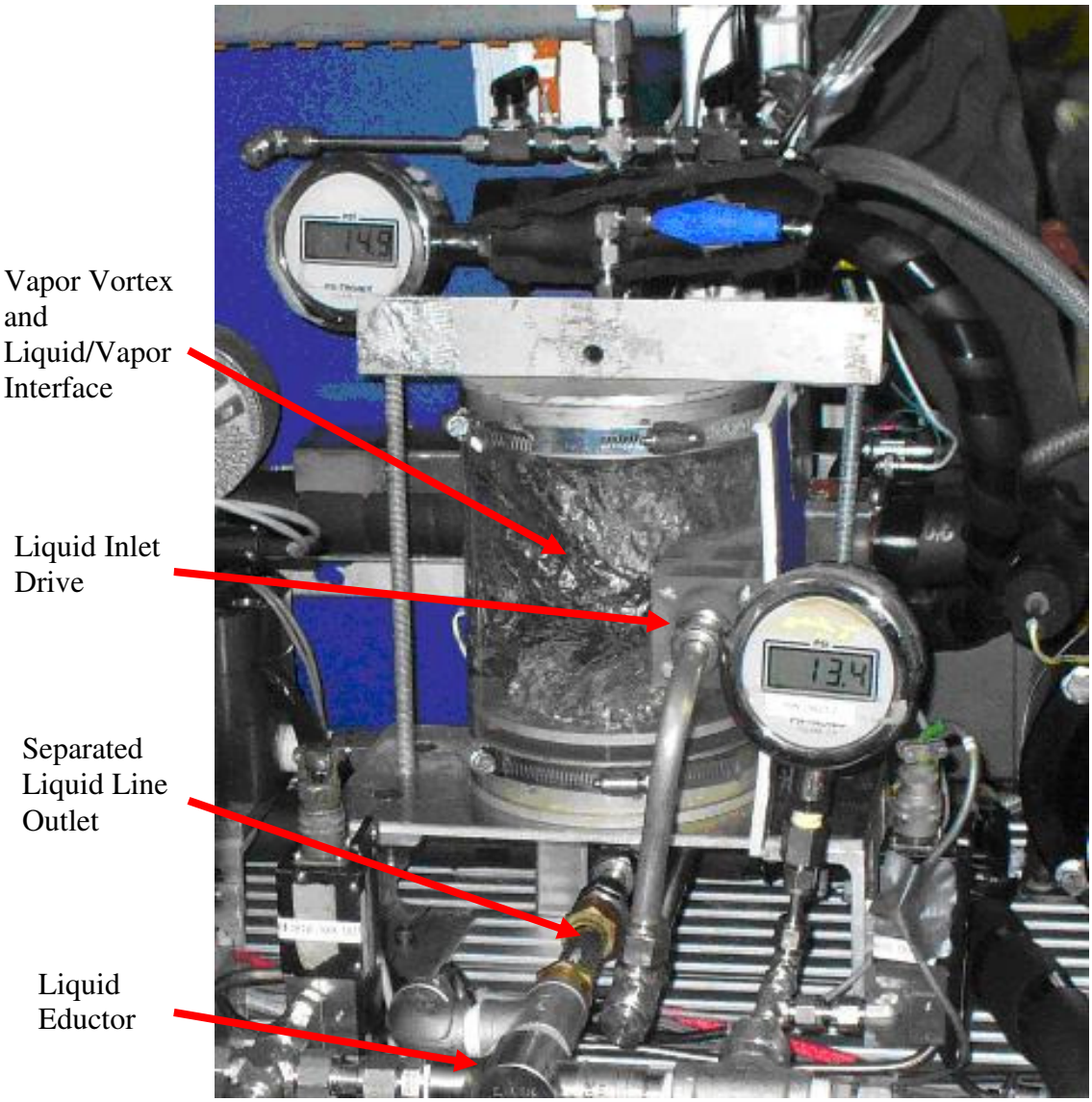

Fig. 38 Saturated separator experiment aboard the NASA aircraft

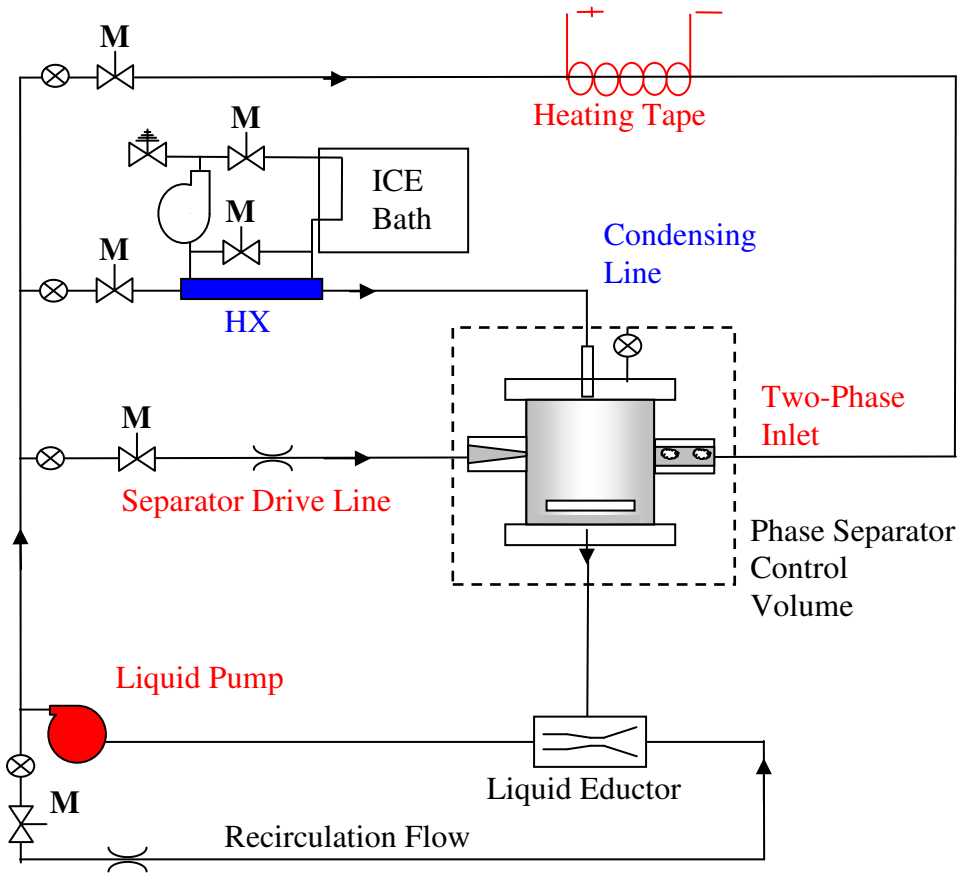

Fig. 39 Separator control volume for energy balance calculations

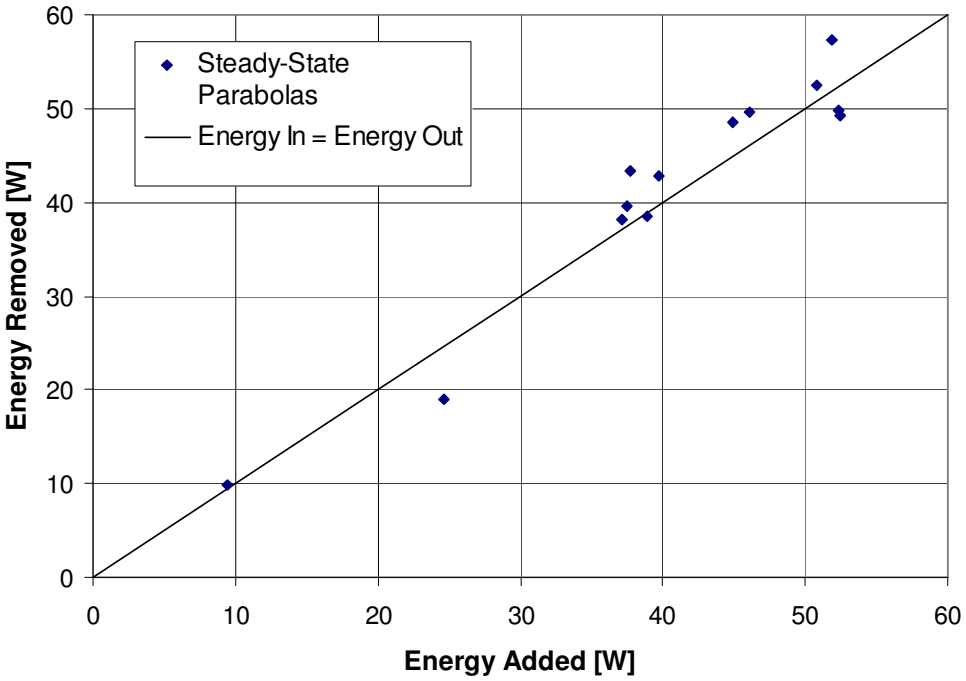

Fig. 40 Steady-state energy balance on the MVS

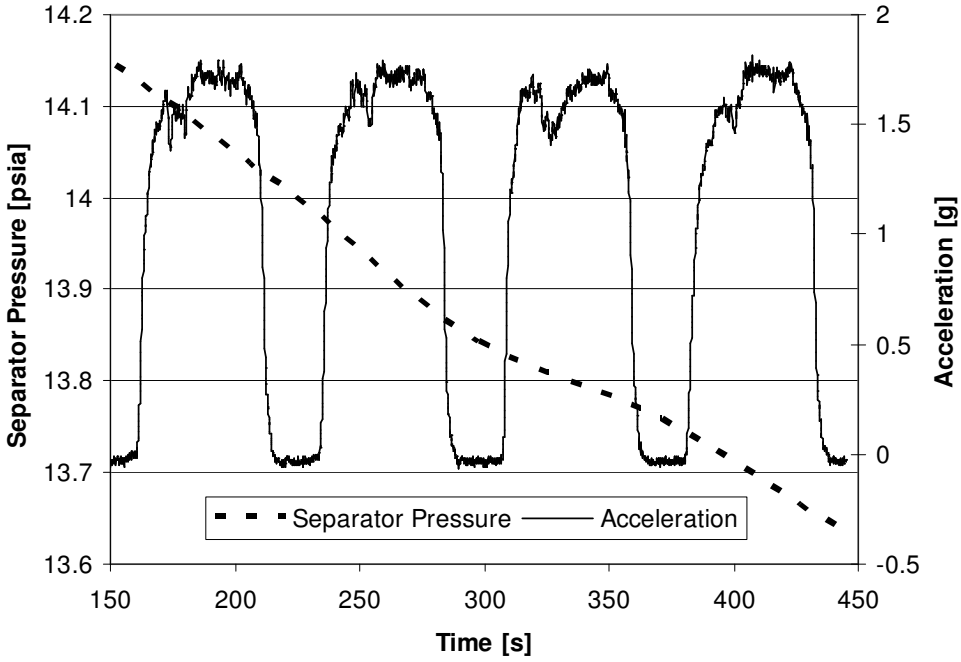

Fig. 41 MVS pressure trace for five parabolas with an average MVS energy removal rate of 50 Watts

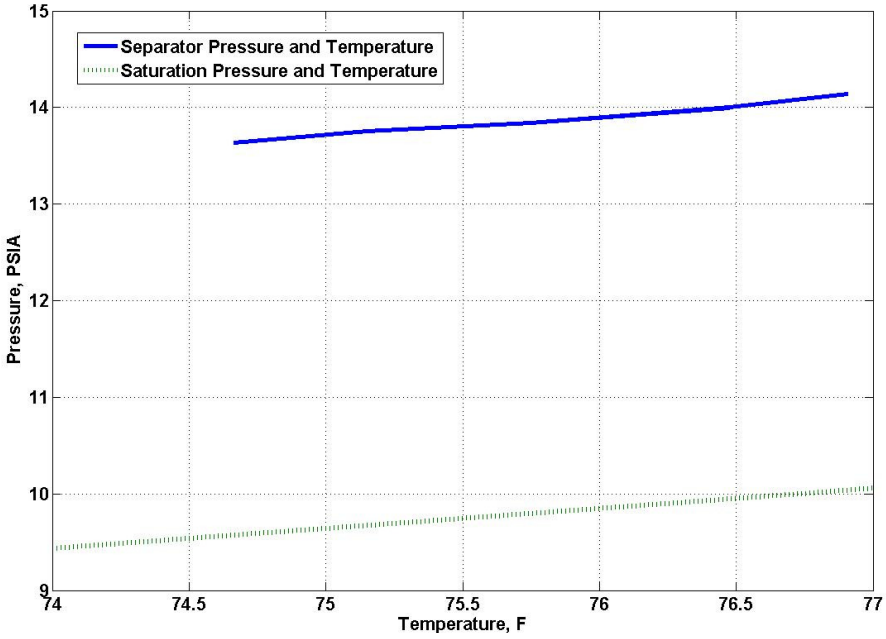

Fig. 42 MVS temperature and pressure for the energy removal period when compared with the saturation curve

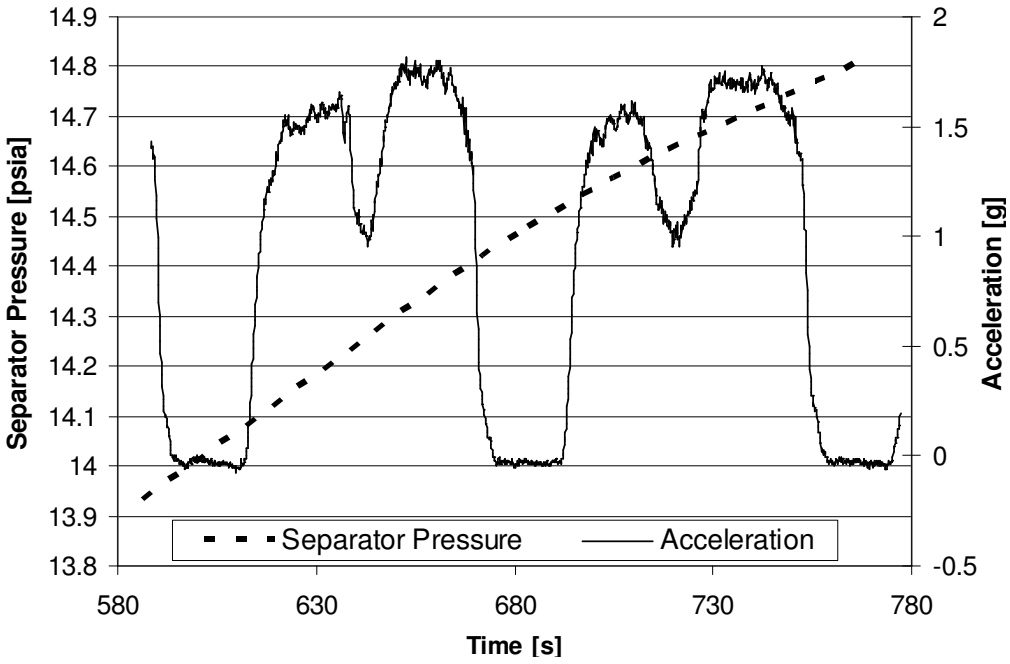

Fig. 43 MVS pressure trace for four parabolas with an average MVS energy addition rate of 60 W

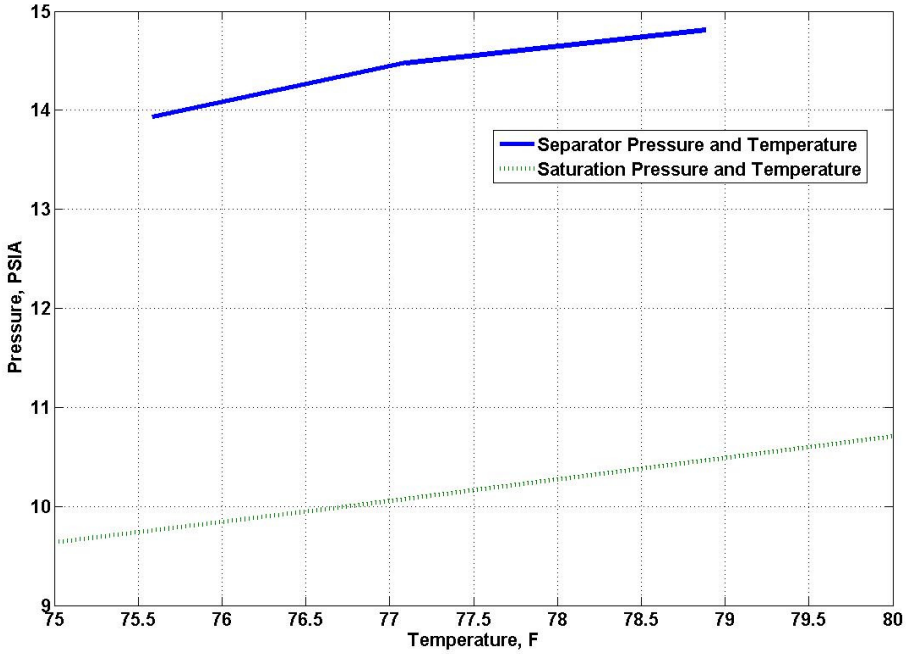

Fig. 44 MVS temperature and pressure for the energy addition period when compared with the saturation curve

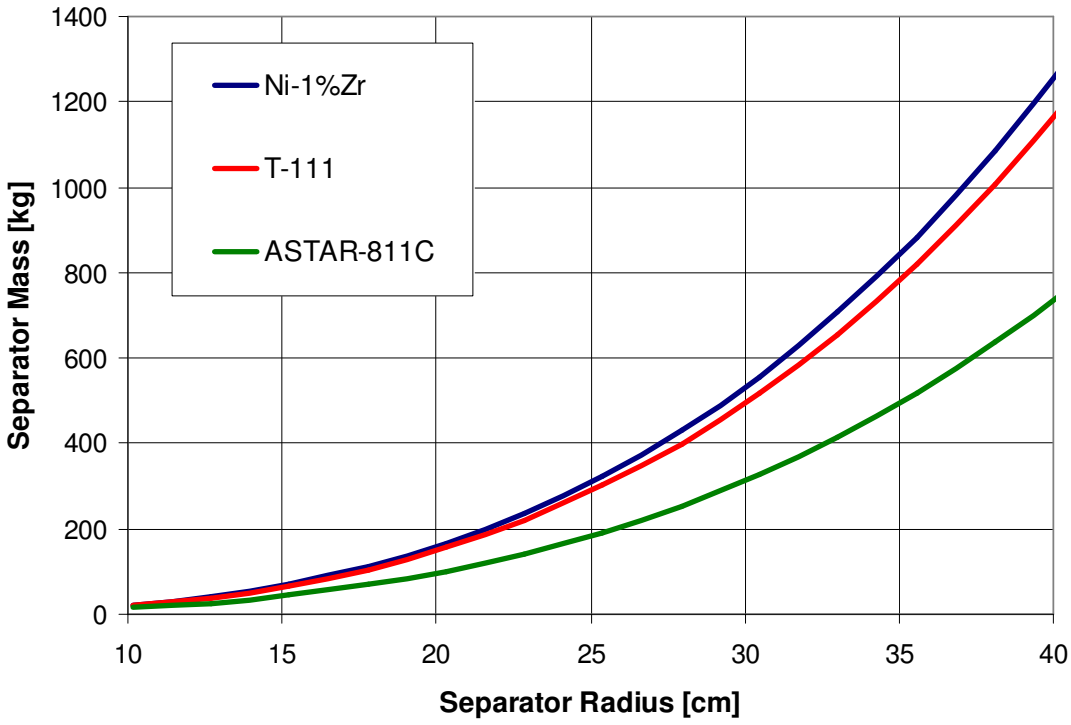

Fig. 45 Separator mass versus radius for operating pressure of 110 psia

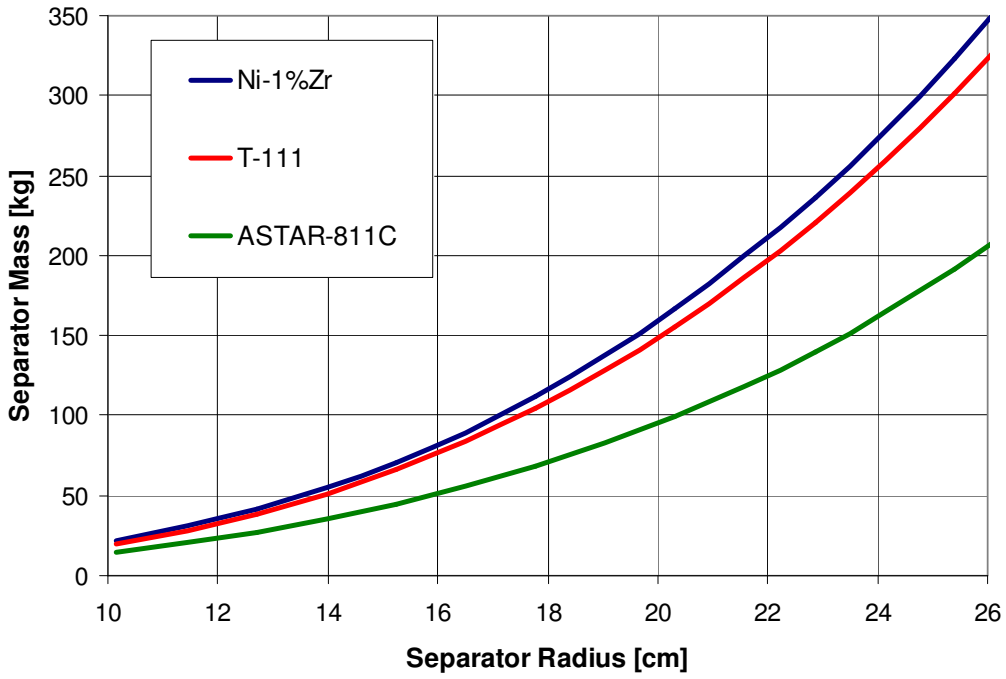

Fig. 46 Separator mass versus radius for operating pressure of 110 psia for diameters between 10 and 26 cm

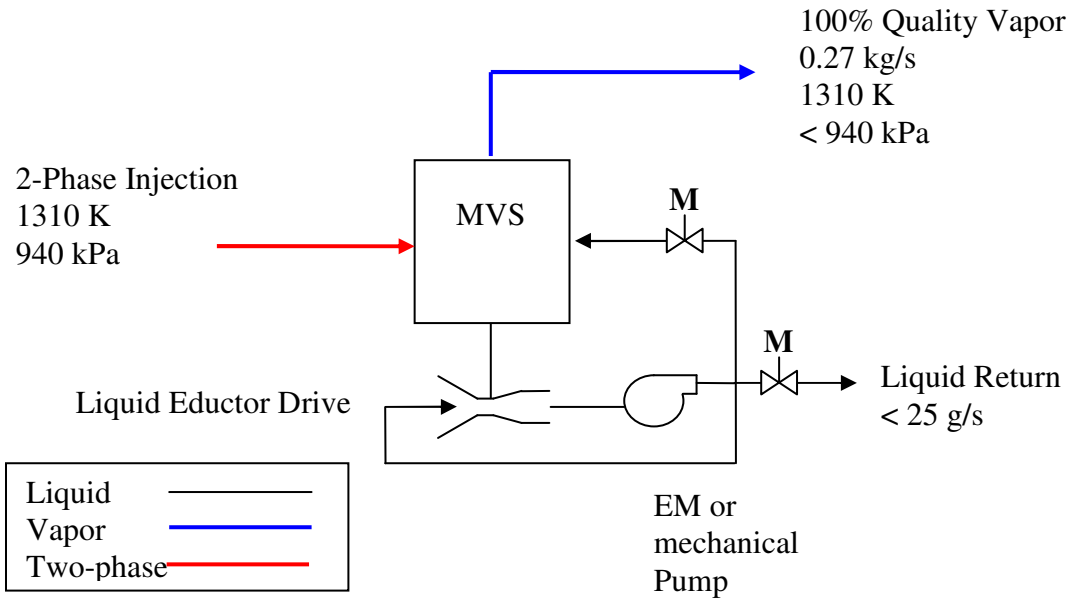

Fig. 47 Separator boiler exit configuration

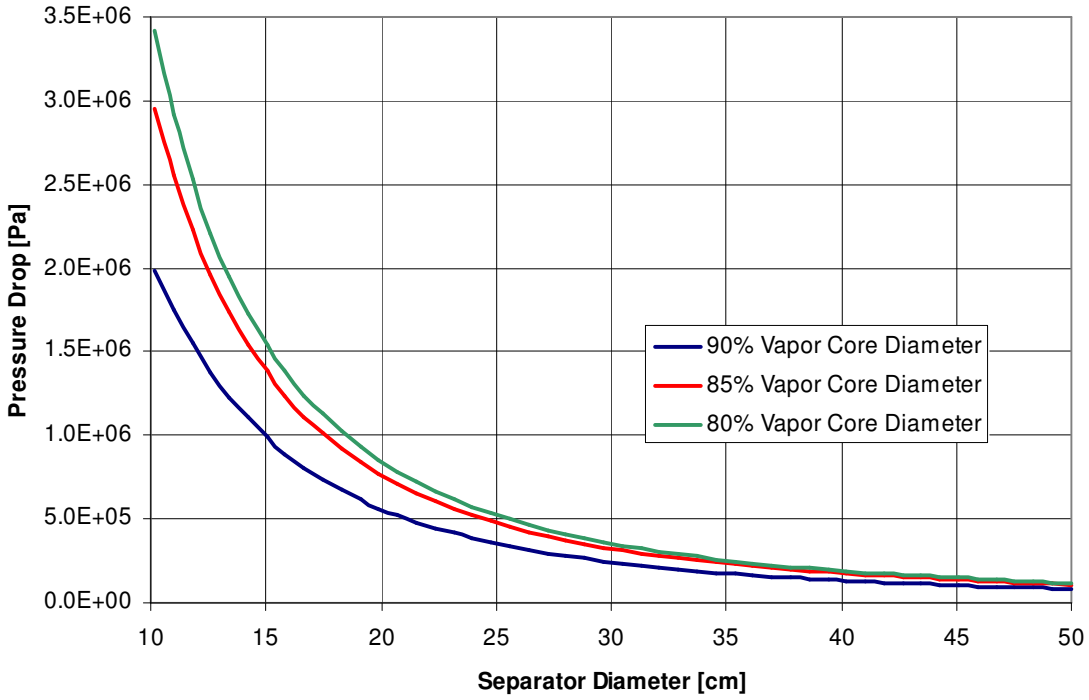

Fig. 48 Separator pressure drop versus separator diameter at 100 kW(e)

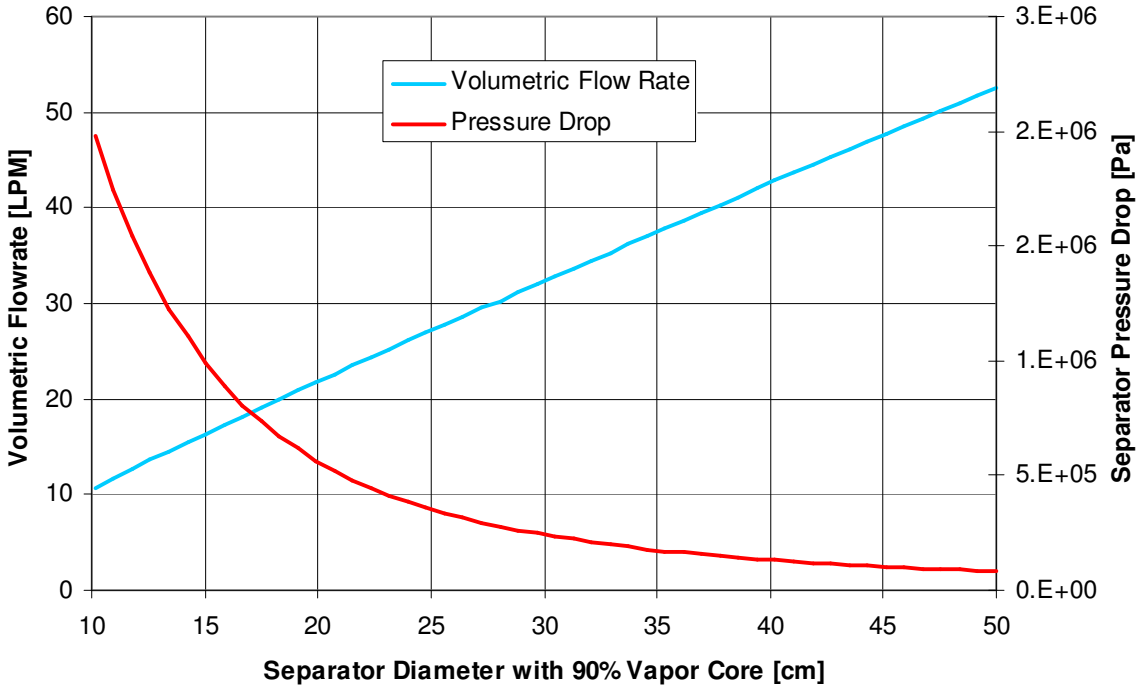

Fig. 49 Separator volumetric flow rate and pressure drop at 100 kW(e)

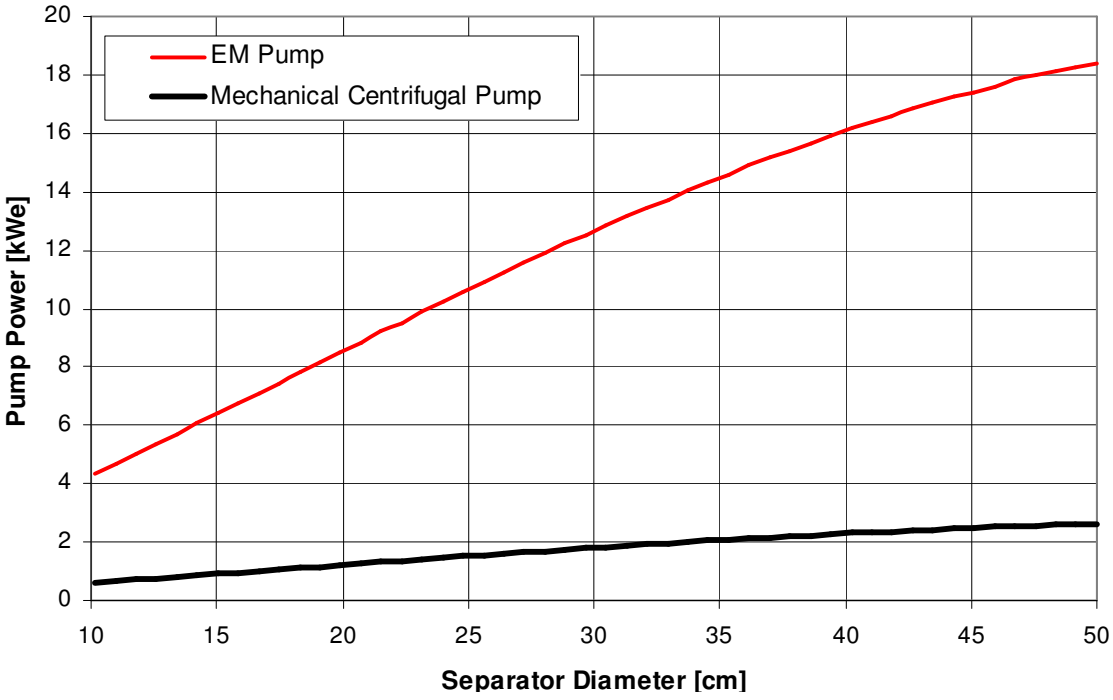

Fig. 50 Pumping power versus separator diameter at 100 kW(e)

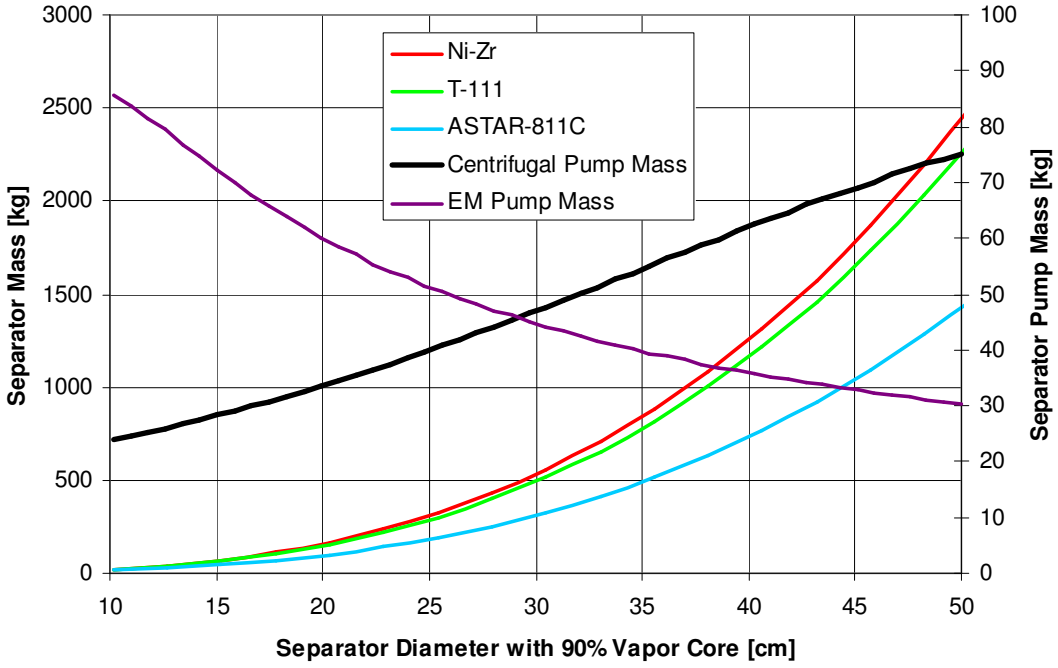

Fig. 51 Separator mass and pump mass versus diameter at 100 kW(e)

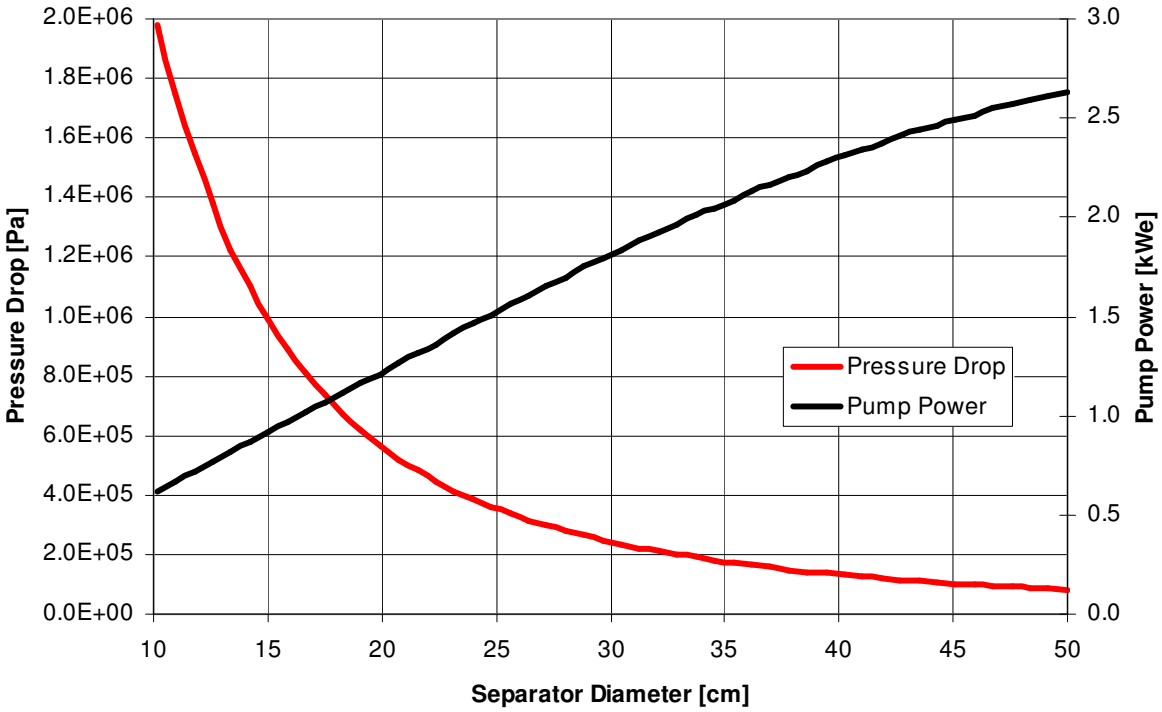

Fig. 52 Separator pressure drop and pump power versus separator diameter with 90% vapor core at 100 kW(e)

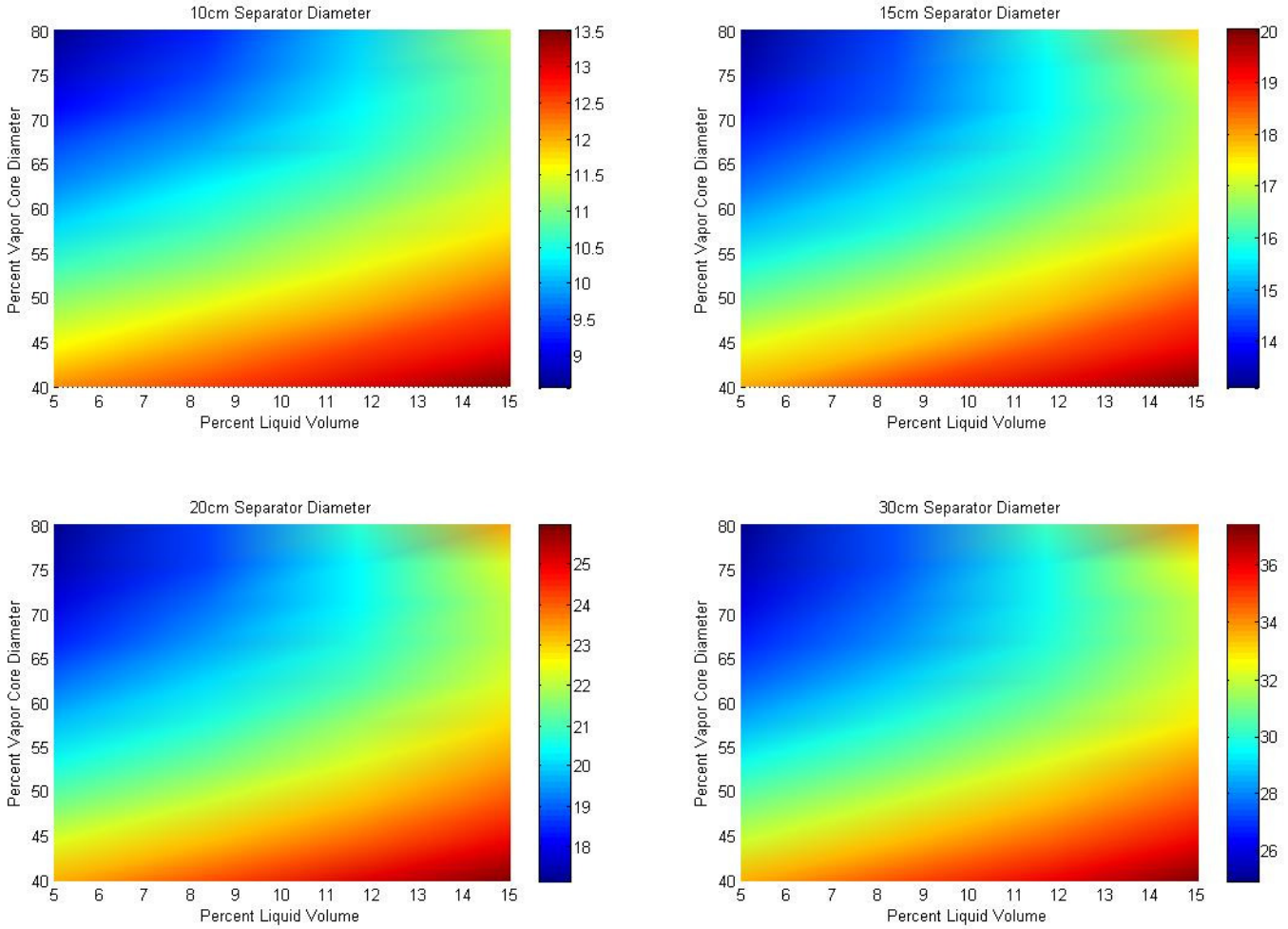

Fig. 53 Separator flow rate in LPM versus vapor core diameter and liquid volume at 100 kW(e)

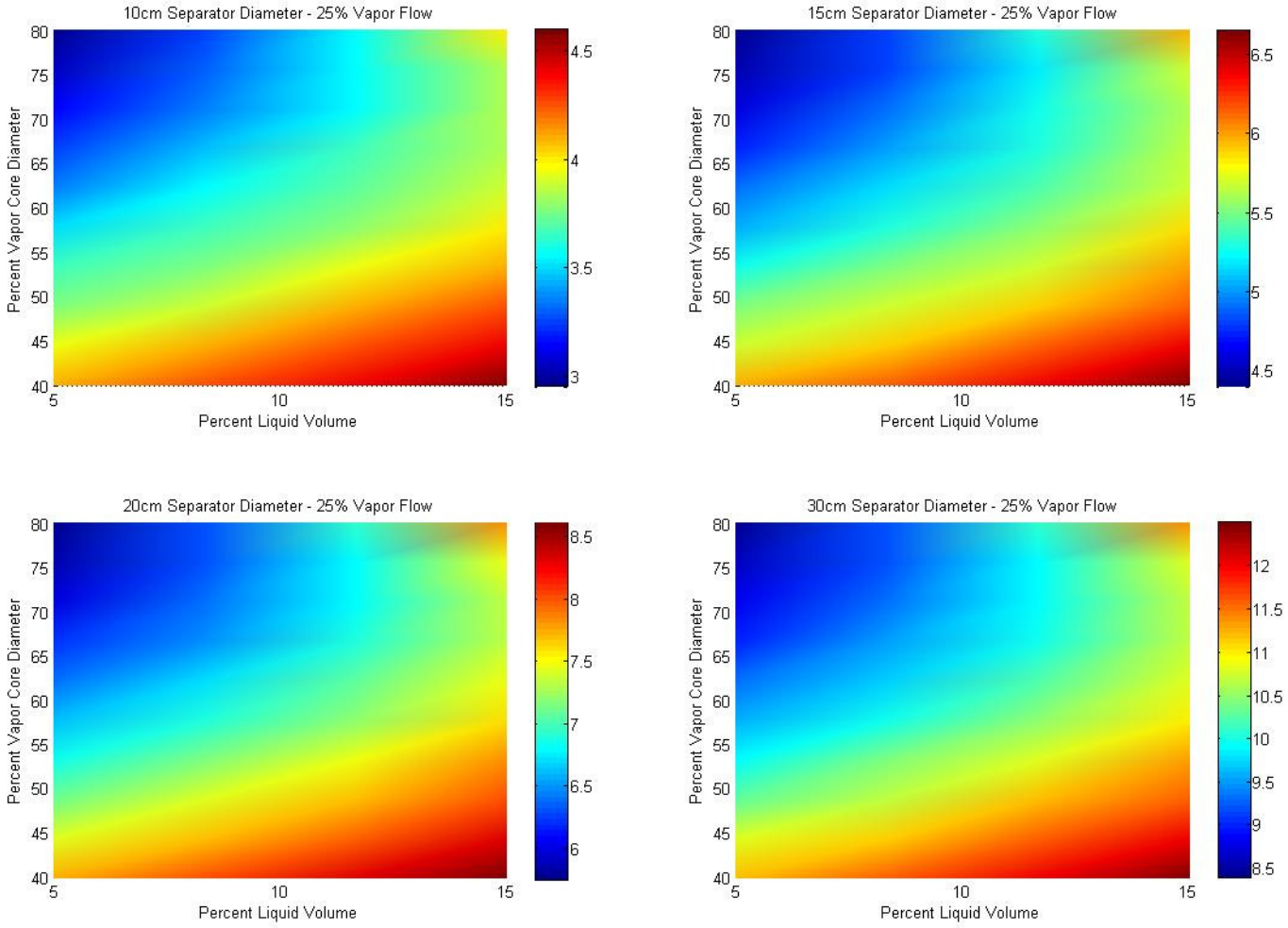

Fig. 54 Separator liquid flow rate in LPM with 25% vapor flow rate at 100 kW(e)

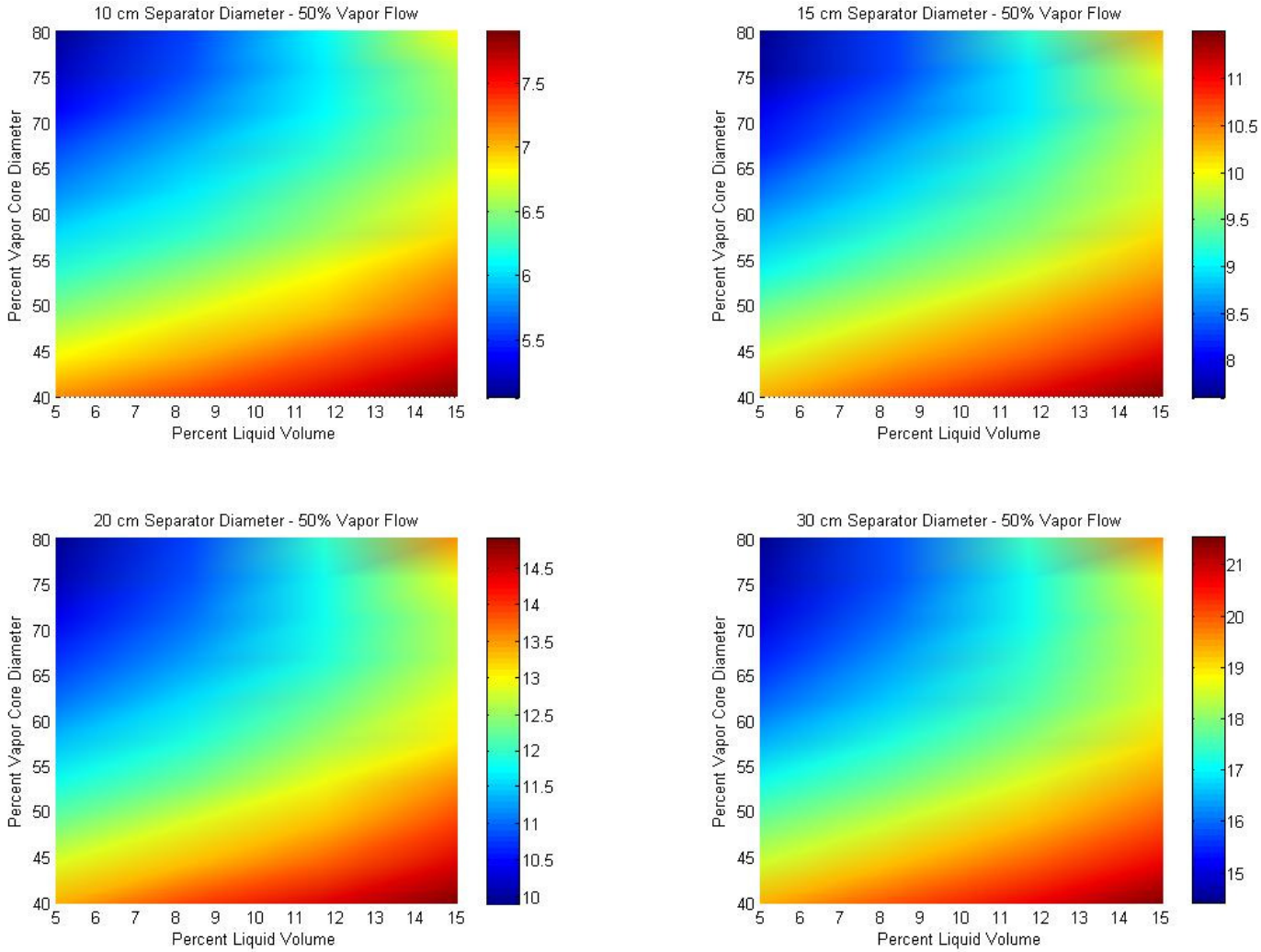

Fig. 55 Separator liquid flow rate in LPM with 50% vapor flow rate at 100 kW(e)

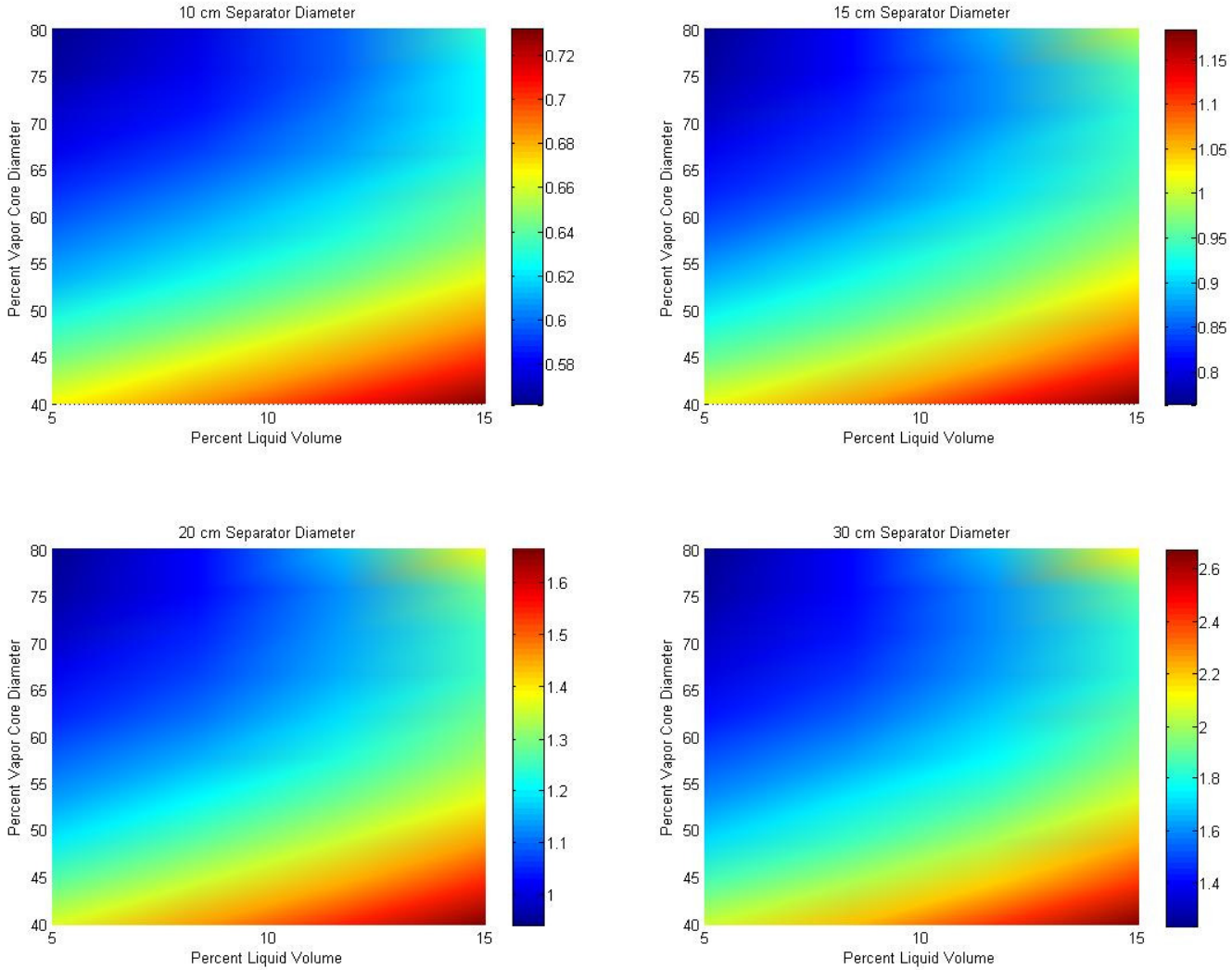

Fig. 56 Separator pumping power in kW(e) versus vapor core diameter and liquid volume

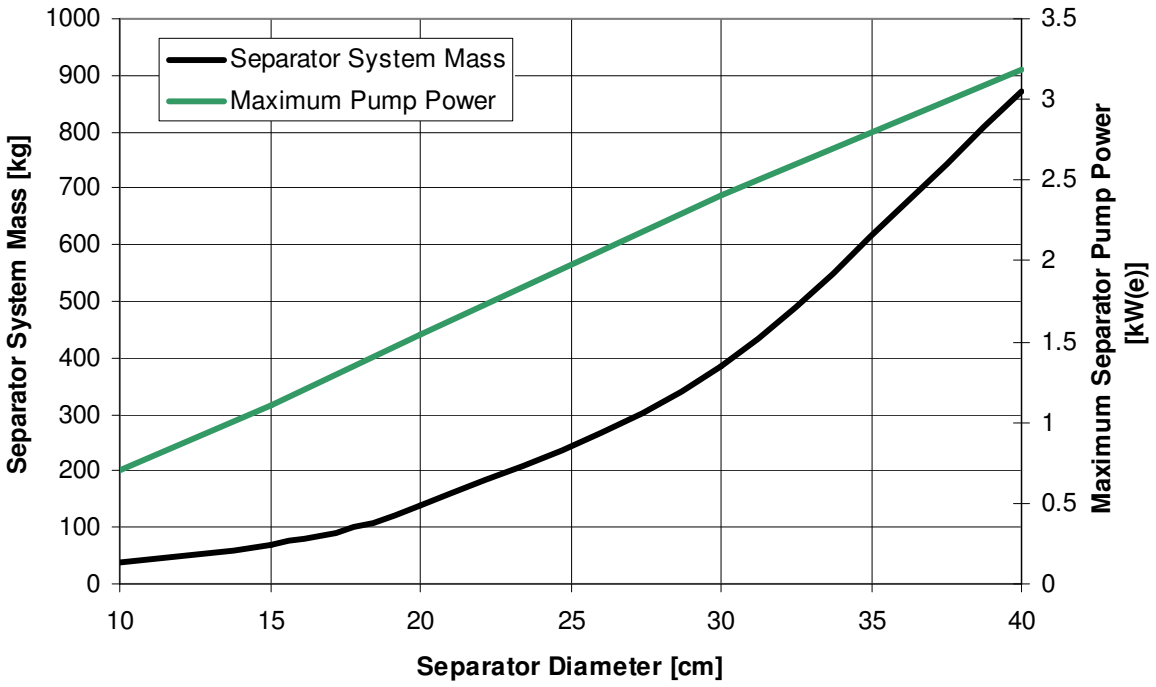

Fig. 57 Separator system mass and pumping power versus separator diameter

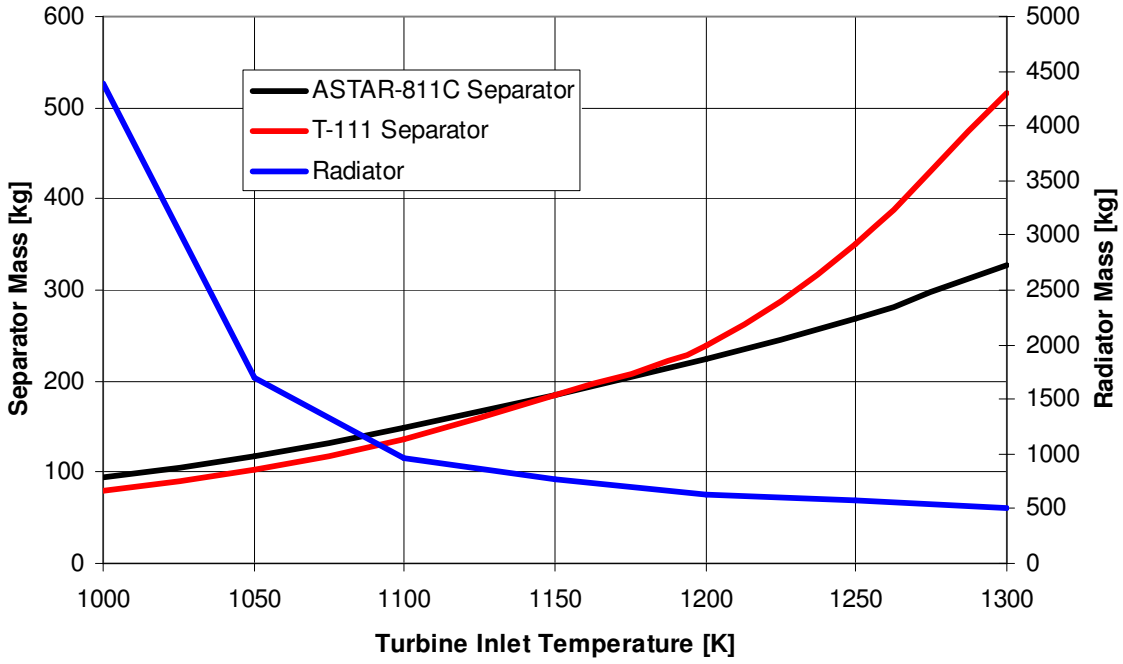

Fig. 58 Separator and radiator mass versus turbine inlet temperature

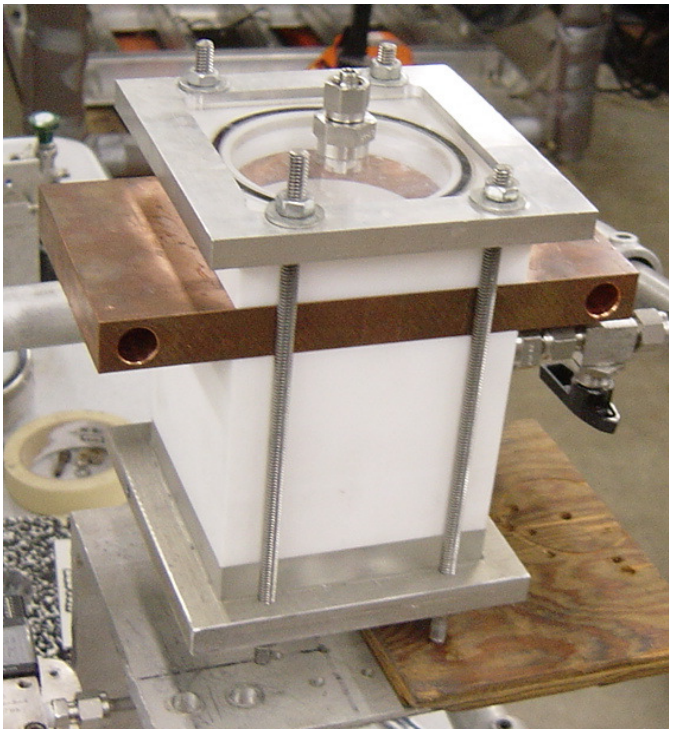

Fig. 59 Boiling vortex phase separator concept

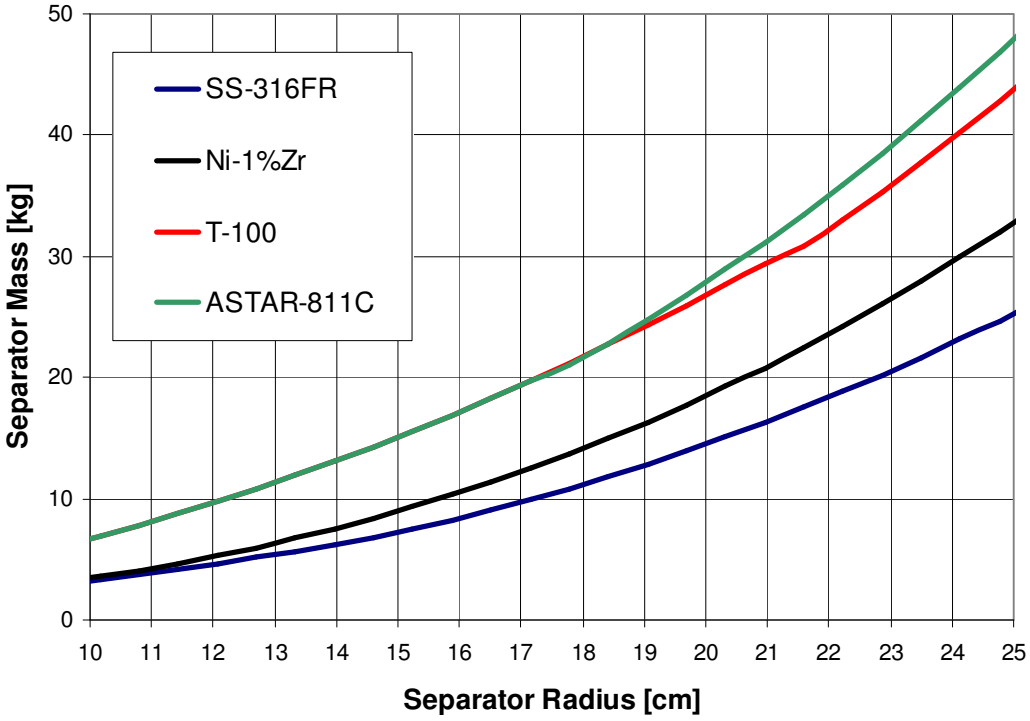

Fig. 60 Separator mass versus radius for operating pressure of 3 psia

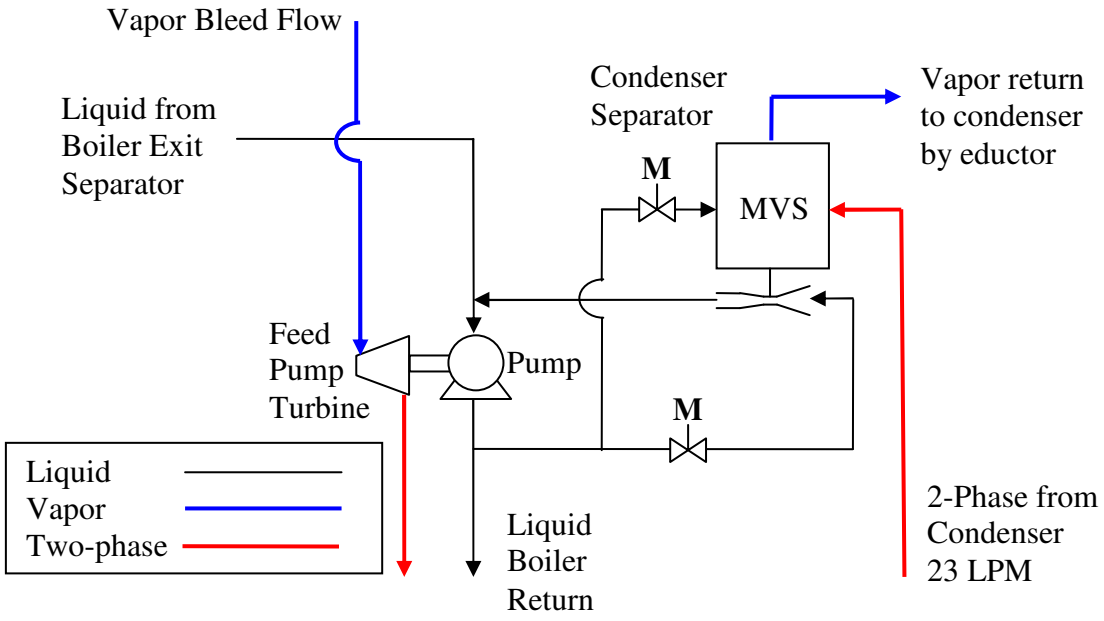

Fig. 61 Separator condenser configuration

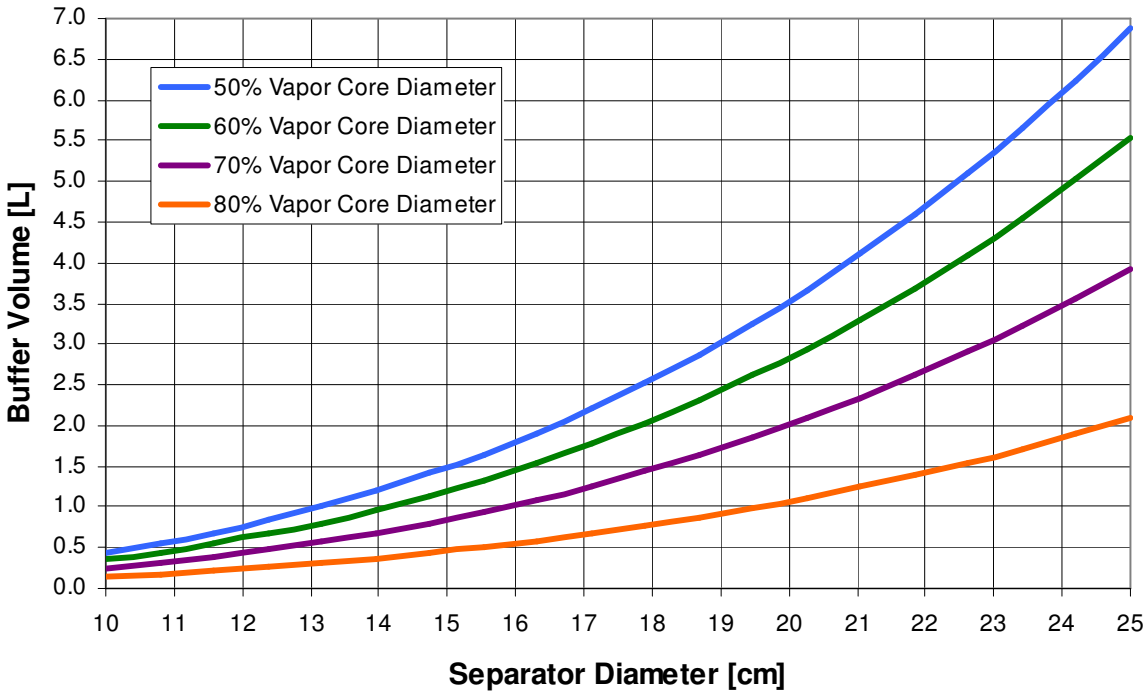

Fig. 62 Buffer volume of the condenser

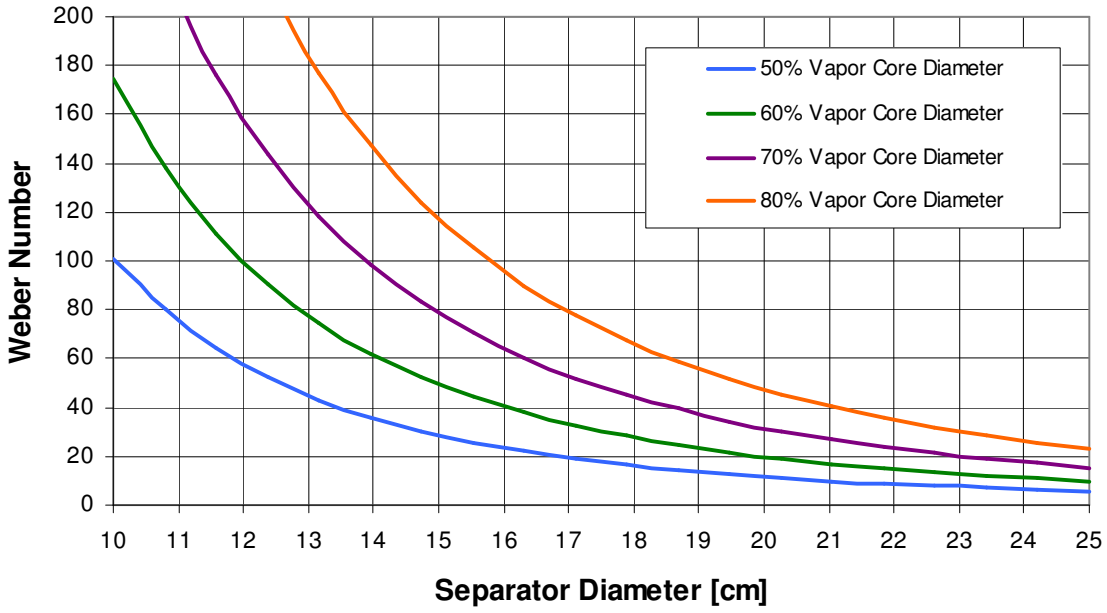

Fig. 63 Condenser separator Weber number for a pump power of 1 kW

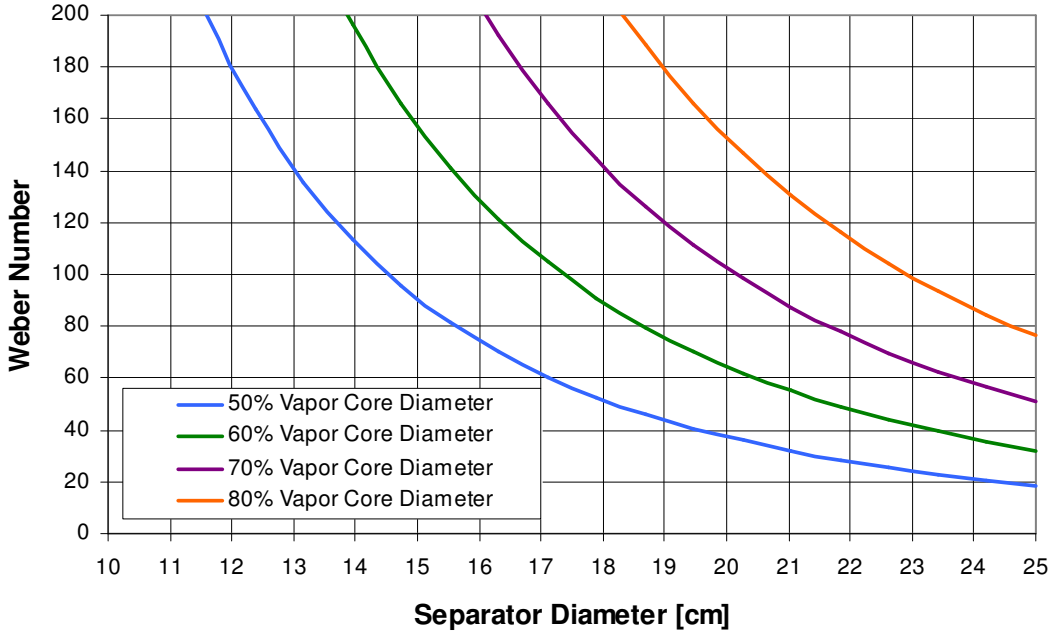

Fig. 64 Condenser separator Weber number for a pump power of 1.1 kW

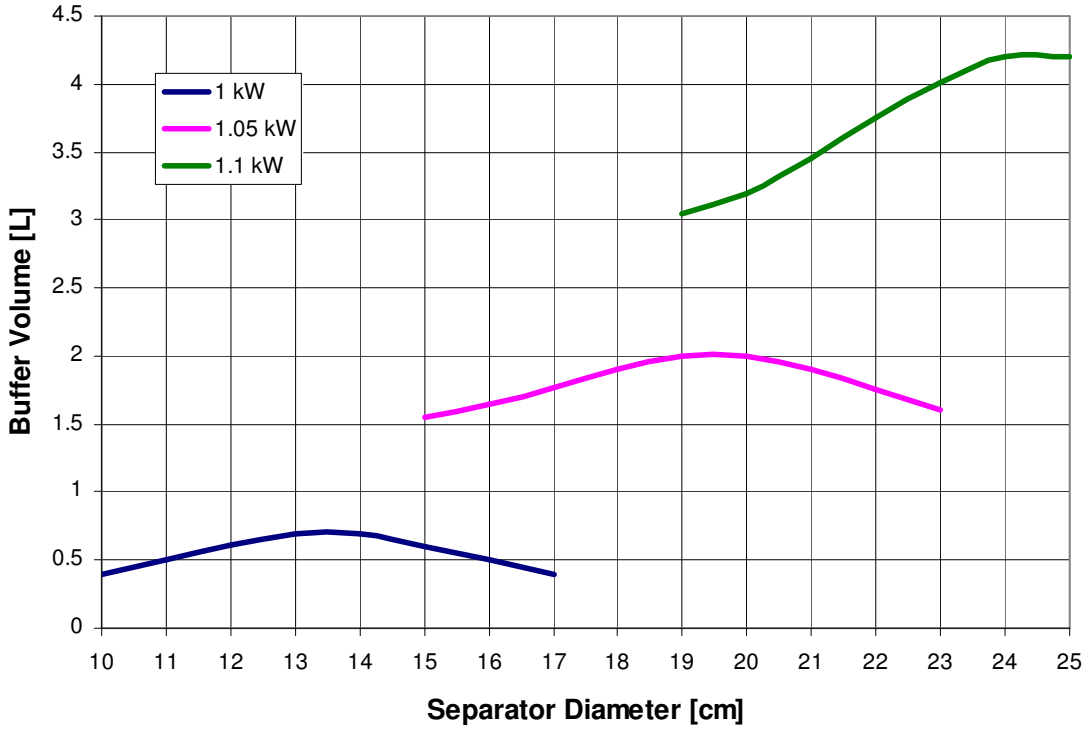

Fig. 65 Buffer volume versus separator diameter for various feed pumping powers

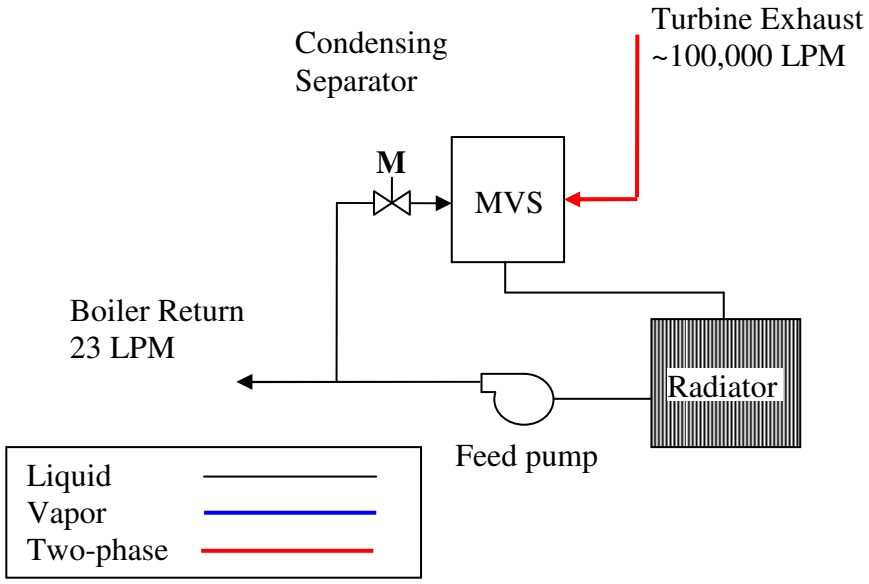

Fig. 66 Sub-cooled separator condenser concept

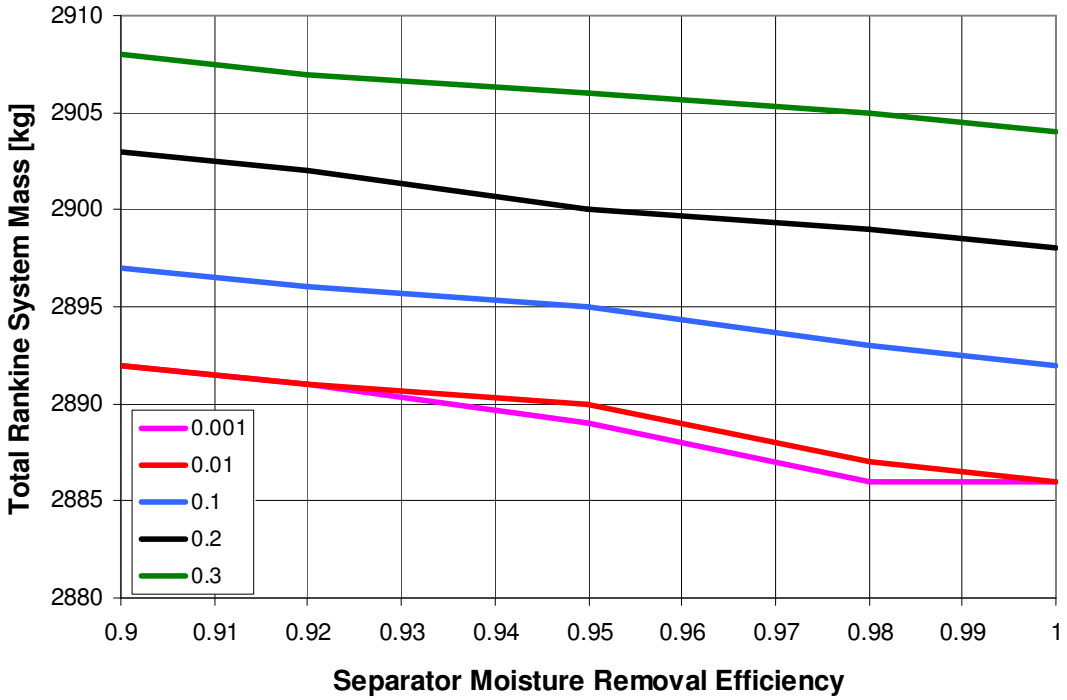

Fig. 67 100 kW(e) external turbine separator efficiency study

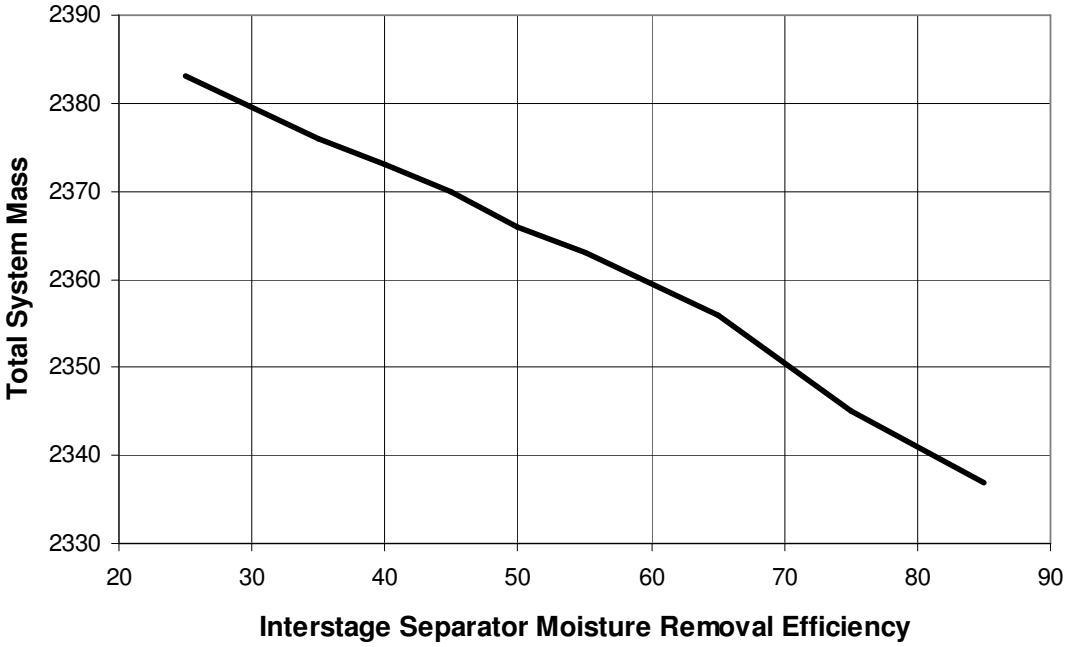

Fig. 68 Total system mass versus interstage separator efficiency

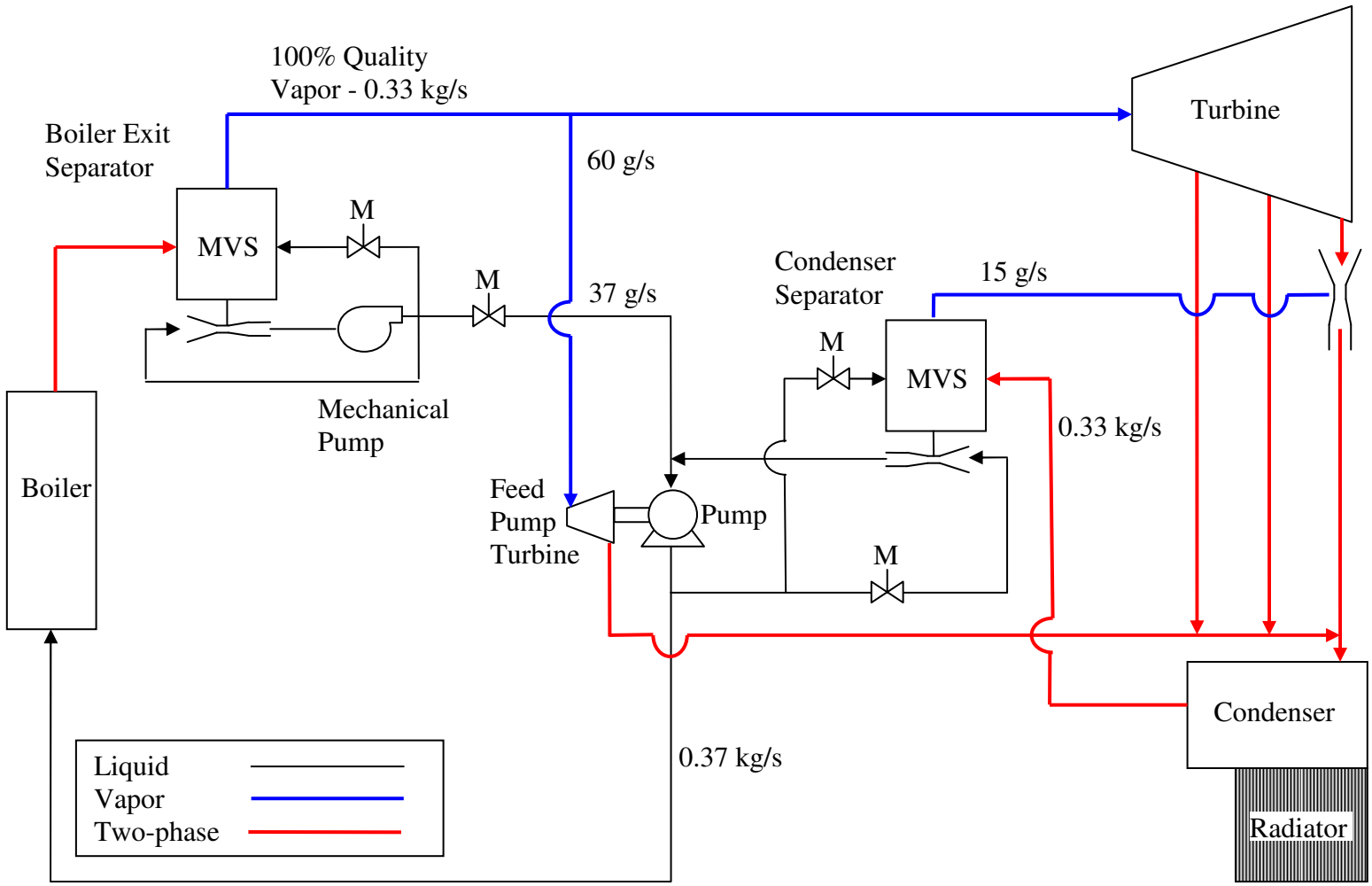

Fig. 69 Rankine cycle piping schematic with passive vortex phase separation

APPENDIX B

B.1 Saturated Potassium Thermodynamic Calculator

FORTRAN 77/90

```
PROGRAM Potassium
      IMPLICIT REAL*4 (A-Z)
      CHARACTER ans

      WRITE(*,*)'Saturated Potassium Properties from T or P?'
      READ(*,*)ans

      IF ((ans .EQ. 't') .OR. (ans .EQ. 'T')) THEN
      WRITE(*,*)'Enter potassium temperature (K),'
      READ(*,*)T
C     converts to Rankine
      T=T*1.8
      TR=T
      CALL KTHERM(T,P,VF,VG,HF,HG,HFG,SF,SG,SFG,SIG)
      CALL KXPORT(TR,MU,K,CP)

      ELSE
      WRITE(*,*)'Enter Potassium Pressure (kPa), '
      READ(*,*)P
C     converts from kPa to ATM
      P=P*0.009869233
      CALL TFROMP(P,TEMP)
      T=TEMP
      TR=T
      CALL KTHERM(T,P,VF,VG,HF,HG,HFG,SF,SG,SFG,SIG)
      CALL KXPORT(TR,MU,K,CP)

      ENDIF

C     Convert units to SI
      RHOG=1/VG*16.018
      RHOF=1/VF*16.018
      T=T/1.8
      P=P/0.009869233
      MU=MU*0.0004134
      CP=CP*4.1868
      K=K*1.73
      WRITE(*,*)'Temperature (K), ',T
      WRITE(*,*)'Pressure (kPa), ',P
      WRITE(*,*)'Vapor Density (kg/m^3), ',RHOG
      WRITE(*,*)'Liquid Density (kg/m^3), ',RHOF
      WRITE(*,*)'Liquid Viscosity (Pa-s), ',MU
      WRITE(*,*)'Specific Heat Capacity (kJ/kg-K), ',CP
      WRITE(*,*)'Thermal Conductivity (W/m-K),',K
      WRITE(*,*)'Surface Tension (N/m), ',SIG

      STOP
      END

C     ******************SUBROUTINE KTHERMO**********************
C     KTHERM RETURNS THERMODYNAMIC PROPERTIES OF POTASSIUM FROM T
C
      SUBROUTINE KTHERM(T,P,VF,VG,HF,HG,HFG,SF,SG,SFG,SIG)
      IMPLICIT REAL*4 (A-Z)
```

```
      INTEGER N1
      CHARACTER FLUID
C       T [Rankine]
      FLUID="POTASSIUM"
 6015 P=EXP(14.10927-18717.2/T-.53299*LOG(T))
C       VF unit = ft^3/lb
      VF=1/(52.768-.0074975*(T-460)-5.255E-07*(T-460)**2
     &   +4.98E-11*(T-460)**3)
      B=-1*ABS(EXP(-8.931+11261.2/T+LOG(T)))
      B1=-1*ABS(EXP(-8.931+11261.2/(2+T)+LOG(2+T)))
      DBDT=(B1-B)/2.
      C=EXP(1.35231+14703.6/T)
      C1=EXP(1.35231+14703.6/(T+2))
      DCDTX=(C1-C)/2.
      D=-1*ABS(EXP(3.3606+18107.1/T))
      D1=-1*ABS(EXP(3.3606+18107.1/(2+T)))
      DDDT=(D1-D)/2.
      E=0.
      V1=.73*T/P
      N1=0
 6085 MUD=P*V1/(.73*T)-1-B/V1-C/V1**2-D/V1**3
      N1=N1+1
      IF (N1 .GT.10) Go TO 6170
      SLOPE=P/(.73*T)+B/V1**2+2*C/V1**3+3*D/V1**4
      V2=V1-MUD/SLOPE
      IF (ABS(V1-V2) .LT. .01) GO TO 6125
      V1=V2
      GO TO 6085
C       VG unit = ft^3/lb-mole
 6125 VG=V2
      HFG=2.72*P*(18717./T-.53299)*(VG/39.1-VF)
      HG0=998.95+.127*T+24836.*EXP(-39375./T)
      HG=HG0+1.987*(T/39.1)*((B-T*DBDT)/VG+(C-T*DCDTX/2)/VG**2
     &   +(D-T*DDDT/3)/VG**3)
      HF=HG-HFG
      SFG=HFG/T
      SG0=.127*LOG(T)+.18075+.7617*EXP(-31126/T)
      SG=SG0-(1.987/39.1)*(LOG(P)-LOG(P*VG/(.73*T))+B/VG+T*DBDT/VG
     &   +C/(2*VG**2)+T*DCDTX/(2*VG**2)+D/(3*VG**3)+T*DDDT/(3*VG**3))
      SF=SG-SFG
      VG=VG/39.1
      TK=T/1.8
      SIG=-0.00007*TK + 0.1378
C
      RETURN
 6170 WRITE (6,6175) T
 6175 FORMAT(" **SOLUTION FOR VG WON'T CONVERGE FOR TEMP = ",F10.3,"**")
      T=T+1
      GO TO 6015
      END
C
C
C     **** POTASSIUM TRANSPORT PROPERTIES SUBROUTINE ******************
      SUBROUTINE KXPORT(TR,MU,K,CP)
      IMPLICIT REAL*4 (A-Z)
      TF=TR-460.
      TC=(TR-492)/1.8
      IF (TR .LT. 1158.) THEN
        MU=EXP(1189.98/TR-1.6286)
      ELSE
        MU=EXP(1698.156/TR-2.0675)
      ENDIF
      K=57.82*(.438-.000222*TC+39.5/(TC+273.2))
      CP=.239*(.84074-3.1688E-04*TC+3.1435E-07*TC**2)
      RHOFL=52.768-.0074975*TF-5.255E-07*TF**2+4.98E-11*TF**3
      RETURN
```

```
      END
C
C
C     **********************TFROMP**************************************
C     CALCULATES SATURATION TEMPERATURE (R) FROM GIVEN PRESSURE (ATM)
      SUBROUTINE TFROMP(P,TEMP)
      T1=1000.
 6315 E=18717.2/T1+.53299*LOG(T1)-14.10927+LOG(P)
      XM=-18717.2/T1**2+.53299/T1
      T2=T1-E/XM
      IF (ABS(T1-T2) .LT. .01) GO TO 6345
      T1=T2
      GO TO 6315
 6345 TEMP=T2
      RETURN
END
```

B.2 Modified ALKASYS-SRPS with Input

FORTRAN 77

Input:

```
100 KW SYSTEM WITH 13 YR LIFE
1, 1, 1100.00, 1.0, 883.0, 0.90, 0.85, 11630., 259.08, 0.0
0.25, 0.25, 0.9, 0.1, 3.5
0.27, 0.46, 0, 194.44, 500.0, 5.555, 5.555, 10.0, 425.0
100, 1, 0.01, 13.
BOILER OUTLET    3.6576   1
TURBINE INLET    1.8288   1
TURBINE OUTLET   1.8288   1
CONDENSER INLET  1.8288   1
CONDENSER OUTLET 1.8288   3
COND.JET OUTLET  2.4384   3
HTR 3 FEED       1.8288   3
HTR 1 FEED       1.2192   3
HTR 2 FEED       1.2192   3
BOILER FEED      3.6576   3
P.TURB. INLET    1.8288   1
P.TURB. OUTLET   2.4384   1
HTR 2 EXTR.      2.4388   1
HTR 2 DRAIN      2.4388   3
HTR 1 SEPS       2.4388   2
HTR 1 MIX        1.2192   1
HTR 1 DRAIN      2.4388   3
HTR 3 EXTR.      2.4388   1
HTR 3 SEPS       2.4388   2
HTR 3 MIX        1.2192   2
HTR 3 DRAIN      2.4388   3
COND. SEPS       1.8288   2
COND.JET RECIRC. 2.4388   3
1110.0, 1, 137.16, 30.48, 3.048, 16718.66, 8580.8, 53.63, 53.63
2, 0.635, 0.0508
5, 600.0, 7.0, 22.0, 0.0232
67.0, 7.0, 85.0, 2.0, 0
```

Output:

```
       ALKASYS/SRPS-RANKINE SYSTEM ANALYSIS-VERSION 2


            100 KW SYSTEM WITH 13 YR LIFE

               REACTOR IS LITHIUM-COOLED
                  WITH SHADOW SHIELD

 ###  INPUT PARAMETERS  ###
   # TURBINE CYCLE #

 THROTTLE TEMP, K            = 1306.   CONDENSER TEMP, K      =  883.
 THROTTLE TEMP, R            = 2351.   CONDENSER TEMP, R      = 1589.
 BOILER VAP. QUALITY         =  1.00   REHEATER DEL T, K      =    0.
 TIP VELOCITY, M/S (FPS)     =  259.08    850.00
 EXHAUST LOSS,J/KG (BTU/LBM) =  11630.      5.00
 DRY STAGE EFF, %            =   85.   NO. OF STAGES          = 10
 NO. OF HEATER STAGES        =  0      PUMP TURB. DEL T, K    =  194.
 JET PUMP FLOW RATIO         = 500.0   PUMP TURB. EFF.        =  0.27
 PUMP EFFICIENCY             =  0.46   GENERATOR EFFICIENCY   =  0.90
 BOILER FEED SUBCOOLING, K   =  425.   CONDENSER SUBCOOLING,K =    6.
 HEATER TERMINAL TEMP.DIF.,K =    6.   DRAIN COOLER DEL T,K   =   10.

 *** NO FEED HEATERS ***

 TEMPERAT. SWITCH FOR RADIATOR MATERIAL, K  = 1110.00

 NB-1%ZR IS THE MATERIAL SELECTED FOR THE PCS

         ROCKETDYNE TURBINE, TURBOPUMP & GENERATOR


#  RADIATOR AND PACKAGING  #

 LOW-TEMP. RADIATOR T, K    =  600.    HI-TEMP. RADIATOR T, K =  839.
 LOW-TEMP. RADIATOR T, R    = 1080.    HI-TEMP. RADIATOR T, R = 1509.
 LAUNCH BAY LENGTH, M       =  22.0    LAUNCH BAY DIAM, M     =   7.0
 HEAT PIPE WALL, CM         = 0.023

    SWALES RADIATOR 0.5m-HP-POTASSIUM/NB-1%ZR


 ###  TURBINE CYCLE CHARACTERISTICS  ###

 GENERATOR OUTPUT  =   115.15 KW(E)    CYCLE EFFICIENCY =  0.2248
 THERMAL INPUT     =   569.11 KW(T)    PLANT EFFICIENCY =  0.2023
 CONDENSER REJECT  =   441.17 KW(T)    MAIN VAPOR FLOW  =   0.597 LB/SEC
 GENERATOR LOSSES  =    12.79 KW(T)                       0.271 KG/S

 STAGE     STAGE FLOW    LIQ. SEP     VAP. SEP    EXTRACT.    STAGE EFF.

  1              0.574       0.000       0.000       0.000     0.83628
  2              0.574       0.000       0.000       0.000     0.81396
  3              0.574       0.000       0.000       0.000     0.79206
  4              0.574       0.000       0.000       0.000     0.77061
  5              0.574       0.055       0.005       0.000     0.74966
  6              0.514       0.000       0.000       0.000     0.82337
```

7	0.514	0.000	0.000	0.000	0.79677
8	0.514	0.000	0.000	0.000	0.77129
9	0.514	0.014	0.004	0.000	0.74688
10	0.496	0.000	0.000	0.000	0.74734

HEATER NO.	1	2	3
FEED FLOW, LB/SEC	0.597	0.597	0.597
FEED TEMP IN, R	0.000	0.000	0.000
FEED ENTHALPY IN, BTU/LB	0.000	0.000	0.000
FEED TEMP OUT, R	0.000	0.000	0.000
FEED ENTHALPY OUT, BTU/LB	0.000	0.000	0.000
VAPOR MIX. FLOW, LB/SEC	0.000	0.000	0.000
VAPOR MIX. VOL. FLOW,FT**3/SEC	0.000	0.000	0.000
VAPOR MIX. TEMP, R	2000.808	0.000	0.000
VAPOR MIX. QUALITY	0.000	0.000	0.000
VAPOR MIX ENTHALPY, BTU/LB	0.000	0.000	0.000
DRAINS TEMP, R	0.000	0.000	0.000
DRAINS ENTHALPY, BTU/LB	0.000	0.000	0.000
HEAT EXCHANGE (COND.), BTU/SEC	0.000	0.000	0.000
LOG MEAN TEMP DIF. (COND.)	0.000	0.000	0.000
HEAT EXCHANGE (D. COOL.), BTU/SEC	0.000	0.000	0.000
LOG MEAN TEMP DIF. (D. COOL.)	0.000	0.000	0.000

FEED PUMP TURBINE

VAPOR FLOW, LB/SEC	0.023
ENTHALPY IN, BTU/LB	1210.735
ENTHALPY OUT, BTU/LB	1178.900
POWER, KW	0.769

FEED PUMP

FEED PUMP FLOW, LB/SEC	0.598
FEED PUMP HEAD, PSI	132.571

CONDENSER

VAPOR MIX. TEMP, R	1589.400
VAPOR MIX. FLOW, LB/SEC	0.597
VAPOR MIX. QUALITY	0.753
VAPOR MIX. ENTHALPY, BTU/LB	961.287
CONDENSATE TEMP, R	1579.401
CONDENSATE ENTHALPY, BTU/LB	306.449

1
SCHEDULE OF PIPING RUNS
PAGE 3

NO.	DESCRIPTION	TEMP R	PRESS PSIA	FLOW LB/S	FLOW CF/S	NO. LINES	UNIT L,FT	I.D. INCH	WALL INCH	TOTAL LBS
1	BOILER OUTLET	2350.800	109.667	0.597	2.997	1	12.0	1.105	0.023	3.666
2	TURBINE INLET	2350.800	109.667	0.574	2.882	1	6.0	1.084	0.023	1.763
3	TURBINE OUTLET	1589.400	2.980	0.496	62.200	1	6.0	5.034	0.020	7.088

```
  4  CONDENSER INLET    1589.400    2.980    0.597   62.907      1      6.0
5.062    0.020    7.128
  5  CONDENSER OUTLET   1579.401    2.980    0.597    0.014      1      6.0
0.500    0.020    0.729
  6  COND.JET OUTLET    1579.401   18.210    0.598    0.014      1      8.0
0.501    0.020    0.973
  7  HTR 3 FEED            0.000  135.551    0.597    0.014      1      6.0
0.500    0.020    0.729
  8  HTR 1 FEED            0.000  135.551    0.597    0.000      1      4.0
0.000    0.020    0.000
  9  HTR 2 FEED            0.000  135.551    0.597    0.000      1      4.0
0.000    0.020    0.000
 10  BOILER FEED        1585.774  135.551    0.597    0.014      1     12.0
0.500    0.020    1.459
 11  P.TURB. INLET      2350.800  109.667    0.023    0.115      1      6.0
0.216    0.020    0.332
 12  P.TURB. OUTLET     2000.808   29.684    0.023    0.374      1      8.0
0.390    0.020    0.767
 13  HTR 2 EXTR.           0.000  109.667    0.000    0.000      1      8.0
0.000    0.020    0.000
 14  HTR 2 DRAIN           0.000  109.667    0.000    0.000      1      8.0
0.000    0.020    0.000
 15  HTR 1 SEPS            0.000    0.000    0.000    0.000      1      8.0
0.000    0.020    0.000
 16  HTR 1 MIX          2000.808   29.684    0.000    0.000      1      4.0
0.000    0.020    0.000
 17  HTR 1 DRAIN           0.000   29.684    0.000    0.000      1      8.0
0.000    0.020    0.000
 18  HTR 3 EXTR.           0.000  109.667    0.000    0.000      1      8.0
0.000    0.020    0.000
 19  HTR 3 SEPS            0.000    0.000    0.000    0.000      1      8.0
0.000    0.020    0.000
 20  HTR 3 MIX             0.000  109.667    0.000    0.000      1      4.0
0.000    0.020    0.000
 21  HTR 3 DRAIN           0.000  109.667    0.000    0.000      1      8.0
0.000    0.020    0.000
 22  COND. SEPS         1957.066   24.369    0.078    0.142      1      6.0
0.510    0.020    0.744
 23  COND.JET RECIRC.   1585.774  135.551    0.001    0.000      1      8.0
0.022    0.020    0.079


TOTAL PIPING WEIGHT   25.458

 # DESIGN CHARACTERISTICS OF FEED HEATERS (USING0.250IN. OD X0.020IN. WALL
TUBING) #

     NO.     PITCH,   SHELL    WALL     LENGTH                              WT/
TOTAL
NO.  TUBES   IN.      DIA,IN   IN       FT        HO       UIC     UID
HTR,LB   WT,LB    SIGMA

                                                          TOTAL HEATER
WEIGHT      0.000

 # CHARACTERISTICS OF TURBINE-GENERATOR #

   MACHINE SPEED, RPM       = 53269.
   TURBINE OD AT INLET, IN  =   0.0
   TURBINE OD AT OUTLET, IN =   0.0
```

```
   TURBINE LENGTH, IN       =   0.0
   TURBINE WEIGHT, LB       =   38.
   GENERATOR OD, IN         =   5.0
   GENERATOR LENGTH, IN     =   6.0
   GENERATOR WEIGHT, LB     =   90.
   TOT. WEIGHT/UNIT, LB     =  128.

 TOT. WEIGHT/ 1 UNITS, LB  =   128.

 TURBINE-PUMP WEIGHT, LB  =    6.4

 POWER COND. WEIGHT, LB  = 1321.2
1

 # CHARACTERISTICS OF RADIATOR #
PAGE 4

 RADIATOR IS CONICAL-CYLINDRICAL   0.000 FT
 HI-TEMP RADIATOR LOAD, KW   =  441.17      LO-TEMP RADIATOR LOAD, KW   =
20.58
 HI-TEMP RADIATOR AREA, M**2 =   26.54      LO-TEMP RADIATOR AREA, M**2 =
3.44
 HI-TEMP RADIATOR WEIGHT, KG =  416.89      LO-TEMP RADIATOR WEIGHT, KG =
82.56
 CONICAL LENGTH, FT          =    0.00      CYLINDRICAL LENGTH, FT      =
0.00
 HEADER DIAMETER, FT         =    0.00      VAPOR HEADER ID, IN         =
0.00
 VAPOR HEADER WALL, IN       =   0.000      VAPOR HEADER WEIGHT, LB     =
0.0
 LIQUID HEADER ID, IN        =    0.00      LIQUID HEADER WALL, IN      =
0.000
 LIQUID HEADER WEIGHT, LB    =     0.0      NIPPLE WEIGHT, LB           =
0.000
 HEAT PIPE WEIGHT, LB        =     0.0      TOTAL RADIATOR WEIGHT, KG   =
499.5
 RADIATOR SP. WT., KG/M**2   =16.66165      TOTAL RADIATOR AREA, M**2   =
30.0

1


### CHARACTERISTICS OF REACTOR ###
PAGE 5

 NET ELECTRIC POWER, KW                          114.0
 POWER CONVERSION EFFICIENCY, %                  20.23
 REACTOR THERMAL POWER, KW                       573.7
 NET THERMAL TO ELECTRIC EFFICIENCY, %           19.87
 ELECTRIC POWER FOR LI PUMP, %                    1.00
 REACTOR COOLANT                                LITHIUM
   FLOW THROUGH CORE, KG/S                       1.364
 MAX. ROD SURFACE HEAT FLUX, W/CM**2             67.0
 PEAKING FACTOR                                   2.0

 TEMPERATURES, K
   REACTOR OUTLET                               1346.0
   REACTOR INLET                                1246.0
   BOILER OUTLET, K SIDE (TURBINE INLET)        1306.0
   BOILER INLET, K SIDE                          881.0
```

PEAK FUEL CENTERLINE		1462.6
PRESSURES	KPA	PSI
LI PUMP INLET	3.9	0.6
LI PUMP OUTLET	30.9	4.5
CORE INLET	27.9	4.0
CORE OUTLET	15.7	2.3
BOILER INLET, LI SIDE	12.2	1.8
BOILER OUTLET, LI SIDE	3.9	0.6
BOILER INLET, K SIDE	934.6	135.6
BOILER OUTLET, K SIDE	756.1	109.7
CORE PROPERTIES		
FULL POWER LIFE, YR		13.0
BURNUP, AT %		
AVERAGE		4.68511
PEAK ROD		5.34066
PEAK PELLET		6.08793
PEAK ROD FISSION GAS RELEASE, %		10.99099
URANIUM LOADING, KG		61.96
INITIAL U-235 CONTENT, WT %		93.212
UN SMEARED DENSITY, % T.D.		85.0
NO. OF FUEL ASSEMBLIES		7.
NO. OF RODS PER ASSEMBLY		19.
NO. OF CONTROL ASSEMBLIES		0.
NO. OF DRUMS		9.
NEUTRON BALANCE		
PRODUCTION - FISSION		0.98000
PRODUCTION - N-2N		0.02020
ABSORPTION		0.55795
LEAKAGE		0.44225
K-EFF (BOL)		1.06059
K-EFF (EOL)		1.02120
DELTA K		
CONTROL REQUIREMENT		0.09059
WORTH OF DRUMS		0.12038
WORTH OF CONTROL ASSEMBLIES		0.00000
NEUTRON FLUX GT 0.1 MEV, N/CM**2-S, CORE		0.16180E+15
PRESSURE VESSEL		0.58928E+14

1
DIMENSIONS
PAGE 6

ROD DIAMETER, CM	1.484
CLAD THICKNESS, CM	0.0635
W LINER THICKNESS, CM	0.0127
ROD PITCH, CM	1.573
HEX CAN WALL THICKNESS, CM	0.050
INTERASSEMBLY GAP, CM	0.015
EFFECTIVE CORE DIAMETER, CM	20.50
CORE LENGTH, CM	29.12
UPPER ALUMINA REFLECTOR, CM	7.50
LOWER ALUMINA REFLECTOR, CM	7.50
GAS PLENUM LENGTH, CM	25.27
TOTAL ROD LENGTH, CM	71.39

CORE LINER THICKNESS, CM	0.050
CORE LINER O.D., CM	20.60
PRESSURE VESSEL I.D., CM	21.04
PRESSURE VESSEL WALL THICKNESS, CM	0.400
DRUM HOLE DIAMETER, CM	9.20
DRUM DIAMETER, CM	9.00
SHIELD INSIDE DIAMETER, CM	40.24
SHIELD OUTSIDE DIA. @ FRONT, CM	96.78
SHIELD OUTSIDE DIA. @ CORE, CM	50.24
SHIELD INSIDE LENGTH, CM	92.43
TUNGSTEN THK @ 18.6 DENSITY, CM	5.95
LIH-SS THK @ 1.024 DENSITY, CM	45.13
MAXIMUM SHIELD THICKNESS, CM	51.08
OUTLET PIPING I.D., CM	3.65
OUTLET PIPING WALL THICKNESS, CM	0.05
RETURN PIPING I.D., CM	3.61
RETURN PIPING WALL THICKNESS, CM	0.050
BOILER SHELL I.D., CM	6.91
BOILER SHELL THICKNESS, CM	0.05
BOILER LENGTH, CM	239.32
TUBE I.D., CM	1.02
TUBE WALL THICKNESS, CM	0.051
TUBE PITCH, CM	1.76
TUBE LENGTH, CM	232.41
NO. OF TUBES	14.
POTASSIUM IN BOILER,L	0.879

WEIGHTS, KG

CORE HARDWARE	109.8
COOLANT IN REACTOR	7.0
PRESSURE VESSEL	23.9
DRUMS AND RADIAL REFLECTOR	49.6
PIPING AND ACCUMULATOR	1.6
LITHIUM PUMP	34.6
BOILER	9.6
TOTAL REACTOR	236.3
SHIELD	838.7
POTASSIUM INVENTORY, L	2.358
POTASSIUM WEIGHT, KG	1.649
K-ACCUMULATOR WEIGHT, KG	1.273

****
* SYSTEM WEIGHT SUMMARY (KG) *
****

REACTOR	236.
SHIELD	839.
TURBINE CYCLE PIPING, HEATERS, AND FEED PUMP WITH DRIVE	16.
TURBINES	17.
GENERATORS	41.
RFMD	8.
ACCUMULATOR	1.3
RADIATOR	499.

CONDENSER	80.
POWER CONDITIONING 1/1	599.
GRAND TOTAL, KG	2337.

WEIGHTS FOR 2x100% PCS

EXTRA BOILER FOR 2/1	10.
POWER COND. FOR 2/1	704.
GRAND TOTAL FOR 2xPCS UNITS, KG	3115.

B.3 High Vapor Flow Separator Sizing Code

MATLAB 7.1

```
%{
High Vapor Flow Separator Sizing Model
Kevin Supak - Spring 2007

This model is based off the volume limited separator design for high vapor flow rate.
Inputs required are the thermodynamic properties,
separator size, liquid layer thickness with no gas injection, and the vapor diameter
fraction.

Additional inputs are minimum bubble radius, vapor flow rate, pump efficiency, pipe area

The output is a surface plot of the flowrate required to operate the separator as a
function of liquid volume fraction and vapor diameter fraction.
%}

clc;
clear all;
format short e;

rho_g = 3.1;                    %vapor density kg/m^3
rho_l = 595;                    %liquid density kg/m^3
mu = 0.000108;                  %dynamic viscosity Pa-s
sigma = 0.047;                  %surface tension N/m
r_bubble = 1000e-6/2;           %minimum bubble radius m
converge = 0.001;
dt = 0.00001;
mdotv = 0.27;                   %vapor flow rate kg/s
pipe_area = 0.000506;           %pipe area m
pump_eff = 0.85;                %pump efficiency

k=1;

d_sep = 0.3;                    %separator size m

layer = linspace(0.1*2.54/100,0.5*2.54/100,4);  %liquid layer thickness IN
dif = linspace(0.4,0.9,10);                     %vapor diameter fraction

[L,D] = meshgrid(layer,dif);


for i=1:1:40


        flow = 20/(1000*60);

        d_core = D(i)*d_sep;
        r_sep = d_sep/2;
        nozh = 0.08888*d_sep;
        nozw = 0.00288888*d_sep;
        noza = nozh*nozw;
        nozl = noza^0.5;
        liq_vol = pi/4*d_sep*(d_sep^2-(d_sep-L(i))^2);
        layer_vol = pi/4*d_sep^3*(1-D(i)^2);

        if (liq_vol > layer_vol)
            stop='volume problem'
            break
        end

        tr_calc = (layer_vol-liq_vol)*rho_g/mdotv;
```

```
for j=1:1:10000
    flow = flow + 0.5/(1000*60);
    time = 0.0;
    vr = 0.0;
    theta = 0.0;
    r = r_sep;
    r_min = d_core/2 + converge;
    lax = pi/4*(d_sep^2-d_core^2);
    vavg = flow/lax;
    nozv = flow/noza;
    w = (0.394*nozl*nozv-2020.0*(mu/rho_l))/r^2;

    while (r > r_min)
        time = time + dt;
        vt = 2*pi*r*w;
        theta = theta + (vt*dt/r)/pi*180;

        while (theta > 360.0)
            theta = theta - 360;
        end

        Re = rho_l*vr*r_bubble*2.0/mu;

        if (Re == 0.0)
            cd = 1.0;

        elseif (Re < 20.0)
                cd = 24./Re*(1+.1315*Re^(0.82-0.05*log(Re)));
        else
                cd = 24.0/Re*(1.0+0.1935*Re^0.6305);
        end

        if (Re == 0.0)

            vterm=r_bubble^2/12.0/mu*(rho_l/rho_g-1.0)*vt^2/r;
        else
            vterm=8.0/3.0*vt^2/cd*r_bubble/r*(1-rho_g/rho_l);

            if (vterm < 0.0)
                strcat('stop: attempted square root of negative')
                break
            end

            vterm = (vterm)^0.5;

        end

        vr = vterm;
        r = r - vr*dt;

    end


    if (abs(tr_calc-time)/tr_calc <= 0.01)

        k

        Dvap(k)     = d_core*100/2.54;
        t_r(k)      = time;
        LPM(k)      = flow*1000*60;
        Omega(k)    = w*60;
        We(k)       = d_core^3*(Omega(k)*2*pi/60)^2*(rho_l-rho_g)/(16*sigma);
        v_noz(k)    = nozv;
        pipe_vel(k) = flow/pipe_area;
        dp_press(k) = (0.5*rho_l*(nozv^2-pipe_vel(k)^2));
        dp_form(k)  = 0.8*0.5*rho_l*nozv^2;
        dp_total(k) = dp_press(k) + dp_form(k);
```

```
            pumpp(k)     = LPM(k)/(1000*60).*dp_total(k)/pump_eff;
            k = k + 1;

            break

        end


        if (j==10000)
            strcat('did not converge at:'), i

        end

    end


end

[Dvap' t_r' LPM' Omega' We' v_noz' dp_press' dp_form' dp_total' pumpp']

LPM = reshape(LPM,10,[]);
L = d_sep*(d_sep^2-(d_sep-L).^2)/d_sep^3;

surf(L*100,D,LPM),shading interp,colorbar
```

VITA

Kevin Robert Supak received his Bachelor of Science degree in aerospace engineering in May 2005 from Texas A&M University. His undergraduate research interests include: spacecraft power and propulsion and fluid mechanics. He entered the nuclear engineering graduate program at Texas A&M University in August 2005 to work with spacecraft nuclear power and propulsion. His current research interests include space power and propulsion, microgravity fluid dynamics, computational modeling, and nuclear physics.

Name:	Kevin Robert Supak
Address:	Texas A&M University Department of Nuclear Engineering MS 3133 College Station, TX 77843
Email Address:	kevinsupak@gmail.com
Education:	B.S., Aerospace Engineering, Texas A&M University, 2005 M.S., Nuclear Engineering, Texas A&M University, 2007